SLOWING DNA TRANSLOCATION IN A BIOLOGICAL PROTEIN α-HEMOLYSIN ION CHANNEL

By

RANULU SAMANTHI SAROJINI DE ZOYSA

Presented to the Faculty of the Graduate School of

The University of Texas at Arlington in Partial Fulfillment

of the Requirements

for the Degree of

DOCTOR OF PHILOSOPHY

THE UNIVERSITY OF TEXAS AT ARLINGTON

May 2011

This dissertation is dedicated to my paternal grandmother whom I call “Mother” in my life and who brought me up with great love, care, and commitment, and whose only dream is to see me fly high in education.

ACKNOWLEDGEMENTS

I would like to express my gratitude to all who contributed to this dissertation in many ways.

I wish to thank, first and foremost, my PhD advisor, Prof. Richard Guan. I would never have been able to complete my dissertation without his support and proper guidance. He has always been there to listen, and to give advice. It is with immense gratitude that I acknowledge his patience, humble and positive attitude, encouragements, and invaluable discussions throughout my graduate studies.

My sincere gratitude goes to the two committee members, Prof. Purnendu Dasgupta and Prof. Daniel Armstrong. Even though the discussions I had with them were limited, their knowledge and wisdom motivated me to seek higher research standards.

I am grateful to UT Arlington's Department of Chemistry for giving me an opportunity to pursue graduate studies. I would like to acknowledge Prof. Rasika Dias and Prof. Gamini Rajapakshe for assisting me in the admission process. Also, I would like to thank all the past and present staff members of the chemistry department for their kind assistance. I am thankful to Prof. Guan's research group members for their help: Dr. Deqiang Wang, Dr. Milan Dissanayaka, Dr. Quito Zhao, Dr. Jyoti Gupta, Dr. Dilani Jayawardhane, and Dr. Mrinal Sengupta. Prof. Guan's lab provided me a very good research atmosphere.

Also, I would like to acknowledge the agencies that funded my research work. We have received research grants from DARPA, NIH, NSF and the Department of Homeland Security.

I wish to offer warm thanks to my good friends for providing support and encouragement.

Most importantly, I wish to thank my family. They always believe in and stood up by me in each and every step of my life.

I am deeply thankful to my dear husband, Buddhika, for his unwavering love, constant support, encouragements, and also for being the joy of my life. I am indebted to my mother and *loku bappa*, to whom I owe everything I am today. They have sacrificed many things in their lives for me. There are no words to express my gratitude towards them. I am deeply grateful to my father and *podi bappa* for the love and support they have given me throughout my life.

I received my primary, secondary and tertiary education in Sri Lanka. My final thanks are due to divine agents who ornamented my motherland with a pearl of great price-a system of free education-half a century ago.

April 14, 2011

ABSTRACT

SLOWING DNA TRANSLOCATION IN A BIOLOGICAL PROTEIN α-HEMOLYSIN ION CHANNEL

RANULU SAMANTHI S.DE ZOYSA, PhD

The University of Texas at Arlington, 2011

Supervising Professor: Richard X. Guan

During the past decade, nanopore DNA sequencing has emerged as a revolutionary prospect towards a “$1000 genome” goal set by U.S. National Institute of Health. In the nanopore approach, electrophoretic movement of polynucleotide molecules through a nanopore would provide transient current blockades that are unique to each molecule. Since kilobase length DNA can be read directly without amplification or use of costly reagents such as enzymes and fluorescent tags, the nanopore approach can significantly reduce the sequencing cost. However, due to the rapid DNA translocation velocity through the nanopore, accurate detection of single nucleotide bases via the electrophoretically driven approach has not yet been achieved with the currently available recording technique. This dissertation work comprises of research that aim to reduce DNA translocation rate by 1) using organic

salts and 2) via pH effect. In addition, nanopore detection of nerve agent hydrolytes and monitoring peptide cleavage are also included in this dissertation.

TABLE OF CONTENTS

LIST OF ILLUSTRATIONS

LIST OF TABLES

CHAPTER 1

INTRODUCTION

1.1 Stochastic nanopore sensing

Stochastic nanopore sensors detect analytes at the single molecule level.[1, 2] This technique utilizes protein ion channels or synthetic nano scale pores to detect molecules that pass through them under an application of external voltage bias.[1] Over 30 years ago, the very first nanopore experiment was conducted in which an ion-conducting channel was formed by placing gramicidin in a planar lipid bilayer.[3] Krasilnikov *et al*. reported the formation of α-Staphylotoxin ion channels in lipid bilayers approximately 20 years ago.[4] In the mid 1990s α-Hemolysin (α-HL) was employed to characterize bio and neutral polymers.[5, 6] Since then, this technique has emerged as a rapid, highly sensitive multifunctional analytical tool.[1] During the last decade, progress has been made in the identification of a wide varity of analytes including anions,[7] cations,[8] reactive molecules,[9] explosives,[10] enantiomers,[11] proteins,[12, 13] bio polymers,[14,15, 16] and organic molecules[17] by using the nanopore technique. Although both biological and artificial nanopores have been used as the sensory element, α-HL protein pore is the most widely used stochastic sensory element at the present time.[12] Structural details of the α-HL protein pore will be discussed in a separate section.

Stochastic nanopore sensors are formed by assembling a protein pore through a lipid bilayer (Figure 1.1a). Detailed experimental protocol for the channel formation is

described in the experimental section. When the nanopore is immersed in an electrolytic buffer solution, applying a voltage bias across the nanopore will cause an ionic current to flow through the nanopore channel. In the absence of analytes, the channel is always open (Figure 1.1b). As the analyte molecules of interest are added to the buffer solution, they start traversing through the pore lumen, creating current modulations (Figure 1.1c and 1.1d). Characterization of the analyte can be achieved from the event signatures, namely dwell time (τ_{off}) and current amplitude (I) values (Figure 1.1d), which are unique to each analyte molecule. Concentration of the analyte is obtained from $1/\tau_{on}$ values of current blockades. Calculation of the mean values of these event signatures are described in the experimental section.

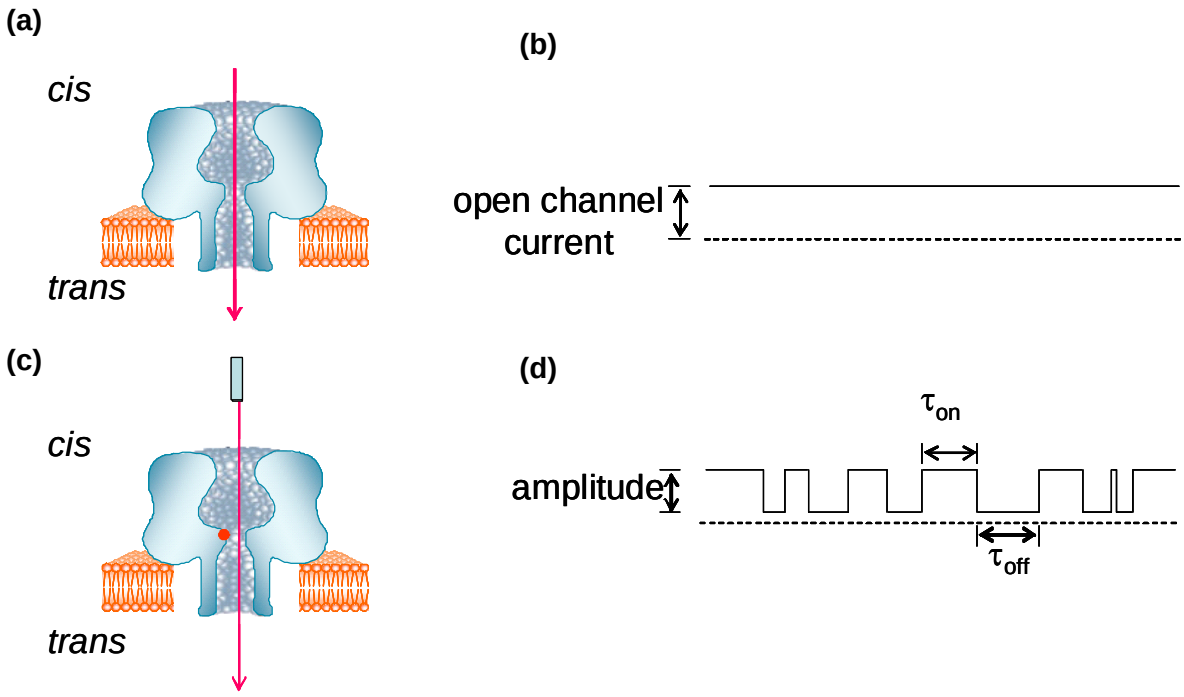

Figure 1.1: Stochastic sensing of single molecules through α-HL nanopore (a)nanopore channel formed through lipid bilayer (b)open channel electrolytic current through nanopore (c)single molecule blockade site within nanopore and (d)resulting current modulation

1.2 α- Hemolysin nanopore

α-Hemolysin (α-HL) are secreted by the human pathogen Staphylococcus Aureus.[18,19] α-HL monomers are water soluble and each monomer has a mass of 33.2-kD.[18] Staphyloccal α-HL is a naturally occurring trans-membrane protein channel. In the presence of a membrane, seven α-HL protein monomers self assemble to form a highly stable, mushroom shaped heptameric channel (232.4 kD) across the membrane (Figure 1.2)[20]. The heptameric protein pore is amphiphlic in nature. Low pH values and high cation concentrations cause reversible channel closures. Although several other biological and synthetic nanopores have been examined, at the present time, α-HL protein is the most widely used sensor element in stochastic nanopore sensing. The α-HL pore is quiet without transient background events, and provides for a very stable sensory element that can withstand harsh conditions. It can easily be genetically engineered with various surface functions, thus permitting convenient detection and characterization of a wide variety of substances.[19,21,22] Three dimensional structure of α-HL has been determined at a 1.9Å resolution via a crystallization strategy.[19] Structure of α-HL and the interactions that occur between various analyte molecules and the pore interiors are being widely experimented. Strongest binding interactions between the analyte molecules and pore occur as the analyte molecules pass through the constriction position having a 1.4nm diameter. Constriction site consists of side chains of Glu 111, Met 113 and Lys 147. Therefore, mutations are performed to change the amino acid residues of the above positions. For instance, the mutant M113F α-HL is obtained by replacing Methionine at position 113 by Phenylalanine. M113F α-HL can be used to detect aromatic compounds based on the aromatic-aromatic interactions between the

analyte molecules and the constriction site of the pore lumen. As α-HL is a heptameric pore, one such change leads to seven changes of the protein pore.[19] However, biological nanopore systems face durability and portability issues due to the fragile lipid bilayer used.[2] Therefore, synthetic nanopores are under investigation to replace their biological counterparts.

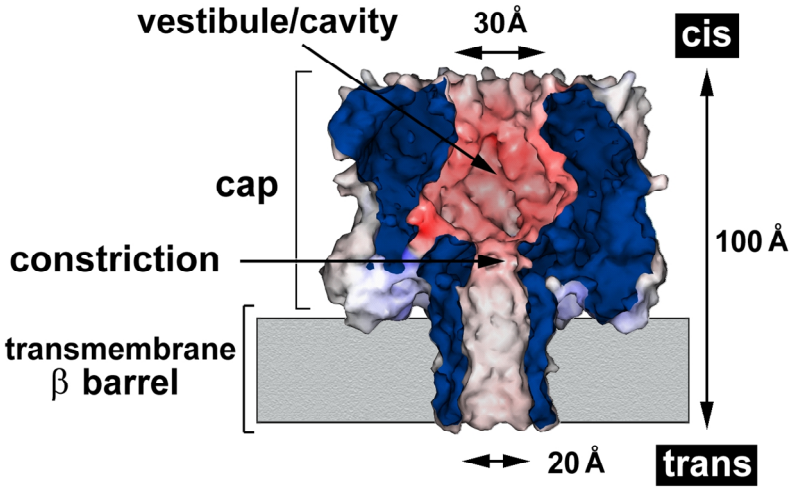

Figure 1.2: Structure and dimensions of α-Hemolysin channel

1.3 Experimental details

1.3.1 Preparation of α-Hemolysin protein pore

Preparation and formation of wild-type and other mutant protein pores have been described elsewhere.[22] Briefly, the mutant α-HL M113F gene is constructed by site-directed mutagenesis. Wild-type and other mutant α-HL monomers are first

synthesized by *in vitro* transcription and translation (IVTT) using the *E. Coli* T7 S30 Extract System for Circular DNA from Promega (Madison, WI). Subsequently, they are assembled into homo-heptamers by adding rabbit red cell membranes and incubating for 1 hour. The heptamers are purified by SDS-polyacrylamide gel electrophoresis and stored in aliquots at -80℃.

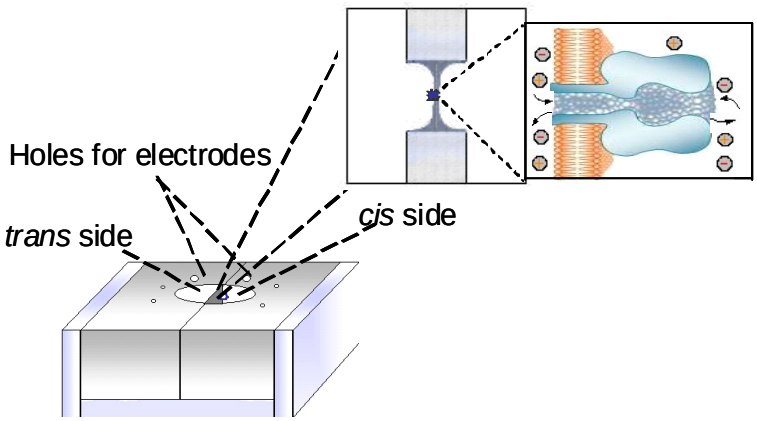

Figure 1.3: Representative experimental chamber

1.3.2 Planar bilayer experiments

Single channel recordings are performed in a teflon chamber. Teflon films are used to divide the chamber into two compartments, *cis* and *trans* (Figure 1.3). Formation of bilayer and single channel recordings have been described elsewhere.[23] Briefly, a lipid bilayer of 1,2-diphytanoyl-sn-Glycero-3-phosphacholine is formed on the aperture in the teflon film by using the Montal-Mueller method[23]. The experiments

are carried out under symmetrical buffer conditions. Each side of the chamber is composed of a 2.0 mL electrolyte solution. For the research work described in this dissertation, 1 M NaCl, 1 M KCl, or 1 M butylmethylimidazolium chloride (BMIM-Cl) are used as the electrolyte solution and buffered with 10 mM Tris·HCl at 22 ± 1 ℃ unless otherwise stated. All experiments are performed at ambient temperature, 22 ± 1 ℃. α-HL protein (with a final concentration of 0.2–2.0 ng·mL^{-1}) is added to the *cis* chamber compartment, which is connected to "ground". α-HL self assembles through the lipid bilayer in a way that the *trans* membrane β barrel of the pore directs towards *trans* compartment of the chamber while the vestibule of the pore directs towards the *cis* compartment. Applying an external voltage bias across the chamber allows electrolyte to flow through the nanopore. Monitoring the current across the two compartments indicate the formation of a nanopore channel. After the formation of a single channel, analyte molecules of interest are added to *cis* or *trans* compartment depending upon the analyte of interest. The interactions of the ananlyte molecules with the pore create current blockades, which are unique to each different analyte (Figure 1.1c&d). Currents are recorded with a patch clamp amplifier (Axopatch 200B, Axon instruments, Foster city, CA, USA). They are low-pass filtered either with an external four-pole Bessel filter at 30 kHz and sampled at 125 kHz or with a built-in four-pole Bessel filter at 10 kHz and sampled at 20 kHz by a computer equipped with a Digidata 1440 A/D converter (Molecular Devices). At least three separate experiments are carried out for each analyte. Detailed protocol for single channel formation and recording has been described elsewhere.[22]

1.4 Data analysis

pClamp software is used to obtain mean residence times (τ_{off} and τ_{on} values) and amplitude values. Mean values of τ_{off} and τ_{on} values are obtained by fitting the amplitude and dwell time histograms to single exponential functions by the Levenberg-Marquardt procedure.[24] Conductance values are obtained by fitting amplitude histograms to Gaussian functions. The mean values of τ_{off} and τ_{on} can be used further to obtain the kinetic and thermodynamic information of the interaction between the protein pore and the analyte using the following equations:

α- HL $\rightleftharpoons$ α- HL- Analyte

$$k_{on} = \frac{1}{\tau_{on}[A]}$$

$$k_{off} = \frac{1}{\tau_{off}}$$

$$K_f = \frac{k_{on}}{k_{off}}$$

$$\Delta G_f = -RT \ln K_f$$

Where,

k_{on} = rate constant of association of α-HL and analyte complex formation

k_{off} = rate constant of dissociation of α-HL and analyte complex formation

τ_{on} = mean residence time of the analyte molecule at open channel stage

τ_{off} = mean residence time of the analyte molecule at blockade level

[A] = analyte concentration

K_f = formation constant of protein-analyte complex

ΔG_f = change in Gibb's free energy formation

R = universal gas constant

T = absolute temperature

1.5 Current status of stochastic nanopore sensing

Stochastic sensing provides a convenient and rapid analytical tool to detect analytes at very low concentrations in solution phase. Technological advancements in protein synthesis, bioengineering, electronics and all the other related fields have brought stochastic sensors closer to reality. However, the fragile lipid bilayer used by the biological nanopore experiment only permits laboratory research. In such experiments, free standing lipid bilayers are typically formed over tiny orifices having 100-120 µm diameters, and lasts usually for several hours.[1, 2] Formation of lipid membranes over smaller orifices having lesser surface areas would provide low noise and small capacitance values and lesser probability of breakage. However, smaller lipid bilayers reduce the probability of protein channel insertion. Further, protein nanopores self assembled in lipid bilayers impose special handling requirements such as shock absorbing lab tables and metal cages. Therefore, it is desirable to develop a portable and durable sensing system. Synthetic nanopores are under investigation to replace their biological counterparts.[2]

Several techniques are being employed to create synthetic nanopores. Nanometer sized holes have been etched in a thinned Si_3N_4 membrane by feedback loop-controlled ion mill.[25, 26] It has been reported that the electron beam of a TEM (transmission electron microscope) can be used to form Si-chip devices.[27] Also, soft lithography, LASER, and carbon nanotubes[28] and hybrid systems[29,30] have been used to fabricate solid state nanopores. Even though the solid state nanopores provide the mechanical robustness and the size tunability, it is extremely difficult to obtain reproducible pore diameters.[2] On the other hand, biological nanopores consistently provide identical pore sizes.[1,2] Moreover, in aqueous solutions the surfaces of synthetic pores can be charged, imposing difficulties with transfer of polynucleotide and charged molecules. In addition, hybrid nanopores have also been proposed by housing a protein pore in an artificial membrane. [2]

Stochastic sensors are highly sensitive to the size and the structure of the given molecules. Given the fact that the molecules of interest create distinguishable event signatures, i.e dwell time and amplitude values, simultaneous detection of several compounds can be readily achieved. The resolution of the nanopore sensor can be further improved by using a nanopore sensor array technique in which each nanopore of the array is engineered with different surface functions. A variety of analytes, including molecules with very similar structures and sizes, can be differentiated in this way[32].

1.6 Nanopore DNA sequencing

1.6.1 Concept

In the mid 1990s, Kasianowicz *et al*. demonstrated that polynucleotides can be threaded through an α-HL nanopore under an external voltage bias.[5] As polynucleotide (PN) molecules translocate through α-HL nanopores that have diameters barely larger than the diameter of single stranded PN, they create transient current blockades. Theoretically, nucleotide bases A, C, T, G and U cause blockades having differentiable dwell times and/or amplitude values, thus permitting the base sequence of PNs to be read. It has been confirmed by PCR reactions that polynucleotides could indeed translocate through the α-HL from *cis* side to the *trans* side. Also, it has been shown that the transition between two segments of nucleotide bases (30 Adenines followed by 70 Cytosines) can be detected.[32]

1.6.2 Potentials and challenges of nanopore DNA sequencing

Currently available DNA sequencing methods are based on modified and improved versions of the conventional Sanger technique.[34] All of these methods require sample preparation which involves expensive and time consuming cloning steps and electrophoretic processes that restrict the read length of DNA strands. Two decades of countless efforts have brought down the sequencing costs significantly. However, with current techniques, it still costs about $10 million to sequence a human genome. Nanopore DNA sequencing has two major advantages over the conventional DNA sequencing methods. Firstly, a nanoscale probe that reads nucleotide sequence does not impose a restriction on read limits of PNs. Secondly, nanopore DNA sequencing obviates time consuming and expensive cloning steps.[34,35] In the recent

review regarding nanopore DNA sequencing, Branton *et.al.* reported that the estimated cost of sequencing a complete human genome would be $40 after the initial instrument expenses.[34] This indeed is a vast reduction in the sequencing cost. An ideal optimized nanopore DNA sequencing device can be described as a portable chip consisting of a very stable sensor element which reads a nucleotide sequence of PNs having kilobase lengths in microsecond time intervals.[35] In spite of the above potential advantages (high speed and low cost), the currently available nanopore DNA sequencing technique is still at the early stage and has not reached a point of commercial viability.[16,33,34]

α-HL nanopores show tremendous sensitivity towards polynucleotide molecules. A wide varitey of successful work has been done to characterize biopolymers with biological and solid state nanopores. Several groups have reported nucleic acid analysis both theoretically and experimentally. For example Keller and colleagues reported that it might be possible to sequence a single stranded DNA by reacting polynucleotide molecules with an exonuclease.[36] Bayley's group used α-HL attached with an aminocyclodextrin adaptor to capture the exact deoxynucleoside monophosphates (dNMPs) released by exonuclease reaction.[37,38] However, a major issue related to this strategy is that the sequencing order may be lost as the reaction continues. Another impressive approach is to attach fluorescent probes to each nucleotide and to obtain the base sequence with the optical readout with massive and parallel nanopore arrays. However in order to realize this scheme, nanofabrication techniques must be further improved to create nanopores with 1.7 to 2 nm diameters.[39]

Another promising approach is to employ tunneling currents through nucleobases that are driven through nanoprobes.[40,41] Thus far, this technique cannot discriminate successive nucleotide bases. Furthermore, it requires all the bases to traverse with an identical orientation.[34] Another novel DNA sequencing approach is based on a metaloxide – silicon capacitor[42,43,44] in which a nanopore is fabricated inside a SiO_2 having a approximately 5nm thickness via a beam of TEM. This technique has insufficient temporal resolution in the identification of individual nucleotides. Sequencing by hybridization incorporates hybridization probes of a known DNA strand to read the base sequence of unknown DNA strand. This approach also faces a problem of identifying the exact location of hybridized pore.[45]

As discussed earlier, α-HL pore consists of a constriction site having a diameter of 1.4-1.5 nm. To achieve single nucleotide resolution, PNs should pass through this constriction site one base at a time.[46] Further, individual nucleotide bases should create distinguishable current modulations that are unique to each nucleotide base. Very small differences between the ionic current blockades caused by successive nucleotide bases are measured in picoamperes. Therefore, to reach the resolution permitted by currently available patch clamp amplifying techniques, individual nucleotides must stay at the constriction site for a longer time, at least longer than 1ms.[34] Currently, the reported translocation speeds of PNs through α-HL are approximately 1 base per 1 μs. To read and detect dwell time measurements having this long, detectors with MHz bandwidths are needed.[47,48,49,50,51] Moreover, there is no way of controlling the capture and the subsequent translocation of a particular DNA molecule which is present in the aqueous solution. Additionally, to precisely read the base sequence, the current fluctuations which occur due to the translocation

dynamics should be minimized. Variability in the orientation of entering molecules (3' or 5' end), translocation and capture rates, and the secondary structures adopted by PNs having different lengths impose practical difficulties in the data analysis and interpretation of the results.

One of the major hurdles of utilizing nanopores to sequence DNA molecules is the rapid DNA translocation velocity. Accurate detection of simple bases is extremely difficult to be achieved with the currently available single channel recording technique. Thus far several strategies have been employed to slow down DNA translocation. These include the decrease of experimental temperature,[14,51] change of applied potential,[51] sequence – specific detection of individual DNA strands,[15] use of DNA-Hemolysin rotaxane formation, and immobilization of DNA strands with streptavidin. In this dissertation, we report two different strategies to slow down DNA translocation significantly.

1.7 Organization of dissertation

The work described in this dissertation is mainly focused on two approaches to slowing down DNA translocation through α-HL protein pores. Chapter 2 describes slowing DNA translocation using an organic salt solution. Chapter 3 describes slowing DNA translocation using an acidic solution. Chapter 4 describes the detection of nerve agent hydrolytes in the α-HL nanopore, and chapter 5 describes real time monitoring of peptide cleavage with a nanopore.

CHAPTER 2

SLOWING DNA TRANSLOCATION THROUGH NANOPORES USING A SOLUTION CONTAINING ORGANIC SALTS

2.1 Introduction

Development of a high-throughput and cost-effective DNA sequencing method provides invaluable information on the biological and biomedical fields, and also makes vital contributions to many areas of high priority research such as forensics, archeology, and anthropology.[51,52] Although significant reductions in DNA sequencing costs have been achieved in the past 25 years, fundamentally different approaches will be required to drastically reduce the cost and increase the speed of routine complete genome sequencing.[52]

Among the various DNA sequencing methods under development, the nanopore approach has emerged as one of the most promising technologies to achieve the "$1000 genome" goal set by the U.S. National Institutes of Health.[54,35,] In the nanopore method, single-stranded DNA (ssDNA) molecules are electrophoretically driven through a nano-channel, and the discrimination of polynucleotides might be achieved based on their different current signatures, represented by residence times and/or current blockage amplitudes in the pore.[5] However, one of the major hurdles of utilizing nanopores to sequence ssDNA molecules is that DNA polymers

translocate through the nanopore very rapidly.[33] For instance, the translocation rate of polydeoxycytosine was ~1 μs/base, whereas that of polydeoxyadenine was ~3μs/base.[14] This rate requires a high temporal resolution for the accurate detection of single bases, which can not be provided by the currently available single-channel recording technique.[34] To increase the nanopore resolution for nucleotide differentiation, many attempts have been made to slow down DNA translocation. It has been shown that a decrease in the experimental temperature allowed ssDNA molecules to be electrophoretically driven through the pore more slowly.[14,53] Further, DNA translocation could be manipulated by changing the applied potential.[50] Other approaches include sequence-specific detection of individual DNA strands,[15] formation of DNA-hemolysin rotaxane,[54] differentiation of nucleotide bases in a host β-cyclodextrin compound,[36] and immobilization of DNA polynucleotides with streptavidin.[55] In addition, it was reported that the detection of DNA sequences could be achieved by using an alternating electric field in a nanopore capacitor.[43]

In this study, we investigate the feasibility of utilizing aqueous solutions of ionic liquids to slow ssDNA translocation in the α-hemolysin pore. The study of ionic liquids is currently an active research area. They have been used in various applications, including organic synthesis,[56] extraction,[57] separation,[58] catalysis,[59] and electrochemical studies.[60] In previous work, a solution containing ionic liquid butylmethylimidazolium chloride (BMIM-Cl) was used as a supporting electrolyte in the nanopore stochastic detection of liquid explosives and mono-valent cations.[10] The results suggested that the use of BMIM-Cl solution instead of the commonly used NaCl/KCl solutions could improve nanopore resolution.

2.2 Experimental methods

2.2.1 Materials and reagents

ssDNA samples, including $(dA)_{20}$, $(dC)_{20}$, $(dT)_{20}$, $(dCdT)_{10}$, and $(dC)_{10}(dT)_{10}$, were purchased from Integrated DNA Technologies, Inc. (Coralville, IA). Lipid 1,2-diphytanoylphosphatidylcholine was obtained from Avanti Polar Lipids (Alabaster, AL). Teflon film was purchased from Goodfellow (Malvern, PA). All of the other reagents including butylmethylimidazolium chloride (BMIM-Cl) and tetramethylammonium chloride (TMA-Cl) were purchased from Sigma Aldrich. All the ssDNA polymers were dissolved in HPLC-grade water (ChromAR, Mallinckrodt Baker). The concentrations of the stock solutions were 4 mM for each of the DNA samples. All the three electrolyte solutions used in this work, i.e., 1 M BMIM-Cl, 1 M TMA-Cl, and 1 M NaCl, were prepared in HPLC-grade water and buffered with 10 mM Tris (pH = 6.0). Preparation and formation of wild-type and mutant protein pores has been described elsewhere. Briefly, the mutant αHL M113F gene was constructed by site-directed mutagenesis. Then, the wild-type and mutant M113F αHL monomer were first synthesized by coupled *in vitro* transcription and translation (IVTT) using the *E. Coli* T7 S30 Extract System for Circular DNA from Promega (Madison, WI). Subsequently, they were assembled into homoheptamers by adding rabbit red cell membranes and incubating for 1 h. The heptamers were purified by SDS-polyacrylamide gel electrophoresis and stored in aliquots at -80℃.

2.2.2 Planar bilayer experiments

The single-channel recording procedure has been described elsewhere. [32, 62] Briefly, a Teflon septum was used to divide the planar bilayer chamber into two compartments, *cis* and *trans*. A lipid bilayer of 1,2-diphytanoyl-sn-Glycero-3-phosphacholine was formed on the aperture in the teflon film by using the Montal-Mueller method.[23] The experiments were carried out under symmetrical buffer conditions with a 2.0 mL solution comprising 1 M butylmethylimidazolium chloride (BMIM-Cl), and 10 mM Tris·HCl (pH 6.0) at 22 ± 1 ℃ unless otherwise stated. Both the αHL protein (with the final concentration of 0.2–2.0 ng·mL^{-1}) and the ssDNA sample were added to the *cis* chamber compartment, which was connected to "ground". The applied potential was +120 mV. Currents were recorded with a patch clamp amplifier (Axopatch 200B, Axon instruments, Foster city, CA, USA). They were low-pass filtered either with an external four-pole Bessel filter at 30 kHz and sampled at 125 kHz or with a built-in four-pole Bessel filter at 10 kHz and sampled at 20 kHz by a computer equipped with a Digidata 1440 A/D converter (Molecular Devices). The final concentrations of ssDNA samples were 10 μM each for the experiments performed at the 30 kHz filter, while those were 4 μM each for the experiments carried out at the 10 kHz filter. At least three separate experiments were carried out for each DNA sample.

2.2.3 Data analysis

Only the events with at least 70% of full blockage were included in the analysis. It is believed that the events with the blockage amplitudes less than 70% of the open channel current are not associated with the translocation of ssDNA polymers through the αHL pore, but instead may be caused by collision with the pore opening or residence only in the channel vestibule.[62] Two significantly different types of events were observed for DNA's transit in the αHL pore in the BMIM-Cl solution: short-lived events with mean residence times of ~ 50 to 100 μs; and long-lived events with mean residence times of milliseconds or larger. Data were analyzed with the following software: pClamp 10.0 (Molecular Devices) and Origin 6.0 (Microcal, Northampton, MA). Conductance values were obtained from the amplitude histograms after the peaks were fit to Gaussian functions. Mean residence time (τ_{off}) values of the short-lived events were obtained from the dwell time histograms by fitting the distributions to Gaussian functions,[14] while those of the long-lived events were obtained by fitting the dwell time distributions to single exponential functions by the Levenberg-Marquardt procedure.[24] It should be noted that the dwell time histograms of the short-lived events could also be fitted to single exponential functions by using larger bin widths, and we found that the mean τ_{off} values obtained using these two different approaches were not significantly different. To obtain the mean residence times of the long-lived events for $(dA)_{20}$, $(dT)_{20}$, $(dCdT)_{10}$, and $(dC)_{10}(dT)_{10}$, the events with duration less than 1 ms were not included, while in the analysis of $(dC)_{20}$, events with duration less than 0.5 ms were ignored to minimize the potential interference from the short event signals. Between 1,330 and 20,000 events were recorded in each of the single channel recording experiments performed at the 30 kHz filter, while

between 280 and 10,000 events were collected in each of the single channel recording experiments carried out at the 10 kHz filter. All the results were reported as mean values ± standard deviation.

To obtain the streaming potentials[63] of protein pores, single-channel current recording experiments were performed under asymmetric conditions: the *cis* chamber compartment contained a 2.0 mL solution comprising either 1 M NaCl or 1 M BMIM-Cl, 10 mM Tris·HCl (pH 6.0), while the *trans* compartment contained 2.0 mL of the same buffer solution plus 1 M urea. Streaming potential $\Delta\phi$ for the protein pore was obtained by linearly fitting the I-V curves, which were recorded from ± 5 mV to ± 50 mV.

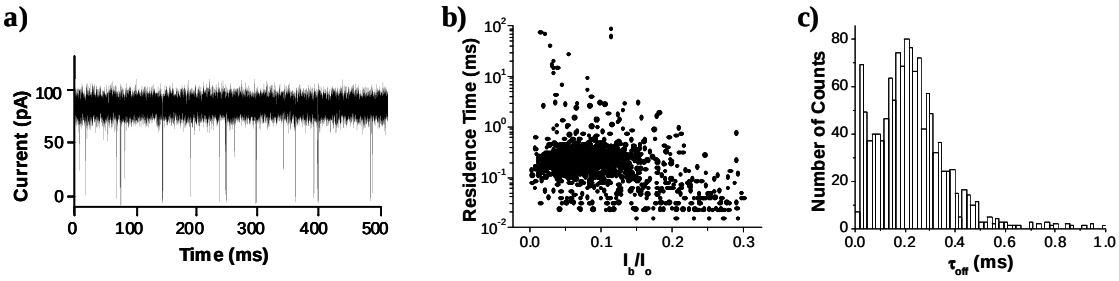

Figure 2.1: Translocation of $(dA)_{20}$ in the mutant $(M113F)_7$ α-HL pore in 1M NaCl solution. (a) Representative single channel current recording trace; (b) scatter plot of event amplitude vs. residence time; and (c) event residence time histogram. I_b/I_o in Figure 1b is normalized blockage residual current, which was obtained by dividing the average blockage residual current of an event by the average open channel current.

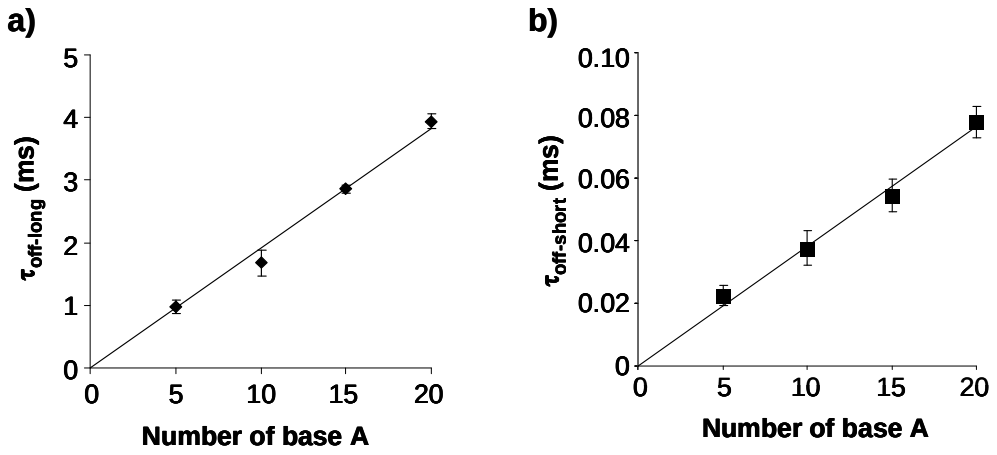

Figure 2.2: Effect of DNA length on the mean residence time of (a) long-lived events; and (b) short-lived events, suggesting that the long duration events are caused by DNA's threading through the α-HL pore. Experiments were performed at +120 mV with the mutant αHL $(M113F)_7$ pore in 1 M BMIM-Cl solution. The currents were low-pass filtered with a four-pole Bessel filter at 30 kHz and sampled at 125 kHz.

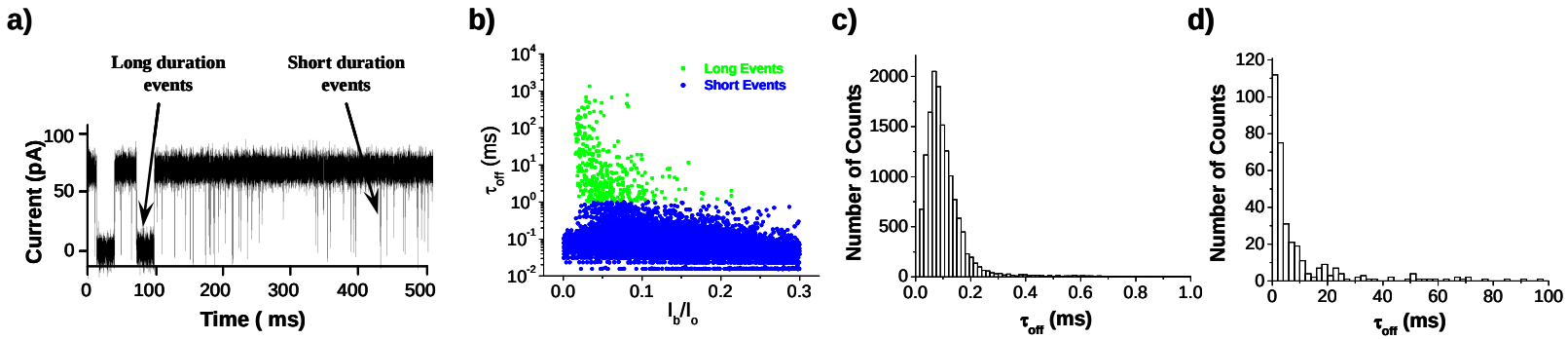

Figure 2.3: Translocation of $(dA)_{20}$ in the mutant $(M113F)_7$ α-HL pore in 1M BMIM-Cl solution. (a) Representative single channel current recording trace; (b) scatter plot of event amplitude vs. residence time; (c) residence time histogram of short-lived events; and (d) residence time histogram of long duration events. I_b/I_o in Figure 2b is normalized blockage residual current, which was obtained by dividing the average blockage residual current of an event by the average open channel current.

2.3 Results and discussion

To investigate the effect of the ionic liquid solution on DNA translocation, the initial experiment was performed at +120 mV with $(dA)_{20}$ in the mutant α-hemolysin (αHL) $(M113F)_7$ pore and using a 1 M BMIM-Cl solution as the supporting electrolyte. The current was low-pass filtered with a four-pole Bessel filter at 30 kHz and sampled at 125 kHz. As a control, the experiment was repeated under the same conditions with the exception that NaCl was substituted for BMIM-Cl as the background electrolyte. The $(M113F)_7$ protein was constructed by replacing the Met residues at position 113 of the wild-type (WT) αHL with Phe amino acids, and has been shown to provide an enhanced resolution for peptide detection compared with that observed with the WT αHL pore.[61] The experimental results showed that, in 1 M NaCl solution, $(dA)_{20}$ produced only a major type of rapid translocation events, although these events could be separated into two subgroups (Figure. 2.1). The mean residence times for the two subgroup events were 190 ± 20 μs, and 40 ± 5 μs, respectively (Figure 2.1). These events might be attributed to the translocation of $(dA)_{20}$ in two different orientations, 5'-first and 3'-first. Note that the observation of two subgroup translocation events with different residence times has been previously reported by Kasianowicz and co-workers in the experiment with the translocation of 210-nt-long poly[U] through the WT αHL channel.[5] Hence, the translocation velocity of $(dA)_{20}$ in the mutant $(M113F)_7$ αHL pore are not significantly different from those well-documented values obtained for the translocation of polydeoxyadenine through the WT αHL pore.[14,53] Similar to the observation made for the translocation of polynucleotides through the WT αHL channel,[5] events with much longer residence times at milliseconds or larger were also occasionally observed for $(dA)_{20}$ in the

$(M113F)_7$ αHL pore (Figure 2.1). These events are believed to be caused by the tangling of polynucleotides to the αHL channel.[5]

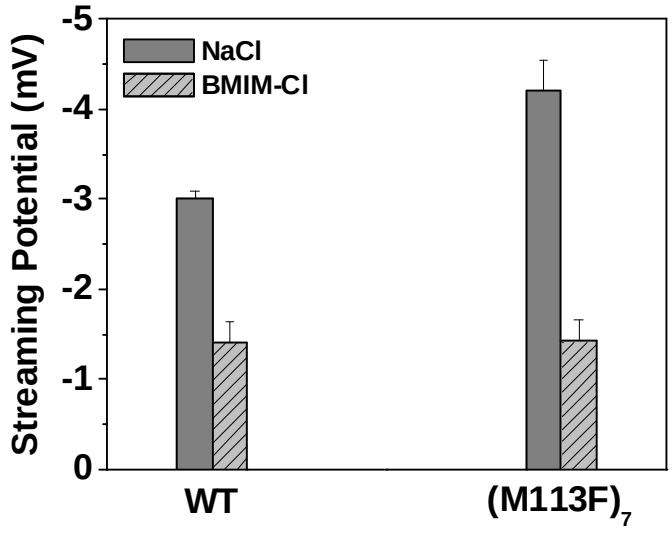

Figure 2.4: Effect of BMIM-Cl solution on the streaming potentials of αHL pores.

In contrast, in 1 M BMIM-Cl solution, two major types of current blockage events were observed for $(dA)_{20}$ (Figure 2.3). One type of events shows a small mean residence time ($\tau_{off\text{-}short}$) and a wide range of current blockage amplitudes (from ~70% to almost full channel blockage), while the other type of events presents a narrow range of current blockage amplitudes and a large mean duration value ($\tau_{off\text{-}long}$) but with a broad distribution of residence times. The mean $\tau_{off\text{-}short}$ and $\tau_{off\text{-}long}$ values were 78 ± 5 μs, and 3.93 ± 0.12 ms, respectively. Since the rise time (= ~0.33/f_c) is ~11 μs at 30 kHz,[64] the vast majority of the rapid DNA translocation events should have

been detected under the experimental conditions employed in this work. It should be mentioned that these long-lived current modulations occurred very frequently (at ~ 5 events per second), although they only accounted for a small portion (~2.5%) of the total current blockages. In part, this was attributed to a ~ 2 fold increase in the frequency of the $(dA)_{20}$ events when the electrolyte BMIM-Cl was substituted for NaCl. In addition, we noticed that, with the change of the electrolyte from 1 M NaCl to 1 M BMIM-Cl, the current value of the open state of a single αHL $(M113F)_7$ channel decreased from 90 ± 4 pA to 62 ± 5 pA at +120 mV. The extent of decrease (i.e., 31%) in our experimental open channel conductance was in agreement with that (i.e., 39%) in the measured conductivities of the bulk solutions (note that the conductivities of 1 M NaCl and 1 M BMIM-Cl solutions were 81.6 mS/cm and 49.9 mS/cm, respectively).[10]

Table 2.1: The residence times and current blockage amplitudes of five ssDNA samples in the $(M113F)_7$ protein pore. Each experimental value represents the mean of three replicate analyses ± one standard deviation. The experiments were performed at +120 mV in 1 M BMIM-Cl solution.

ssDNA sample	Residence Time (ms)	Residual Current (pA)	Current Blockage (%)
$(dA)_{20}$	4.02 ± 0.17	2.9 ± 0.2	95.3 ± 0.4
$(dC)_{20}$	1.96 ± 0.22	7.0 ± 0.4	88.7 ± 0.6
$(dT)_{20}$	3.00 ± 0.25	2.8 ± 0.2	95.4 ± 0.3
$(dCdT)_{10}$	5.13 ± 0.91	4.0 ± 0.3	93.6 ± 0.5
$(dC)_{10}(dT)_{10}$	6.40 ± 0.19	4.9 ± 0.2	92.2 ± 0.4

Table 2.2: The residence times and current blockage amplitudes of five ssDNA samples in the wild-type αHL protein channel. Each experimental value represents the mean of three replicate analyses ± one standard deviation. The experiments were performed at +120 mV in 1 M BMIM-Cl solution.

ssDNA sample	Residence Time (ms)	Residual Current (pA)	Current Blockage (%)
$(dA)_{20}$	2.37 ± 0.20	2.8 ± 0.2	95.6 ± 0.3
$(dC)_{20}$	1.65 ± 0.23	4.1 ± 0.3	93.5 ± 0.4
$(dT)_{20}$	2.17 ± 0.10	0.8 ± 0.1	98.6 ± 0.1
$(dCdT)_{10}$	3.00 ± 0.20	1.3 ± 0.1	98.0 ± 0.2
$(dC)_{10}(dT)_{10}$	4.79 ± 0.71	3.3 ± 0.3	94.8 ± 0.5

To investigate whether these long-live events are caused by $(dA)_{20}$'s threading through the αHL pore or rather they are attributed to the sticking of these DNA polymers to the channel, a series of polydeoxyadenine polymers with different lengths were examined with the mutant αHL $(M113F)_7$ protein channel in 1 M BMIM-Cl solution. Our experimental results show that, with an increase in the DNA length, the mean residence time of the long-lived events increased linearly (Figure 2.2.a). This clearly suggests that these long-lived events were not due to the tangling of the $(dA)_{20}$ molecule to the channel or binding of one or more bases of the polymer to the protein pore for long periods of time with intermittent short periods of rapid translocation, but rather caused by the slower translocation of the DNA molecule as a whole. And hence, the long duration events are suitable for the analysis of the length and structure of a polynucleotide molecule. In terms of the short-lived events, we noticed that $(dA)_5$ (with a mean $\tau_{off\text{-}short}$ value of 22.5 ± 3.1 μs) was still in the linear range of the plot of the event residence time vs. DNA length (Fig. 3b). In contrast, a linear relationship between the event residence time and polymer length was observed only when DNA polymers longer than ~ 12 bases were electrophoretically driven through the WT αHL pore in the KCl solution.[50, 53] Therefore, this suggests that the use of ionic liquid solutions coupled with the engineered protein pores provides a potential means to improve the resolution of the nanopore to the nucleotide differentiation, especially in the analysis of short DNA polymers.

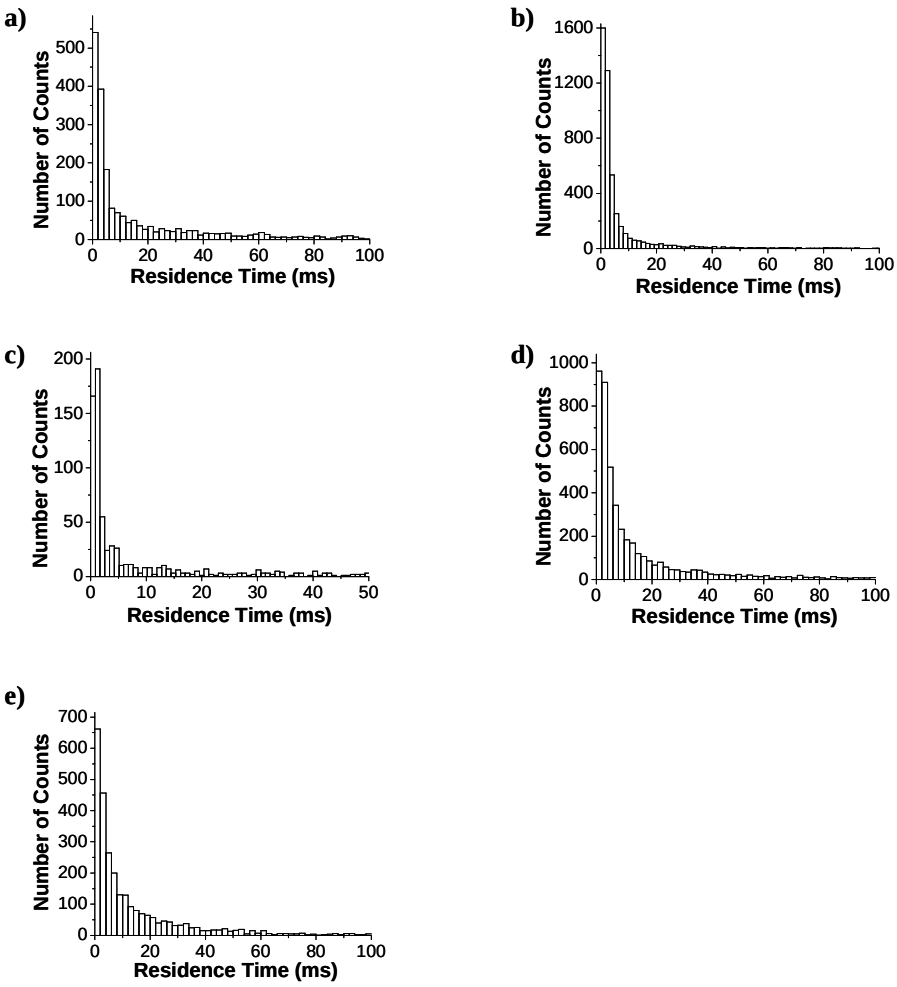

Figure 2.5: Event dwell time histograms of (a) $(dA)_{20}$; (b) $(dT)_{20}$; c) $(dC)_{20}$; (d) $(dC)_{10}(dT)_{10}$; and (e) $(dCdT)_{10}$. Experiments were performed at +120 mV with the mutant αHL $(M113F)_7$ pore in 1 M BMIM-Cl solution. The currents were low-pass filtered with a four-pole Bessel filter at 10 kHz and sampled at 20 kHz. Events with residence times longer than 100 ms (or 50 ms for $(dC)_{20}$) were also observed but not displayed in the histogram

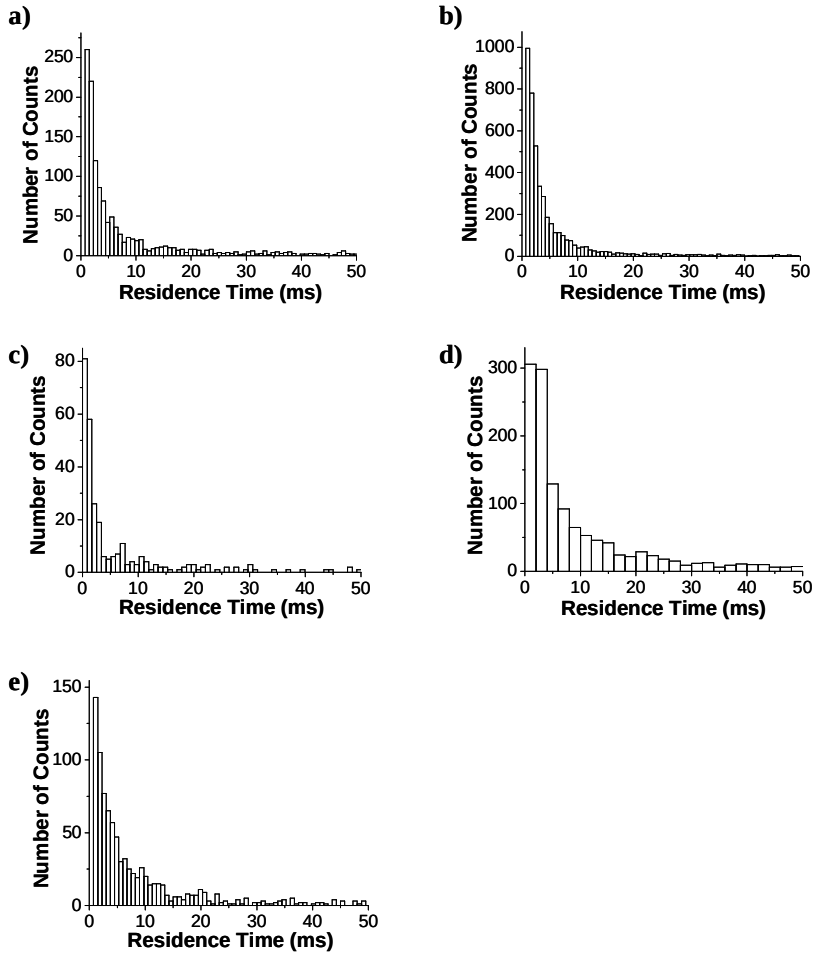

Figure 2.6: Event dwell time histograms of (a) $(dA)_{20}$; (b) $(dT)_{20}$; c) $(dC)_{20}$; (d) $(dC)_{10}(dT)_{10}$; and (e) $(dCdT)_{10}$. Experiments were performed at +120 mV with the wild-type αHL pore in 1 M BMIM-Cl solution. The currents were low-pass filtered with a four-pole Bessel filter at 10 kHz and sampled at 20 kHz. Events with residence times longer than 50 ms were also observed but not displayed in the histograms.

It should be noted that such long duration translocation events of polydeoxyadenine have not been previously reported,[14] although $(dT)_{50}$ produced events with duration at ~3.7 ms in the WT αHL pore in 1 M KCl solution.[62] In this work, we focus on the pertinent long residence time events and investigate whether they can be employed to differentiate between various nucleotides. The large duration events have a significant advantage over the short-lived events since high measurement bandwidths are not necessary and hence significantly reduced measurement noise could be achieved. For this purpose, five ssDNA samples, including $(dA)_{20}$, $(dC)_{20}$, $(dT)_{20}$, $(dCdT)_{10}$, and $(dC)_{10}(dT)_{10}$, were examined with the same mutant $(M113F)_7$ pore in the BMIM-Cl solution at a filter frequency of 10 kHz and sampled at 20 kHz. As was found for $(dA)_{20}$, all of the four additional DNA molecules produced large residence time events (Figure. 2.5). The mean residence times and amplitudes of these long-lived events for the five different DNA samples are summarized in Table 1. The translocation rates for various DNA polymers (201 μs/base for $(dA)_{20}$, 98 μs/base for $(dC)_{20}$, 150 μs/base for $(dT)_{20}$, 256 μs/base for $(dCdT)_{10}$, and 320 μs/base for $(dC)_{10}(dT)_{10}$) obtained were ~2 orders of magnitude larger than the well-documented rates of ~1 to 3 μs/base with the translocation of 100-mer DNA polymers through the WT αHL channel in the KCl solution at room temperature.[14, 53] This clearly shows that the use of BMIM-Cl solution instead of NaCl/KCl solutions significantly slows DNA translocation and provides a much enhanced resolution/sensitivity. This increased nanopore resolution coupled with the different event blockage amplitudes produced by different nucleotides (Table 2.1) permits the convenient differentiation between the five DNA molecules examined.

To further document the utilization of ionic liquid solutions as an effective means to slow the translocation of DNA polymers in nanopores, the WT αHL pore was used instead of the mutant $(M113F)_7$ protein to examine the same series of DNA samples in 1M BMIM-Cl solution. Similar to the observation made for the DNA translocation through the $(M113F)_7$ pore in the BMIM-Cl solution, all the five tested DNA samples produced long duration events (Figure 2.6). The mean residence times and amplitudes of these long-lived events for the five different DNA samples are summarized in Table 2. Although the residence time values were smaller than those obtained in the $(M113F)_7$ protein pore, the translocation rates of various polynucleotides at 82.5 μs/base – 240 μs/base were still ~10^2 fold larger than those in KCl or NaCl solutions. The difference in the residence times for the DNA translocation through two different protein pores may be attributed to the change in the van der Waals volumes of amino acids at position 113 of the αHL channels (V_M (124 Å^3) < V_F (135 Å^3)).[65] All together, these results suggest that the BMIM-Cl solution is essential to obtaining the long duration DNA events in the αHL pore, while mutant protein pore plays a smaller role.

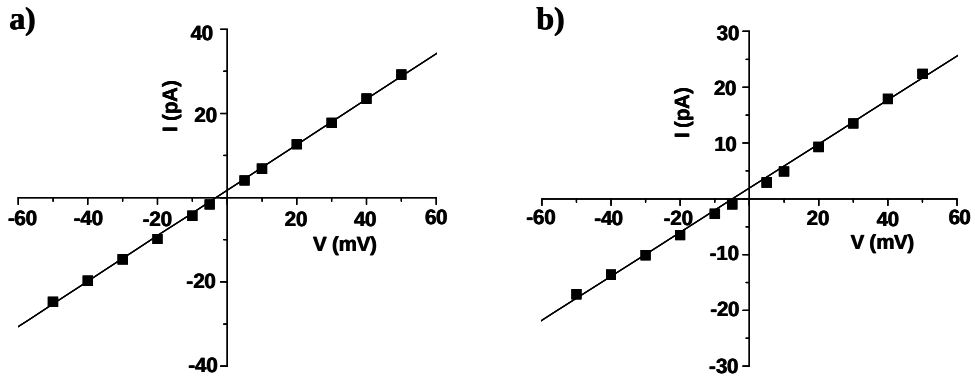

Figure 2.7: Determination of the streaming potentials of αHL channels in NaCl solution. I-V curves for the (a) wild-type and (b) mutant $(M113F)_7$ αHL protein pores based on recordings made with *cis*: 1 M NaCl, 10 mM Tris·HCl (pH 6.0); *trans:* the same buffer solution as *cis* plus 1 M urea. Streaming potentials obtained were -3.0 mV, and -4.2 mV for the wild-type and mutant $(M113F)_7$ αHL pores, respectively.

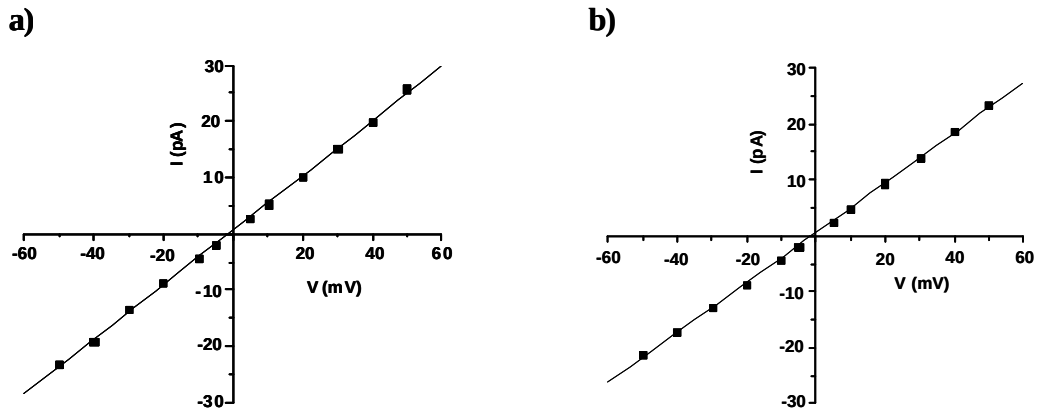

Figure 2.8: Determination of the streaming potentials of αHL channels in BMIM-Cl solution. I-V curves for the (a) wild-type and (b) mutant $(M113F)_7$ αHL pores based on recordings made with *cis*: 1 M BMIM-Cl, 10 mM Tris·HCl (pH 6.0); *trans:* the same buffer solution as *cis* plus 1 M urea. The streaming potentials obtained for both the wild-type and mutant $(M113F)_7$ αHL pores were -1.4 mV.

The significant increase in the residence time of DNA translocation in the ionic liquid BMIM-Cl solution over the NaCl/KCl solution might be attributed to several possible reasons, e.g., the changes in the viscosity of the medium and in the charge selectivity of the pore. Under a specific applied voltage bias, e.g., +120 mV in this work, the DNA translocation process is mainly determined by the interaction of the polynucleotides and the αHL pore, and the migration rate of the nucleotide molecules. The latter is primarily dependent on the diffusion of the polymer and the charge selectivity of the pore. Our previous research showed that the viscosity of the

BMIM-Cl solution was only 71% greater than that of the NaCl solution.[10] Hence, such a small change in the viscosity of the medium could not explain the observed large DNA residence times[66] (note that the diffusion coefficient of an ion is inversely related to the viscosity of the medium). On the other hand, the actual charge selectivity of the pore could not be obtained due to the lack of data for the activity coefficient of BMIM-Cl solution. However, our experiments showed that, when BMIM-Cl solution was used instead of NaCl, the values for the streaming potentials in both the WT and mutant $(M113F)_7$ αHL pores reduced significantly (Figure 2.4). For example, in 1 M NaCl solution, the streaming potentials in the wild-type and mutant $(M113F)_7$ αHL pores were -3.0 ± 0.1 mV and -4.2 ± 0.35 mV, respectively (Figure 2.7). In contrast, in 1 M BMIM-Cl, those values were -1.41 ± 0.22 mV, and -1.43 ± 0.24 mV, respectively (Figure 2.8). It should be noted that a smaller streaming potential of the pore indicates a more even transport of solvent by cations and anions, leading to a drop in the preferential charge selectivity to either cation or anion.[22] Thus, our results suggest that the weakly anion selective WT or mutant $(M113F)_7$ αHL pore in the NaCl/KCl solution is becoming more neutral in the BMIM-Cl solution. However, previous work suggests that although the frequency of DNA translocation events could be significantly affected by the charge selectivity of a protein pore, the translocation time is not greatly altered.[67] In addition, the constant impact of the charge selectivity of the protein pore on molecular transport (e.g., the event residence time)[22,68]could not explain our observation that the long-lived events only accounted for a small portion of the total events.

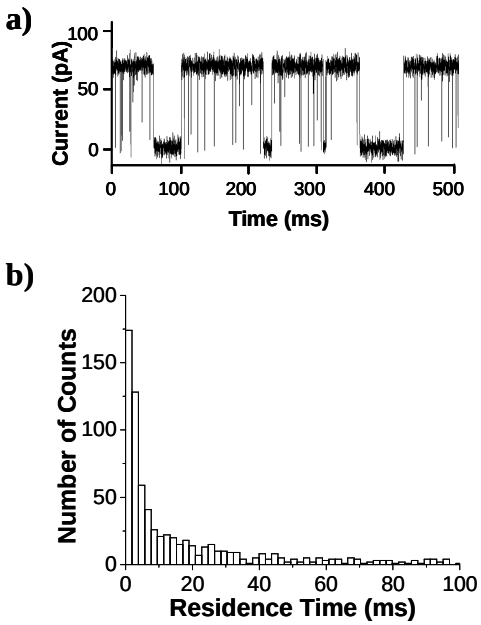

Figure 2.9: Translocation of $(dA)_{20}$ in the mutant $(M113F)_7$ αHL pore in 1 M tetramethylammonium chloride solution. (a) Representative single channel current recording trace, and (b) dwell time histogram of long duration events. Experiments were performed at +120 mV. The currents were low-pass filtered with a four-pole Bessel filter at 10 kHz and sampled at 20 kHz. Events with residence times longer than 100 ms were also observed but not displayed in the histogram.

Contrary to the observation that poly(dA) translocates through the αHL pore more slowly than poly(dCdT) in the KCl solution,[53] the residence time of $(dCdT)_{10}$ events were larger than that of $(dA)_{20}$ with the BMIM-Cl solution. This suggests that the interaction between nucleotides and the protein pore could be significantly influenced by the presence of the imidazolium cation. It is known that the diameter of the constriction region of the αHL pore is only slightly larger than the diameter of a ssDNA polymer.[69] Thus, in order for a ssDNA molecule to translocate through the

αHL pore, the counter-ions need to be squeezed in the narrow water-filled space surrounding the DNA.[70] Compared with the naked K^+ (radius: 1.33 Å) or Na^+ (radius: 0.97 Å),[71] the bulky $BMIM^+$ (length: 11.0 Å; width: 5.8 Å)[72] is much larger. Furthermore, recent studies have suggested that the interaction between $BMIM^+$ and DNA is very strong, so much so that DNA could be extracted by ionic liquid BMIM-PF_6 solution.[73] The strong interaction between $BMIM^+$ and DNA might be attributed to the interaction of the bulky organic $BMIM^+$ and P-O bonds of phosphate groups in the DNA molecule,[73] and/or the electrostatic interaction between $BMIM^+$ and DNA.[74] Therefore, it is not unreasonable that it would be much more difficult to squeeze DNA molecules through the narrow αHL pore in BMIM-Cl than in KCl or NaCl solution. Considering that the long-lived $(dA)_{20}$ events only accounted for 2.5% of the total events and the significant difference in the residence times of two types of events, it is likely that the large duration events were attributed to the threading of the DNA-$BMIM^+$ complex through the pore. In contrast, the short-lived events were due to the translocation of uncomplexed DNA molecules or the rapid entrance/exit of the DNA-$BMIM^+$ complex at the *cis* opening of the channel (e.g., the DNA-$BMIM^+$ complex enters the vestibule, moves toward the β-barrel but does not traverse through the limiting aperture, but instead retracts backward to the *cis* side and exits). We are leaning toward the latter interpretation of the short-lived events. Further experiments are required to resolve the origin of these events.

2.4 Conclusions

In summary, we have demonstrated that by using electrolyte solutions which contain organic salts instead of NaCl/KCl, a ~ 2 order of magnitude reduction in the velocity of DNA translocation through protein pores can be achieved. Compared with other physical conditions, such as temperature, ionic strength, viscosity, etc.[75] the effect of organic salts on DNA translocation was far more significant. It is likely that the strategy used in this work could be employed together with other experimental conditions by synthetic nanopores[76,77,78] to substantially decrease the rapid DNA translocation velocity. Further experimental, theoretical, and computational research is necessary to understand and clarify how the organic salt solutions slow down the DNA translocation in the nanopores.

CHAPTER 3

TRANSLOCATION OF SINGLE STRANDED DNA THROUGH THE α-HEMOLYSIN PROTEIN NANOPORES IN ACIDIC SOLUTIONS

3.1 Introduction

Nanopore stochastic sensing is currently an active research area, characterized by highly-sensitive, rapid, and multi-functional detection capabilities.[1] In nanopore sensing, the passage of analytes of interest through a nano-channel (or pore) at an fixed applied potential cause current modulations. The mean residence time and amplitude of the recorded events allows to determine the identity of the analyte, while the frequency of occurrence of the current modulations could be used to find its concentration.[61] In addition to the development of ultrasensitive sensors for a wide range of substances,[7, 8, 10-12, 17, 79-83] these nanometer-sized channels offer exciting new possibilities for studying covalent and non-covalent bonding interactions,[9, 22, 84] investigating biomolecular folding and unfolding,[85, 86] probing enzyme kinetics,[87] as well as analyzing and even sequencing DNA molecules.[5, 14, 15, 25,62, 88-91] The hypothesis for DNA sequencing in a nanopore is that when a single-stranded DNA (ssDNA) sample is electrophoretically driven through the pore, it is possible to read its base sequence if each nucleotide of the polymer produces a characteristic current modulation. Since kilobase length DNA can be read directly without amplification or use of costly reagents such as enzymes and fluorescent tags, the nanopore approach can significantly reduce the sequencing cost, and has emerged as one of

the most promising technologies to achieve the "$1000 genome" goal set by the U.S. National Institutes of Health.[52] However, due to the rapid DNA translocation velocity through the nanopore, accurate detection of single nucleotide bases via the electrophoretically driven nanopore approach has not yet been achieved with the currently available single-channel recording technique.[33]

To increase the nanopore resolution for nucleotide differentiation, three major approaches have been used in the past decade to slow DNA translocation. These include modification of the structures of both nanopores and DNA molecules, and manipulation of experimental physical conditions. Note that the molecular transport and binding kinetics inside a channel are strongly dependent on the nature of the pore, the species passing through the channel, as well as the experimental conditions. It has been reported that enhanced translocation of ssDNA molecules through α-hemolysin protein channels could be achieved by manipulation of the internal charge within the pore.[67] By attaching chemical tags to DNA bases[92] or immobilization of DNA polynucleotides with streptavidin,[55] prolonged DNA residence time in the pore could be obtained. Furthermore, experimental physical conditions such as temperature, voltage bias, viscosity, electrolyte, and application of an alternating electric field were also found useful to control the DNA translocation rate.[10, 43, 50, 53, 66] Other approaches include use of a host compound,[36] and a polymerase.[93]

It should be noted that nanopore experiments are usually carried out at or near physiological pH. Although the detection of single-stranded and double-stranded DNA in the nanopore at alkaline pH has been attempted,[94] thus far, to the best of our

knowledge, there have been no systematic studies of the effect of pH on DNA translocation through the nanopore, especially at acidic solutions. Here, we report that acidic electrolyte solutions could be used as an effective means to significantly reduce the velocity of DNA translocation through the α-hemolysin pore.

3.2 Experimental methods

3.2.1 Materials and reagents

The wild type α-hemolysin protein was synthesized by coupled *in vitro* transcription and translation as described previously. ssDNA samples were purchased from Integrated DNA Technologies, Inc. (Coralville, IA) and Sigma Aldrich. Lipid 1,2-diphytanoylphosphatidylcholine was obtained from Avanti Polar Lipids (Alabaster, AL). Teflon films were purchased from Goodfellow (Malvern, PA). All of the other reagents were purchased from Sigma Aldrich. All the ssDNA polymers were dissolved in HPLC-grade water (ChromAR, Mallinckrodt Baker). The concentrations of the stock solutions were 4 mM for each of the DNA samples. All the electrolyte solutions used in this work were prepared in HPLC-grade water, which contained 1 M NaCl and 10 mM NaH_2PO_4, with the pH of the solutions adjusted to 3.0 - 7.5.

3.2.2 Planar bilayer experiments

The single-channel recording procedure has been described elsewhere.[10] Briefly, a planar bilayer chamber was divided into two compartments, *cis* and *trans*, by a Teflon septum. A lipid bilayer of 1,2-diphytanoyl-sn-Glycero-3-phosphacholine was formed on a ~120 μm-diameter aperture in the teflon film by using the Montal-Mueller method. The experiments were performed under a series of symmetrical conditions with a 2.0 mL solution comprising 1 M NaCl and 10 mM NaH_2PO_4, with the pH of the solutions adjusted to 3.0 - 7.5 at 22 ± 1 °C unless otherwise stated. Both the αHL protein (with the final concentration of 0.2–2.0 $ng \cdot mL^{-1}$) and the ssDNA sample were added to the *cis* chamber compartment, which was connected to "ground". The applied potential was +120 mV. Currents were recorded with a patch clamp amplifier (Axopatch 200B, Axon instruments, Foster city, CA, USA). They were low-pass filtered with an external four-pole Bessel filter at 30 kHz and sampled at 125 kHz by a computer equipped with a Digidata 1440 A/D converter (Molecular Devices). The final concentrations of ssDNA samples were 10 μM each. At least three separate experiments were carried out for each DNA sample.

3.2.3 Data analysis

Data were analyzed with pClamp 10.1 (Molecular devices), QuB **(**www.*qub***.**buffalo.edu), and Origin 6.0 (Microcal, Northampton, MA) software. Current modulation events that caused at least 70% blockade of the open channel were taken into consideration to calculate the corresponding mean residence values and amplitude values. It has been well established that the events with less than 70% blockades are attributed to residence only in the channel vestibule or the

collisions of the ssDNA molecules by the pore mouth.[62] Mean conductance and residence time values were obtained from the amplitude histograms and the dwell time histograms, respectively by fitting the distributions to Gaussian and/or single exponential functions. It has been reported that the mean residence time values obtained using either Gaussian fitting or single exponential fitting were not significantly different.[10] Between 3,000 and 25,000 events were recorded in each of the single channel recording experiments. All the results were reported as mean values ± standard deviation. Note that when DNA interacted with the αHL pore in solutions with pH values ranging from 3.0 to 5.0, two significantly different types of events with different blockage amplitudes and residence times (i.e., deep blockades and shallow blockades) were observed (Figure 3.5). To minimize the potential interference from the shallow blockades, only the events with duration larger than 0.5 ms and having more than 97% channel block were included to analyze the mean residence times of the deep blockades. Such events accounted for more than 95% of the current modulations that led to at least 97% blockade of the open channel. To calculate the percentage of the deep blockage events in the total events in such experiments, the frequency of the deep blockage events (f_{deep}) and the overall frequency of all the DNA events (f) are calculated. Then, the percentage was obtained by dividing f_{deep} by f.

3.3 Results and discussion

The initial experiment was carried out at +120 mV with $(dA)_{20}$ in the wild type α-hemolysin pore in 1 M NaCl solutions having various pH ranging from 3.0 to 6.0. The

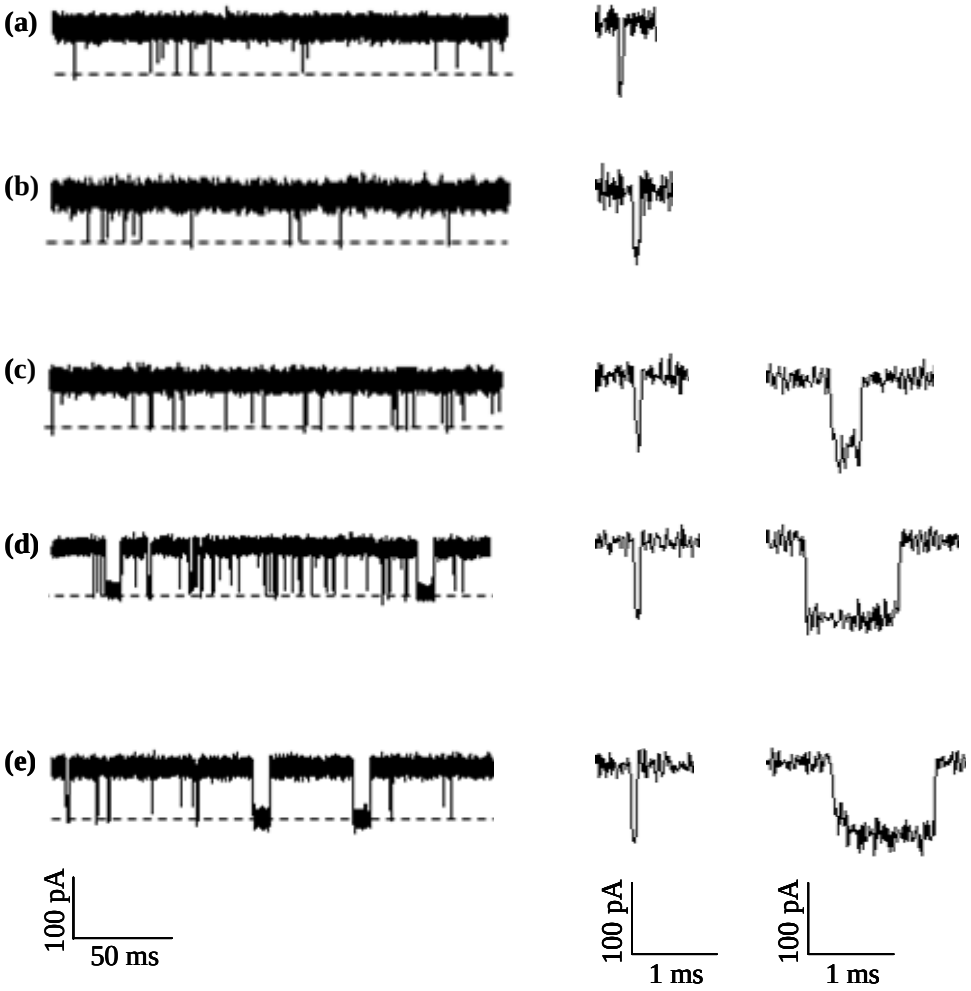

Figure 3.1:Translocation of $(dA)_{20}$ in the wild-type αHL pore in 1M NaCl solutions having various pH values: (a) pH 7.5; (b) pH 6.0; (c) pH 5.0; (d) pH 4.0; and (e) pH 3.0. (*Left*) Representative single channel current recording traces; (*Middle*) Typical shallow blockades shown at expanded time scales; and (*Right*) Typical deep blockades shown at expanded time scales. The experiments were performed at +120 mV

control experiment was performed in a solution containing 1 M NaCl with a pH of 7.5. As shown in Figures 4.1 and 4.2, at pH 6.0 and pH 7.5, only one major type of short-lived translocation events was observed with mean residence times of 83 ± 11, and

70 ± 10 μs, respectively. In sharp contrast, in all of the other three examined acidic electrolyte solutions, two significantly different types of events with different blockage amplitudes (i.e., deep blockades and shallow blockades) were observed. The deep blockades show a narrow range of amplitudes (~98% channel block) and a large mean duration value but with a broad distribution of residence times, while shallow blockades present a small mean residence time and a wide range of current blockage amplitudes (from ~70% to almost full channel block). Table 4.1 illustrates the results of the statistical translocation properties of $(dA)_{20}$ in five different pH solutions, including the mean residence times and residual currents of the deep blockades and shallow blockades, as well as the percentage of deep blockades in the total events. It is apparent from this table that with a decrease in the pH value of the electrolyte solution, the percentage of deep blockades increases. At pH 3.0, 19.5 ± 1.0 % of the total events belonged to the deep blockades with a mean residence time of 1210 ± 156 μs. Furthermore, as pH decreases, the mean residence time of the shallow blockades is almost unchanged, while that of the deep blockades increases significantly until pH 4.0, after which the event mean duration does not vary much. As an importance aside, we noticed that, when the pH of the solution decreased from 7.5 to 3.0, the overall frequency of $(dA)_{20}$ events first increased and then decreased. It should be noted that although current modulations with residence times at milliseconds or larger were occasionally (~1-2 events / min) observed in the absence of DNA samples (Figure. 3.6), the frequent (> 300 events / min) long-lived deep blockades obtained after addition of DNA to the electrolyte solution with a pH of 3.0 or 4.0 ruled out the possibility that such events were due to the channel gating.

As mentioned in the introduction, to utilize the nanopore technique for analyzing/sequencing DNA, it is imperative to slow down DNA translocation since in this case, high measurement bandwidths are not necessary for the detection of current modulations induced by the DNA translocation through the nanopore. The major advantages of lower bandwidth measurements include smaller data storages and significantly reduced measurement noise, which allow more convenient data analysis and an enhanced resolution to the discrimination of various polynucleotides. The mean residence time of the deep blockage events of $(dA)_{20}$ at pH 3.0 or pH 4.0 was ~ 17 - 18 folds larger than that of $(dA)_{20}$ events at pH 7.5. Therefore, in an electrolyte solution having a lower pH, the nanopore resolution to DNA analysis should be improved if these deep blockage events are attributed to translocation. Moreover, as the pH of the electrolyte solution decreased from 7.5 to 3.0, the open channel current increased by 14.7% (from 97.7 ± 1.4 pA to 112.1 ± 2.4 pA). The pH dependence of the open channel current has been observed by Kasianowicz and Bezrukov, which was proposed to be attributed to the reversible binding of protons to ionizable residues inside the channel.[6] The increase in the open channel current offers the potential to increase the S/N ratio, thus providing a further improvement in the capability of the nanopore to differentiate polynucleotides.

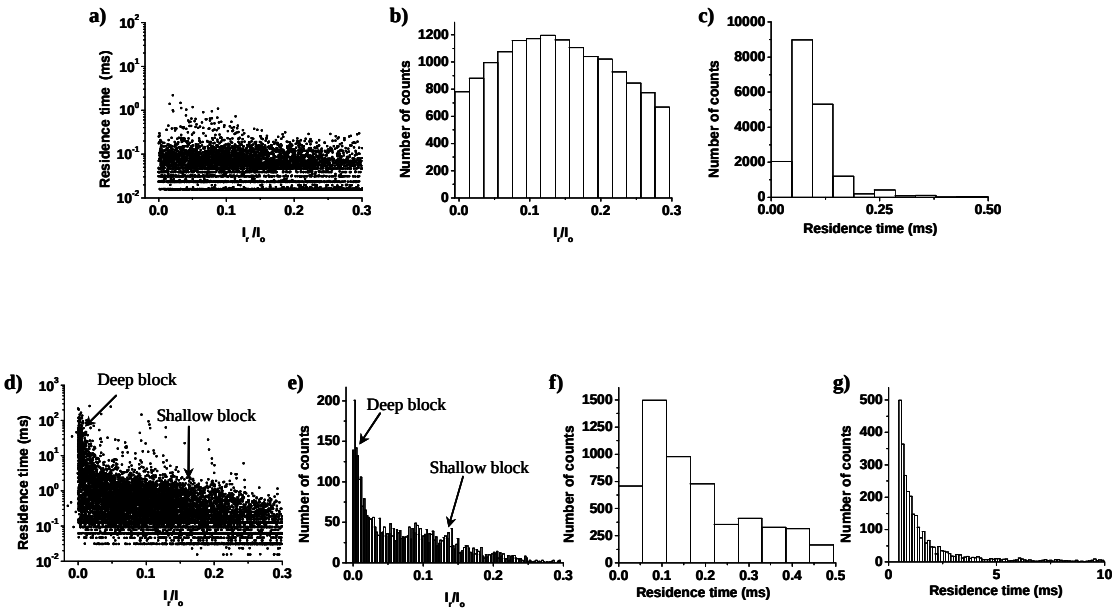

Figure 3.2: Blockage characteristics of $(dA)_{20}$ in the wild-type αHL pore at pH 7.5 and pH 3.0. (a) Scatter plot of event amplitude vs. residence time; (b) event amplitude histogram; and (c) event residence time histogram for the translocation of $(dA)_{20}$ in the αHL pore at pH 7.5. (d) Scatter plot of event amplitude vs. residence time; (e) event amplitude histograms, showing two types of blockades (deep and shallow); and (f) and (g) event residence time histograms of the shallow blockades and deep blockades, respectively, for the interaction of $(dA)_{20}$ with the αHL pore at pH 3.0. I_r/I_o in Figures. 2a, 2b, 2d, and 2e is normalized blockage residual current, which was obtained by dividing the average blockage residual current of an event by the average open channel current. The experiments were performed at +120 mV.

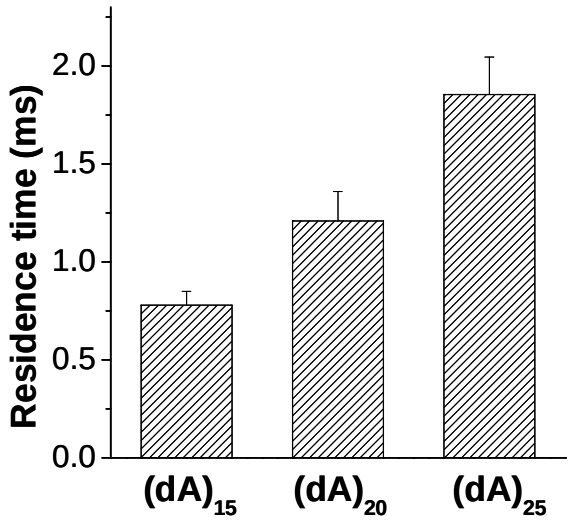

Figure 3.3: Effect of DNA length on the mean residence time of deep blockades, suggesting that these events are caused by DNA's threading through the αHL pore. Experiments were performed at +120 mV with the wild-type αHL pore in a 1 M NaCl solution at pH 3.0.

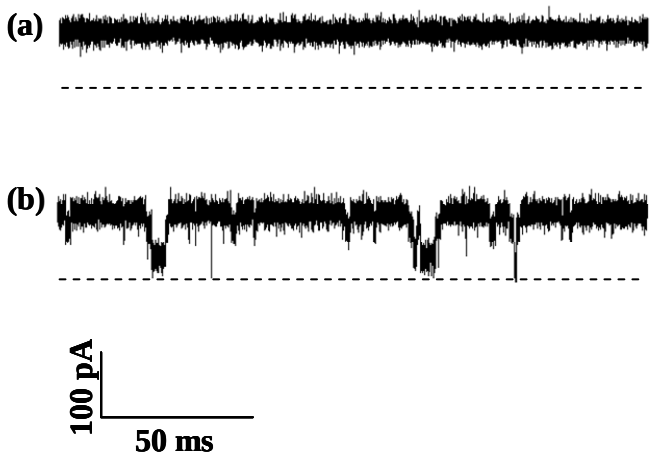

Figure 3.4: Single channel recordings of a 3-mer ssDNA at (a) pH 7.5; and (b) pH 3.0, showing the viability of utilizing acidic electrolyte solutions for the detection of short DNA samples. Experiments were performed at +120 mV with a DNA sample (sequence: TTT) in the wild-type αHL pore in 1 M NaCl.

To investigate whether these deep blockades are caused by the translocation of $(dA)_{20}$ through the αHL pore or rather they are attributed to the sticking of these DNA polymers to the channel or binding of one or more bases of the polymer to the protein pore for long periods of time with intermittent short periods of rapid translocation, two additional polydeoxyadenine samples with different lengths were examined with the wild-type αHL pore in a solution containing 1 M NaCl at pH 3.0. As shown in Figure

3.3, with an increase in the DNA length, the mean residence time of the deep blockades increased, thus clearly suggesting that these deep blockades were not due to the tangling of the $(dA)_{20}$ molecule to the channel, but rather caused by the slower threading of the DNA molecule through the pore. Note that it has been well established that the current blockage events having the residence time not dependent on the polymer length are due to the polynucleotides' collision with or binding to the pore, while those with the dwell time sensitive to the sample length depict actual DNA translocations.[50, 53] Moreover, the mean residence time of the deep blockades decreased with an increase in the applied potential (data not shown), thus providing further evidence that these events were attributed to translocation.

To investigate whether an acidic electrolyte solution could be used as an effective approach to increase the nanopore resolution for DNA analysis instead of the commonly used buffer solution at/near physiological pH, three additional 20-mer ssDNA samples, including $(dT)_{20}$, $(dCdT)_{10}$, and $(dAdG)_{10}$, were examined with the wild-type αHL pore in 1 M NaCl at pH 3.0. As was found for $(dA)_{20}$, all of the three additional DNA molecules produced both deep blockades and shallow blockades. The mean residence times and amplitudes of the deep blockades and shallow blockades as well as the percentage of deep blockage events for these three 20-mer DNA samples are summarized in Table 2. From the table, we can see that, in terms of the deep blockades, the translocation rates of ~65 to 287 μs/base for various polynucleotides were typically at least ~ 20 folds larger than the well-documented rates of ~1 to 3 μs/base with the translocation of 100-mer DNA polymers through the WT αHL channel in the 1 M KCl solution with/near physiological pH at room temperature.[14] Therefore, at a lower pH, various DNA polymers indeed translocate

through the wild-type αHL pore at a slower velocity. The different event means residence time and amplitudes as well as different percentages of deep blockades produced by different nucleotides (Tables 4.1 and 4.2) may permit the convenient discrimination among the four DNA molecules examined.

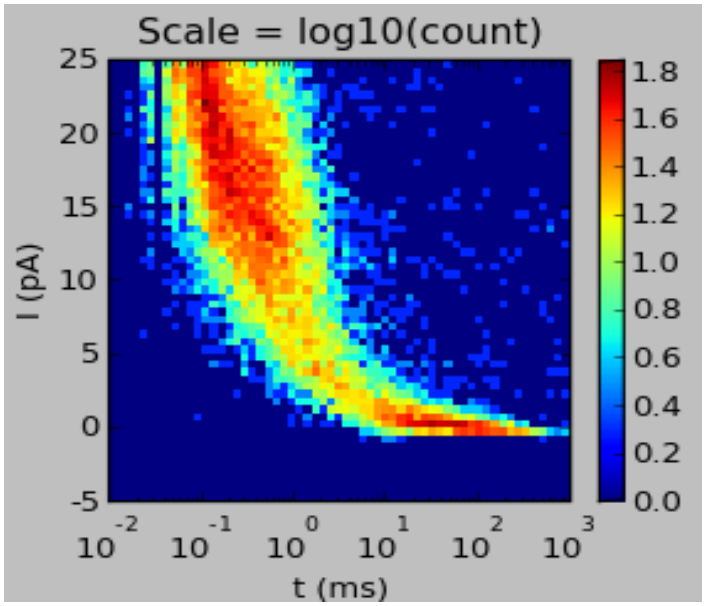

Figure 3.5: Event density plot, showing two types of blockades (deep and shallow). Experiments were performed at +120 mV with the wild-type αHL pore in a 1 M NaCl solution at pH 3.0 in the presence of 10 μM $(dA)_{20}$.

Due to the enhanced resolution, the feasibility of utilizing nanopores to analyze very short polynucleotides in acidic solutions was then investigated. A 3-mer ssDNA sample with a sequence of TTT was examined in the wild-type αHL pore in a 1 M NaCl solution with a pH of 3.0. The control experiment was carried out in 1 M NaCl at pH 7.5. Note that such a short DNA sample has not yet been able to be detected by using the electrophoretically-driven nanopore approach before. As shown in Figure 3.4, the 3-mer DNA sample indeed produced current modulations at pH 3.0, while no DNA events could be identified at pH 7.5. The ability to detect short DNA molecules offers the potential to use nanopore technique as a rapid effective approach to detect, characterize, and even sequence DNA samples. The study of other short (e.g., 2-mer, 4-mer, etc.) DNA molecules in the αHL pore at pH 3.0 is currently in progress.

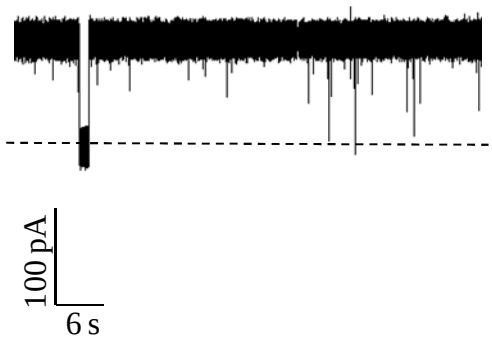

Figure 3.6: Representative single channel current recording of the wild-type αHL pore in a 1 M NaCl solution at pH 3.0 in the absence of ssDNA samples. The experiments were performed at +120 mV. The trace was low-pass filtered at 10 kHz.

It is worthwhile to probe the underlying reasons why DNA samples produce two significantly different types of events (i.e., deep blockades and shallow blockades) in acidic solutions, and why DNA polymers translocate through the αHL pore at a slower velocity but with a larger frequency at acidic pH than at physiological pH. One possible cause is that the pH of the electrolyte solution affects the net charge of nucleic acids. It is well-known that at physiological pH, DNA has a net negative charge since the phosphate components of the DNA backbone are deprotonated, whereas the purine or pyrimidine bases are in a neutral form. It has been estimated that the effective charge per nucleotide is substantially less than 1 electron charge in nanopore experiments.[95,96] With a decrease in the pH of the solution, the phosphate groups can accept the protons in the electrolyte and hence the phosphate ionization equilibrium will shift, leading to a reduction in the effective negative charge of the DNA molecule. At pH values below 4.0, even the purine and pyrimidine bases will be protonated, which further reduces the net negative charge of the DNA. And thus a slower DNA migration in the nanopore could be expected at a fixed applied potential, e.g., +120 mV in this work. Furthermore, the change in the pH value of the solution affects the charge selectivity of the protein pore. Bayley and co-workers' research showed that when the pH of the electrolyte solution decreased from 11.0 to 7.5 and then to 5.0, the charge selectivity of the wild-type αHL pore changed from cation-selective to weakly anion selective, and then to anion selective.[68] Therefore, a decrease in the pH can enhance DNA translocation due to the enhanced electroosmotic flow, which was supported by our experimental result that a ~8 fold increase in the event frequency was observed when the pH of the solution decreased from 7.5 to 4.0. This is similar to the observation made for the translocation of a 92-nt single-stranded DNA through the $(M113R)_7$ pore vs. the wild-type pore, in which a

~10 fold increase in the event frequency was found.[67] Note that, in this case, the $(M113R)_7$ pore was anion selective, while the wild-type αHL pore was weakly anion selective.

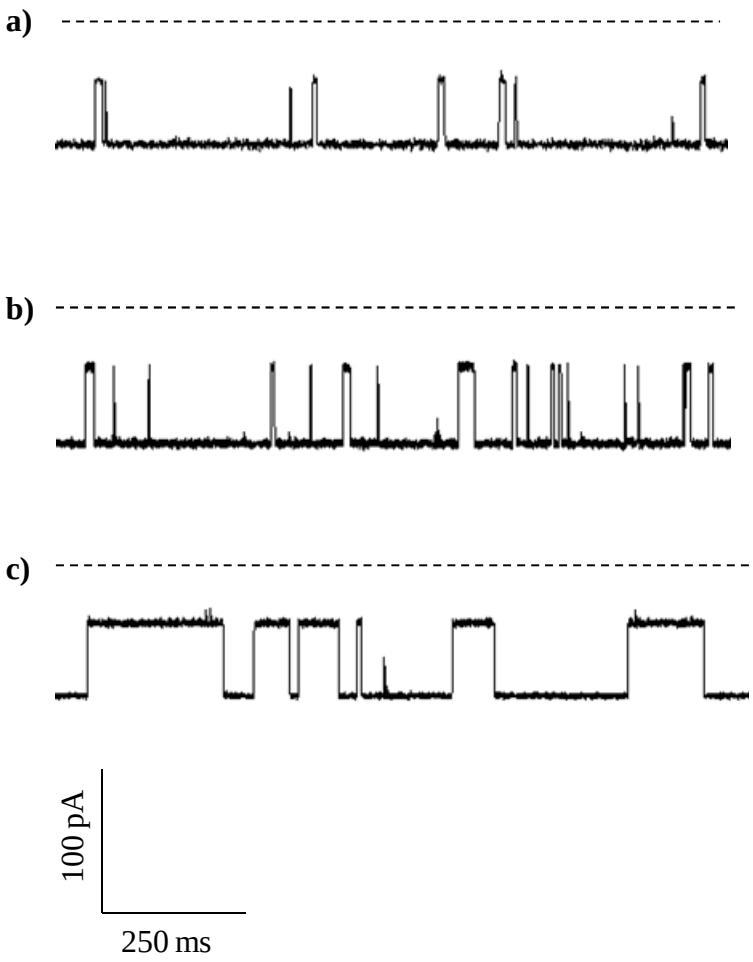

Figure 3.7: Representative single channel recordings of the mutant αHL $(M113K)_3(M113Y\text{-}D8)_4$ pore in the presence of 40 μM β-cyclodextrin at (a) pH 6.5; (b) pH 5.0; and (c) pH 3.0, showing a stronger interaction between β-cyclodextrin and the protein pore obtained at a lower pH. Experiments were performed at -120 mV in 1 M NaCl and 10 mM NaH_2PO_4.

However, the constant impact of both the net charge of the DNA molecule and the charge selectivity of the protein pore on molecular transport (e.g., the event residence time)[22, 68] could not explain our observation that two quite different types of events were produced when DNA translocated through the αHL pore in acidic solutions. In our earlier study, we found that the translocation of DNA through the αHL pore in a solution containing organic salts (e.g., BMIM-Cl) also produced two different types of events, in which the deep blockades were proposed to be attributed to the threading of the DNA-$BMIM^+$ complex through the pore, whereas the shallow blockades were due to the translocation of uncomplexed DNA molecules or the rapid entrance/exit of the DNA-$BMIM^+$ complex at the *cis* opening of the channel.[10] Similarly, we are leaning toward the interpretation that the occurrence of two types of events in acid solutions is due to the pH effect on DNA secondary structure. It has been well established that a solution with a lower pH can promote the formation of DNA secondary structure. In order to translocate such a DNA molecule through the pore, the helical structure of the DNA must be disrupted, and thus a longer residence time could be expected. In contrast, the shallow blockades may be attributed to the translocation of coiled DNA molecules or the rapid entrance/exit of the helical DNA at the *cis* opening of the channel. In this case, after the helical DNA molecule enters the vestibule and moves toward the β-barrel, it fails to translocate through the limiting aperture but instead escapes backwards and exits from the *cis* entrance of the pore. Further experiments and/or computational modeling are required to resolve the origin of these events.

Table 3.1: Effect of pH on the translocation of $(dA)_{20}$ through the wild-type αHL pore. Each experimental value represents the mean of three replicate analyses ± one standard deviation. Experiments were performed at +120 mV in 1M NaCl solutions with various pH values.

pH	Mean residence time (μs)		Mean current blockage (%)		Percentage of deep block	Event frequency (s^{-1})	Open channel current (pA)
	Shallow block	Deep block	Shallow block	Deep block			
7.5	70 ± 10	n.o.[a]	87.7 ± 1.5	n.o.[a]	n.o.[a]	17.0 ± 3.9	97.7 ± 1.4
6.0	83 ± 11	n.o.[a]	77.5 ± 1.9	n.o.[a]	n.o.[a]	27.9 ± 5.7	94.2 ± 2.4
5.0	86 ± 11	350 ± 52	84.3 ± 2.0	97.2 ± 0.5	1.2 ± 0.3	66.1 ± 10.1	92.1 ± 3.9
4.0	116 ± 28	1250 ± 111	85.6 ± 1.5	98.4 ± 0.3	18.5 ± 4.4	133.2 ± 35.2	108.3 ± 1.4
3.0	80 ± 10	1210 ± 156	83.0 ± 3.2	98.8 ± 0.2	19.5 ± 1.0	26.8 ± 9.3	112.1 ± 2.4

Table 3.2: Summary of statistical translocation properties of three ssDNA samples in the wild-type αHL pore at pH 3.0. Each experimental value represents the mean of three replicate analyses ± one standard deviation. Experiments were performed at +120mV.

ssDNA sample	Mean residence time (μs)		Mean current blockage (%)		Percentage of deep block
	Shallow block	Deep block	Shallow block	Deep block	
$(dT)_{20}$	190 ± 23	1295 ± 215	92.1 ± 0.3	98.1 ± 0.5	41.9 ± 3.9
$(dAdG)_{10}$	195 ± 20	5740 ± 254	80.7 ± 2.0	94.6 ± 0.1	49.8 ± 1.9
$(dCdT)_{10}$	166 ± 15	2746 ± 266	87.8 ± 1.2	98.6 ± 0.4	48.2 ± 16.1

3.4 Conclusions

The work presented here demonstrates that the translocation of single-stranded DNA through the α-hemolysin pore is strongly affected by the pH of the electrolyte solution. Besides the rapid translocation events (~ 4 to 10 μs per base), another type of events with significantly reduced translocation rates (~ 60 to 287 μs per base) are observed at low pH. Furthermore, the open channel current increases with a decrease in the pH of the electrolyte solution, offering the potential to increase the S/N ratio and hence providing a further improvement in the capability of the nanopore to differentiate polynucleotides. In addition to be used as an effective approach to slow DNA translocation in the nanopore, manipulation of the pH of the electrolyte solution may provide a potential means to greatly enhance the sensitivity of the nanopore for the detection of various compounds (Figure 3.7), which may find useful application in stochastic sensing.

CHAPTER 4

DETECTION OF NERVE AGENT HYDROLYTES IN AN ENGINEERED NANOPORE

4.1 Introduction

Organophosphorus chemical agents (i.e. nerve gases) are the most toxic group in chemical warfare agents.[97] They can irreversibly bind to acetylcholine esterase, an enzyme which affects the accumulation of the neurotransmitter acetylcholine, thus disrupting the nervous system.[97] As these chemical agents are degraded into less toxic hydrolytes, the detection of nerve agent degradation products can verify the presence or disposal of the lethal organophosphorus warfare agents.[98] Thus far, numerous techniques have been developed for the detection of these nerve agents, as well as their degradation products and stimulants. These include gas chromatography,[99] liquid chromatography,[100] ion chromatography,[101] capillary electrophoresis,[102] gas chromatography-mass spectrometry,[103,104] liquid chromatography-mass spectrometry,[105] quartz-crystal microbalance,[106] surface acoustic wave[107,108] metal oxide semiconductor,[109,110] functionalized liquid crystal,[111] microcantilever,[112] interferometry,[113] enzymatic assays,[114,115,116]molecularly imprinted polymers,[117] colorimetric method,[118] fluorescent detection,[119,120] electrochemical analysis,[121,116]sensor array,[122,123] and lab-on-chip technique.[124] However, the technology currently available is certainly not compatible with our needs in terms of

sensitivity, selectivity, portability, low cost, ease of use, and rapid response.[117,125] Hence, improved analytical capability for the detection of nerve gases and their degradation products remains a high priority need in our continuing defense against future terrorist attacks.

Here, we report a nanopore stochastic sensing method for the detection of the hydrolysis products of the potent nerve gases. Stochastic sensing can detect analytes at the single-molecule level, in which a single transmembrane protein channel, most often the heptameric α-hemolysin (αHL), is embedded in a planar lipid bilayer.[1] Nanopore detection is achieved by monitoring the ionic current flowing through the single pore at a fixed applied potential. Typically a buffer solution containing a high salt concentration (e.g., 1 M NaCl or KCl) at or near pH 7.4 (i.e., physiological pH) is used to produce the open channel current which is monitored. Individual binding events are detected as transient blockades in the recorded current. This approach reveals both the identity and the concentration of an analyte: the former by its characteristic current signature, typically the dwell time (τ_{off}) of the analyte coupled with the extent of current block (amplitude) it creates, and the latter from the frequency of occurrence ($1/\tau_{on}$) of the binding events. Engineered versions of αHL have been used as stochastic sensing elements for the identification and quantification of a wide variety of substances,[1] including cations,[8] anions,[7] explosives,[79,10] proteins,[12,13] DNA,[54,15] and reactive molecules.[9] The detection of small organic molecules was also achieved by lodging cyclodextrin (CD) adapters within the wild-type αHL protein pore.[17] To stabilize the βCD-αHL interaction, tight-binding mutant pores (e.g., $(M113F)_7$) were developed, where the residence time

(tens of seconds) of βCD were ~10,000 fold larger than that of the wild-type αHL.[68] However, βCD produced additional frequent current modulation spikes in these mutant pores, and this high background would interfere with the detection of target analytes. Hence, the detection limit of the method was not improved. Previous work also demonstrated that significantly reduced βCD background spike events were observed in the mutant pore $(M113F/K147N)_7$, although it bound βCD less strongly than the $(M113F)_7$[11, 126] pore. Recently, it was reported that βCD could be covalently attached to the αHL protein nanopore, thus eliminating the pore/βCD gating entirely to facilitate the analyte detection.[37] In this work, we report a rapid and sensitive stochastic nanopore sensing method for the detection of nerve agent hydrolytes using the $(M113F/K147N)_7$ protein pore and βCD as a molecular adapter. Indeed this is the first time nerve agent degradation products have been detected using the nanopore sensing technique. Although the planar lipid bilayer formed in the traditional single channel recording device (e.g., Teflon cell) is fragile, recent studies have demonstrated the viability of utilizing nanopore technique for high-throuput and deployable sensing application. For example, a bilayer with life time of at least 2 weeks could be obtained using glass nanopore membrane.[127] Furthermore, it has also been reported that a single αHL pore embedded in a planar phospholipid bilayer could be sandwiched between two agarose layers which gel in situ and make a robust and portable single-channel chip, that may be transported, stored, and used repeatedly.[126]

4.2 Experimental section

4.2.1 Reagents

Cyclohexyl methylphosphonic acid (CMPA or GF acid), isopropyl methylphosphonic acid, diisopropyl methylphosphonate, and ethyl hydrogen dimethylamidophosphate were purchased from Cerilliant Corporation (Round Rock, Texas). Pinacolyl methylphosphonate (PMPA or GD acid), 2-(diisopropylamino)-ethanethiol, methyl phosphonic acid, ethyl methylphosphonate, 2-(dimethylamino)ethanethiol hydrochloride, 2-diethylaminoethanethiol hydrochloride, diazinon, parathion, malathion, and amifostine were obtained from Sigma (St. Louis, MO). All these analytes were dissolved either in HPLC-grade water (ChromAR, Mallinckrodt chemicals), or acetonitrile from EMD Chemicals Inc. (Darmstadt, Germany). And the concentrations of all the stock solutions were 10 mM. All other reagents were purchased from Sigma (St. Louis, MO).

Four contaminated water samples were prepared in the laboratory in 10-mL glass vials by spiking the stock solutions of nerve agent hydrolysis products in tap water. After spiking, the samples were fully vortex mixed and stored in a 4 ℃ freezer overnight before the experiments were performed. Specifically, sample 1 contained 100 μM of methyl phosphonic acid, ethyl methylphosphonic acid, and 2-(dimethylamino) ethanethiol. In addition to these three nerve agent degradation products, samples 2 – 4 contained additional PMPA at various concentrations. The concentrations of PMPA for these three samples were 10, 15, and 20 μM, respectively.

4.2.2 Preparation and formation of protein pore

Mutant αHL genes were constructed by side-directed mutagenesis (Mutagenex, Piscataway, NJ) with a WT αHL gene in a T7 vector (pT7–αHL), which has been described elsewhere.[22] Briefly, mutant αHL monomers were first synthesized by coupled *in vitro* transcription and translation (IVTT) using the *E. Coli* T7 S30 Extract System for Circular DNA from Promega (Madison, WI). Subsequently, they were assembled into homoheptamers by adding rabbit red cell membranes and incubating for 2 h. The heptamers were purified by SDS-polyacrylamide gel electrophoresis and stored in aliquots at -80℃.

4.2.3 Planar bilayer recording

Single-channel recordings were carried out as described at 22 ± 1 °C. The *cis* and *trans* compartments of the chamber were separated by a Teflon septum (25 μm thick; Goodfellow, Malvern, PA, USA). An aperture (150 μm) in the septum was pretreated with 10% (v/v) hexadecane (Aldrich; Milwaukee, WI) in *n*-pentane (Burdick & Jackson; Muskegon, MI). A bilayer of 10 mg/mL 1,2-diphytanoylphosphatidylcholine (Avanti Polar Lipids; Alabaster, AL, USA) in *n*-pentane was formed on the aperture. The formation of the bilayer was achieved by using the Montal-Mueller (i.e., monolayer folding) method,[23] and monitored by using a function generator (BK precision 4012A; Yorba Linda, CA, USA). Unless otherwise noted, the experiments were performed under symmetrical buffer conditions with each compartment containing a 2.0 mL solution of 1 M NaCl and 10 mM Tris·HCl (pH 7.5). The αHL protein was added to the *cis* compartment, which was connected to "ground". In such a way, after insertion of a single αHL channel, its mushroom cap

would be located in the *cis* compartment, while the β-barrel of the αHL would insert into the lipid bilayer and connect with the *trans* of the chamber device. The final concentration of the αHL protein was 0.2–2.0 ng·mL^{-1}. With an exception to the assay of contaminated water samples, all of the other experiments were performed with addition of β-cyclodextrin (βCD) and PMPA (or CMPA) to the *trans* compartment immediately after the insertion of a single αHL channel. In the experiments with the contaminated water samples, 1.0 mL contaminated water sample was first mixed with 1.0 mL buffer solution consisting of 2.0 M NaCl and 20 mM Tris·HCl (pH 7.5). Then, the 2.0-mL mixture solution was added to the *trans* compartment, while a 2.0 mL solution of 1 M NaCl and 10 mM Tris·HCl (pH 7.5) was added to the *cis* compartment. After insertion of a single αHL pore, 40 μM βCD was additionally added to the *trans* compartment. The transmembrane potential, which was applied with Ag/AgCl electrodes with 3% agarose bridges (Sigma) containing 3 M KCl (EMD Chemicals Inc; Darmstadt, Germany), was -80 mV, unless otherwise noted. A negative potential indicates a lower potential in the *trans* chamber of the apparatus. Currents were recorded with a patch clamp amplifier (Axopatch 200B, Molecular Devices; Sunnyvale, CA, USA). They were low-pass filtered with a built-in four-pole Bessel filter at 2 kHz and sampled at 10 kHz by a computer equipped with a Digidata 1440 A/D converter (Molecular Devices). To shield against ambient electrical noise, a metal box was used to serve as a Faraday cage, inside which the bilayer recording amplifying headstage, stirring system, chamber, and chamber holder were enclosed.

4.3 Data analysis

Data were analyzed with the following software: pClamp 10.0 (Molecular Devices) and Origin 7.0 (Microcal, Northampton, MA). Conductance values were obtained from the amplitude histograms after the peaks were fit to Gaussian functions. τ_{on} and τ_{off} values for the analytes were obtained from dwell time histograms by fitting the distributions to single exponential functions by the Levenberg-Marquardt procedure. Kinetic and thermodynamic constants were calculated by using $k_{off} = 1/\tau_{off}$, $k_{on} = 1/(C\tau_{on})$, and $K_f = k_{on}/k_{off}$, where C is the concentration of the analyte.

4.4 Molecular graphics

The model of $(M113F/K147N)_7$ was derived from the structure of the wild-type αHL pore (PDB: 7AHL) with the "mutate" function of SPOCK 6.3. Mutations were performed by reading the new amino acid from the library in the $SP_AALIB directory, and superimposing the Cα_Cβ bond onto the wild-type residue based on Mackay's quaternion method. The model of βCD was produced with HyperChem7.5 (Hypercube, Inc., Gainesville, FL, USA). After export as PDB files, representations of the mutant with bound βCD were produced with RasWin (version 2.7.3). The structures of PMPA and CMPA were drawn in ChemDraw Ultra (CambridgeSoft, version 7.0).

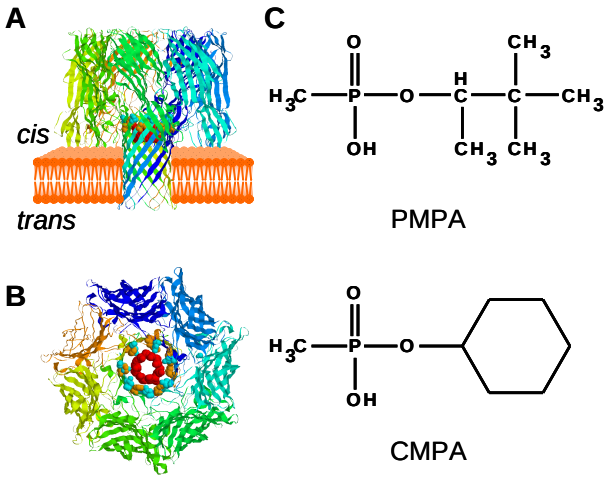

Figure 4.1: Molecular graphics representation of the staphylococcal αHL protein with βCD lodged in the lumen of the channel. (A) Side view of the $(M113F/K147N)_7$ pore; and (B) View into the $(M113F/K147N)_7$ pore from the *cis* side of the lipid bilayer, highlighting positions 113 (orange) and 147 (cyan), where the naturally occurring Met and Lys residues have been substituted with Phe and Asn, respectively, while the red color represents the βCD molecule. (C) Structures of PMPA and CMPA.

4.5 Results and discussion

4.5.1 Nanopore sensing element and its response

In this study, the engineered αHL $(M113F/K147N)_7$ pore, with βCD lodged in the lumen of the channel (as depicted in Figures 4.1A and 1B) as a molecular adapter, was employed as the stochastic sensing element. PMPA and CMPA (Figure 4.1.C), hydrolysis products of GD and GF, respectively, were employed as analytes. It is well established that βCD can be used as a host compound to capture and hence sense organic molecules.[128,129] When βCD is bound to the αHL pore, the channel is partially blocked and the open channel current drops. When a guest molecule is captured by βCD, and the resultant host-guest complex is bound to the pore, the channel is blocked to a larger extent with a further decrease in the observed current.[17] It should be noted that, whether the observed current arose from the insertion of a single αHL channel into the lipid bilayer or not could be conveniently judged from the planar bilayer recording experiment. Since the bilayer lipid membrane typically exhibits a sealing resistance on the order of 100–200 GΩ,[130] it can isolate the electrolyte solutions in the two chamber compartments very well. Under an applied potential of e.g., 40 mV, the current will be 0 pA even if the proteins have been added to the *cis* compartment, but have not yet inserted into the bilayer. After one αHL protein channel inserts into the bilayer, the two chamber compartments (*cis* and *trans*) will be connected. Thus, a sudden current jump will be observed. The single channel currents for the wild-type and various mutant αHL protein pores were well documented, usually about 21 – 32 pA in 1 M NaCl solution under an applied potential of 40 mV depending on the protein pore used.[68] If two

αHL channels insert into the bilayer, the current will be doubled, around 42-64 pA. All the experimental results reported in this work were obtained with a single αHL channel and no double openings were seen in the recorded entire trace.

Our experiments showed that in 1 M NaCl solution, βCD bound to the mutant $(M113F/K147N)_7$ protein very tightly, with a mean dwell time of 1.2 ± 0.1 s at an applied -80 mV potential. With βCD's binding to the pore, the channel current dropped from 58.8 ± 3.2 pA to 9.9 ± 1.2 pA (n = 10) (Figure 2.A). If PMPA or CMPA was additionally added to the mutant $(M113F/K147N)_7$ αHL pore, the blocking event by the βCD·PMPA or βCD·CMPA complex further reduced the current to 0.08 ± 0.06 pA (n=5), or 0.31 ± 0.09 pA (n=5), respectively (Figure 3.2.B and 2.C). The association rate constants (k_{on}) of βCD·PMPA and βCD·CMPA were 6.5 ± 0.7 × 10^6 $M^{-1}{\cdot}S^{-1}$ (n=3), and 2.5 ± 0.3 × 10^6 $M^{-1}{\cdot}S^{-1}$ (n=3), respectively, while the dissociation rate constants (k_{off}) were 1.2 ± 0.1 × 10^3 S^{-1} (n=3), and 1.6 ± 0.2 × 10^3 S^{-1} (n=3), respectively. Thus, the overall reaction formation constants (K_f) at 23 ^oC for βCD·PMPA and βCD·CMPA were 5.4 ± 0.5 × 10^3 M^{-1} and 1.5 ± 0.3 × 10^3 M^{-1} (n=3), respectively. This suggests that PMPA has a stronger binding affinity to βCD than CMPA does. It should be noted that, other engineered αHL pores, including $(M113F/G145F/K147N)_7$ and $(M113F/T143F/G145F/K147N)_7$ were also examined with βCD and PMPA/CMPA. These two nerve agent hydrolytes produced similar current blockage events to those observed in the $(M113F/K147N)_7$ pore, although βCD showed much weaker bindings toward both the pores (data not shown).

4.5.2 Effect of voltage on sensor resolution

The events of PMPA showed much smaller dwell times (τ_{off}), indicating much weaker host-guest interactions occurred in the protein pore, at positively applied potentials than at negatively applied voltages. Hence, the voltage effect on the detection of 10 μM PMPA was investigated using the $(M113F/K147N)_7$ pore and in the presence of 40 μM βCD with an applied potential ranging from –40 mV to –120 mV. With an increase in the applied voltage, both the dwell time and frequency of the host molecule βCD events decreased, while the amplitude of the analyte PMPA events increased. As shown in Fig. 3.3, with the increase of the applied voltage from -40 to -120 mV, the dwell time (τ_{off}) of the host molecule βCD decreased from 5.03 ± 0.13 s to 0.78 ± 0.24 s, the βCD event frequency ($1/\tau_{on}$) decreased from 4.38 ± 0.04 s^{-1} to 0.27 ± 0.05 s^{-1}, while the amplitude of PMPA events increased from 3.74 ± 0.30 pA to 16.01 ± 0.27 pA. For the sensitive detection of PMPA, a large mean amplitude of PMPA events as well as large event dwell time and high frequency for the host molecule βCD were desired. In addition, it should be mentioned that, with the increase of the applied potential, the lipid bilayer used in the experiments would become less stable. The combined results (Figure 4.3) suggests that -80 mV was the optimum applied voltage for our sensor system since all the three parameters (i.e., dwell time, event frequency, and amplitude) had relatively large values at this potential.

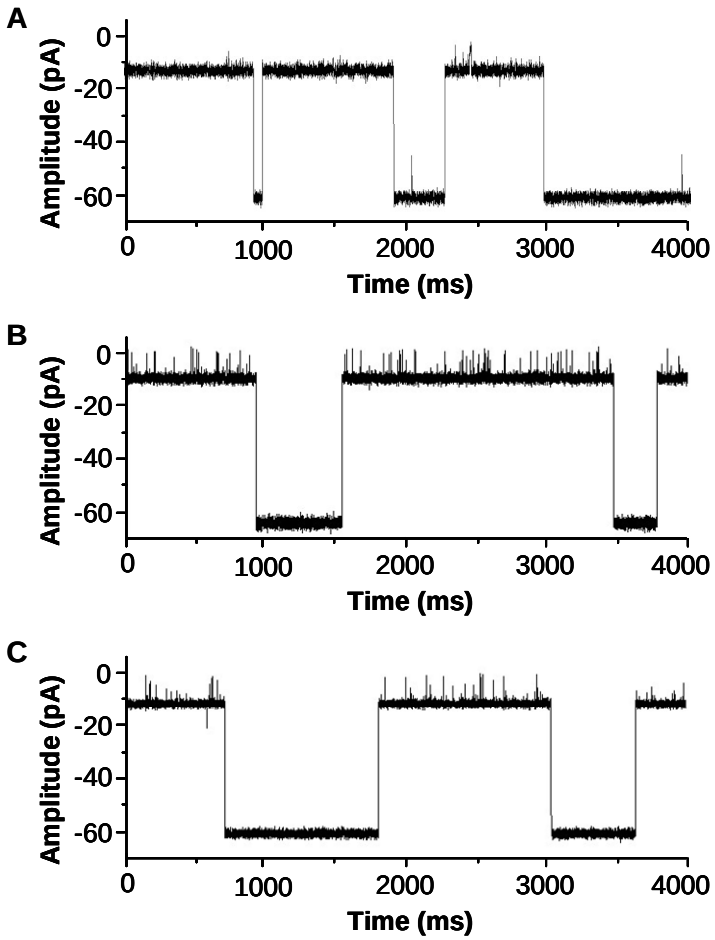

Figure 4.2: Typical single channel current recording traces, showing the detection of PMPA and CMPA. (A) Without PMPA/CMPA; (B) 2 µM PMPA; and (C) 2 µM CMPA. The experiments were performed at -80 mV in 1 M NaCl and 10 mM Tris·HCl (pH 7.5), and in the presence of 40 µM βCD.

4.5.3 Characteristics of the nanopore stochastic sensor

To demonstrate the nanopore sensor to be of analytical use, the effect of the concentration of PMPA and CMPA on the event frequency ($1/\tau_{on}$), dwell time (τ_{off}), and amplitude was investigated. Our experiments (Figures 4.4.A and B) showed that the event mean dwell time and amplitude were unvaried with the increase of the concentration of added PMPA (ranging from 500 nM to 10 µM) and CMPA (ranging from 500 nM to 8 µM). Therefore, amplitude and dwell time can be used as signatures for identifying different organophosphates, specifically, PMPA and CMPA. The experimental results (Figure 4.C) also demonstrated that the event frequency ($1/\tau_{on}$) was linearly related to the concentration of PMPA and CMPA, which provides a basis for quantifying these analytes (Figure 4.6). The sensitivities of the method for the detection of PMPA and CMPA were 4.47 $\mu M \cdot S^{-1}$ and 2.31 $\mu M \cdot S^{-1}$, respectively. The detection limits for PMPA and CMPA were 53 nM (i.e., 0.01 mg/L) and 102 nM (i.e., 0.02 mg/L), respectively. The detection limit was defined as the concentration corresponding to three times the standard deviation of a blank signal. These values are significantly lower than the discharge limits required by US Army (0.1% in w/v, i.e., 1000 mg/L).[131] It should be noted that, to obtain such detection limits, 10 min recording time is enough to collect 300 - 500 events depending on whether the analyte is PMPA or CMPA, from which convincing mean values of the analyte signatures (e.g., τ_{off}, τ_{on}, and amplitude) could be obtained statistically (see “Data analysis” section for detail**).**

4.5.4 Nanopore selectivity

Sarin hydrolysis products (i.e., isopropyl methylphosphonic acid, and diisopropyl methylphosphonic acid), VX hydrolysis products (i.e., 2-(diethylamino) ethanethiol, 2-(dimethylamino) ethanethiol, 2-(diisopropylamino)-ethanethiol, ethyl methylphosphonic acid, methyl phosphonic acid), tabun hydrolyte (i.e., ethyl hydrogen dimethylamidophosphate), and some common toxic organophosphates including diazinon, parathion, malathion and amifostine were also tested with the nanopore sensor. However, no current blockage events were observed when the concentrations of these analytes were lower than 500 μM, suggesting that the sensing system is very selective toward PMPA and CMPA. It should be noted that the structures of some nerve agent hydrolytes used in this selectivity study, such as isopropyl methylphosphonic acid, ethyl methylphosphonic acid, methyl phosphonic acid, etc., were similar to those of PMPA and CMPA. It is likely that the interactions between these compounds and βCD are much weaker than those between βCD and PMPA/CMPA so that they could not be captured by βCD for long time enough to produce observable events in our single-channel recording experiments (note that the instrument resolution is about 100 μs). The detection of VX and Sarin hydrolytes are currently under way by using other engineered αHL pores in the presence of αCD and βCD derivatives. It should be mentioned that, in general, βCD-based host-guest systems are not specific. A number of organic molecules with proper size will be captured by βCD and produce current blockage events, including, e.g., ibuprofen and thalidomide.[11] However, since different compounds produce different signatures (e.g., dwell time and/or amplitude) in the protein nanopore, PMPA and CMPA could be differentiated against common chemicals. For example, the dwell time of

thalidomide was ~0.2 ms,[11] while those of PMPA and CMPA were 0.83 ms, and 0.62 ms, respectively. Therefore, our method offers the potential for rapid screening of PMPA and CMPA. To further improve the selectivity and resolution of the nanopore sensor, development of other engineered αHL pores and utilization of more specific (non-βCD) approaches to the detection of nerve agent hydrolytes are now in progress.

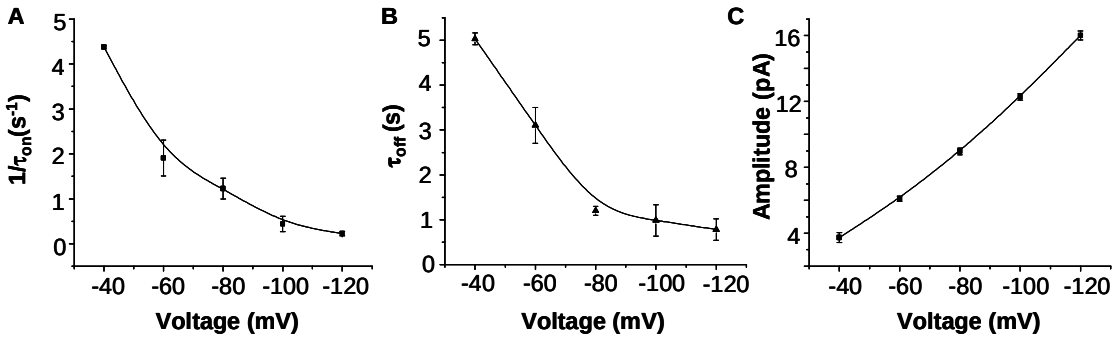

Figure 4.3: The effect of applied potential on (A) $1/\tau_{on}$ and (B) τ_{off} of the βCD events, as well as (C) amplitude of PMPA events. The experiments were performed in1 M NaCl and 10 mM Tris·HCl (pH 7.5) and were repeated at least three times. Each data point in the figure was average of these experiments. The error bars represented the standard deviations of each data point. Both βCD and PMPA were added to the *trans,* while the mutant αHL protein $(M113K/F147N)_7$ was added to the *cis* compartment. The concentration of βCD was 40 μM, and that of PMPA was 10 μM.

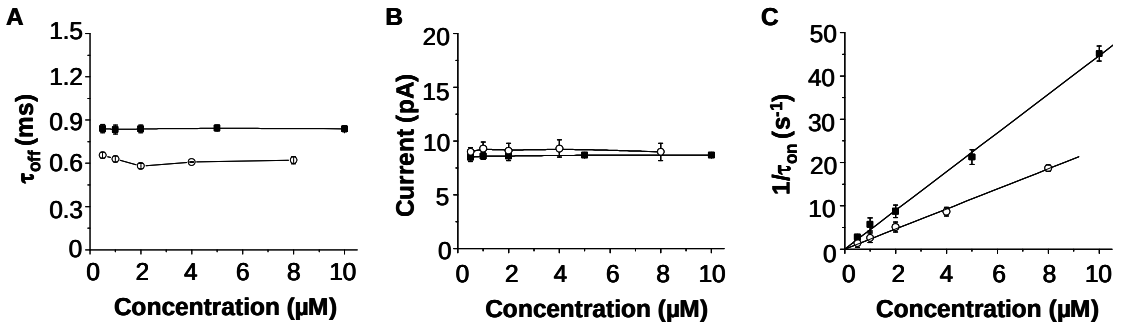

Figure 4.4: Effect of analyte concentration on current blocking events. (■) PMPA; and (○) CMPA. (A) Plot of τ_{off} as a function of PMPA/CMPA concentration, showing the mean dwell time of events was unchanged with the increasing concentration of added organophosphate, (B) Plot of amplitude as a function of PMPA/CMPA concentration, indicating the mean amplitude was unvaried with the changing concentration, where the amplitude was defined as the extent of current blockage, and (C) Plot of $1/\tau_{on}$ as a function of PMPA/CMPA concentration, demonstrating that the event frequency was linearly related to the concentration of added PMPA/CMPA. The experiments were performed at –80 mV in 1 M NaCl and 10 mM Tris·HCl (pH 7.5) and were repeated at least three times. Each data point in the figure was average of these experiments. The error bars represented the standard deviations of each data point. Both βCD and PMPA or CMPA were added to the *trans,* while the mutant αHL protein $(M113K/F147N)_7$ was added to the *cis* compartment. The concentration of βCD was 40 μM.

4.5.5 Salt effect on the sensitivity of the stochastic sensor

To investigate whether the salt effect[22] can be used as an effective approach to significantly increase the resolution and sensitivity for the stochastic detection of PMPA and CPMA, PMPA detection was performed in a series of NaCl solutions at different concentrations, including 0.1 M, 0.5 M, 1 M, 3 M, and 5 M. As shown in Figure 4.7 with the increase of NaCl concentration, both the dwell time and amplitude of the PMPA events increased, and hence a higher sensor resolution was obtained. For example, in 0.5 M NaCl solution, the event mean dwell time of PMPA was 0.54 $\pm$ 0.04 ms, while the amplitude was 4.37 $\pm$ 0.38 pA at -80 mV. In sharp contrast, in 5 M NaCl solution, the dwell time of PMPA was increased to 6.85 $\pm$ 0.17 ms, while the amplitude was 42.27 $\pm$ 0.25 pA. Therefore, an increase of the salt concentration from 0.5 M to 5 M resulted in a 12.7 fold increase in event dwell time, indicating that the binding between PMPA and βCD indeed becomes much stronger with the increase in the electrolyte concentration. Note that the larger the event dwell time, the smaller the dissociation rate constant k_{off}. It should be noted that, when the salt concentration reduced to 0.1 M, the open channel was 5.85 pA. After β-CD's binding to the pore, the residual current was very small (only 1.42 pA), suggesting that salt concentrations less than 0.1 M were not suitable for analyte detection. Furthermore, no PMPA events were identified in 0.1 M NaCl solution.

Table 4.1: Recovery of PMPA from liquid samples[a] by use of the nanopore stochastic sensing method. Each experimental value represents the mean of three replicate analyses ± one standard deviation. The experiments were performed at -80 mV with mutant aHL (M113K/F147N)$_7$ pore in the presence of 40 μM βCD.

Sample number	Theoretical value (μM)	Experimental value ± SD (μM)
1	0	nd[b]
2	10.0	10.6 ± 0.4
3	15.0	14.2 ± 0.9
4	20.0	18.8 ± 1.7

[a]All of the four liquid samples contained additional 100 μM of methyl phosphonic acid, ethyl methylphosphonic acid, and 2-(dimethylamino) ethanethiol. [b]nd: not detected.

4.5.6 Assay of contaminated water samples

To demonstrate the utility of the developed nanopore method for the analysis of PMPA or CMPA in the environmental monitoring applications, two experiments were performed. In the first experiment, two contaminated tap water samples were examined by using the nanopore sensor. Sample 1 contained 100 μM of methyl phosphonic acid, ethyl methylphosphonic acid, and 2-(dimethylamino) ethanethiol, while in addition to the three nerve agent degradation products, sample 2 contained an additional 10 μM PMPA. The preparation of contaminated water samples was described in the Experimental Section. Our experiments showed that no current blockage events were observed for sample 1, whereas sample 2 caused current modulations with a mean dwell time τ_{off} of 0.82 ± 0.10 ms (note that the dwell time for

a single PMPA standard solution was 0.83 ± 0.04 ms). This suggest that the developed nanopore sensing method can indeed differentiate the target compound from false positives, and even allow the accurate identification of PMPA in the presence of a mixture of structure-similar compounds. To investigate whether the nanopore method can be employed to quantify PMPA for field application, another experiment was carried out, in which two additional contaminated water samples were tested. Similar to sample 2, in addition to 100 μM of methyl phosphonic acid, ethyl methylphosphonic acid, and 2-(dimethylamino) ethanethiol, samples 3 and 4 also contained additional PMPA, but with different concentrations at 15 μM, and 20 μM, respectively. Once again, current blockage events were observed for these two samples. The results for all the four tested liquid samples are summarized in Table 1. The concentration values obtained for samples 2 – 4 were 10.6 ± 0.4 μM, 14.2 ± 0.9 μM, and 18.8 ± 1.7 μM, respectively. These values are in agreement with their corresponding theoretical values, thus clearly demonstrating the viability of utilizing the nanopore sensor for quantification of PMPA in liquid samples.

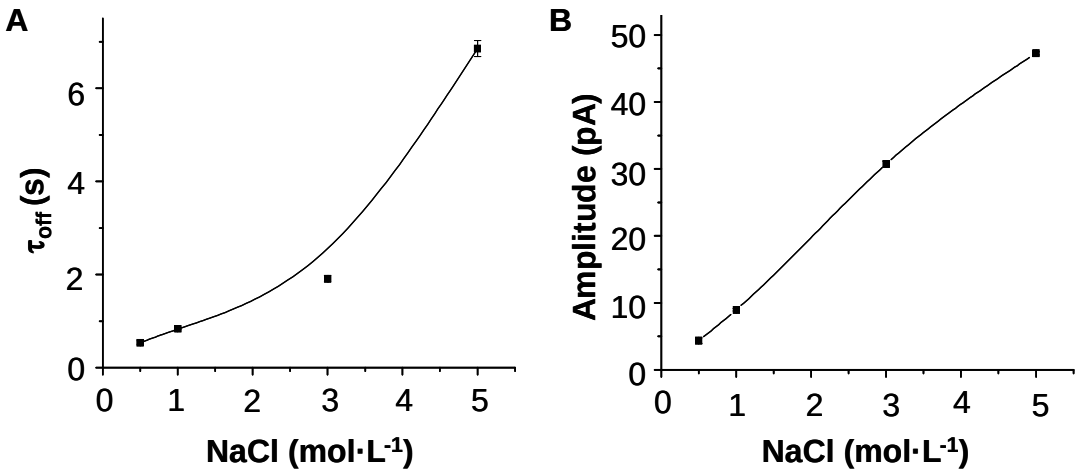

Figure 4.5 Salt effect on PMPA detection. (A) Plot of τ_{off} as a function of NaCl concentration, and (B) Plot of amplitude vs. NaCl concentration, showing both the mean dwell time and amplitude of the PMPA events increased with the increasing NaCl concentration. Each data point in the figure was average of three experiments. The error bars represented the standard deviations of each data point.

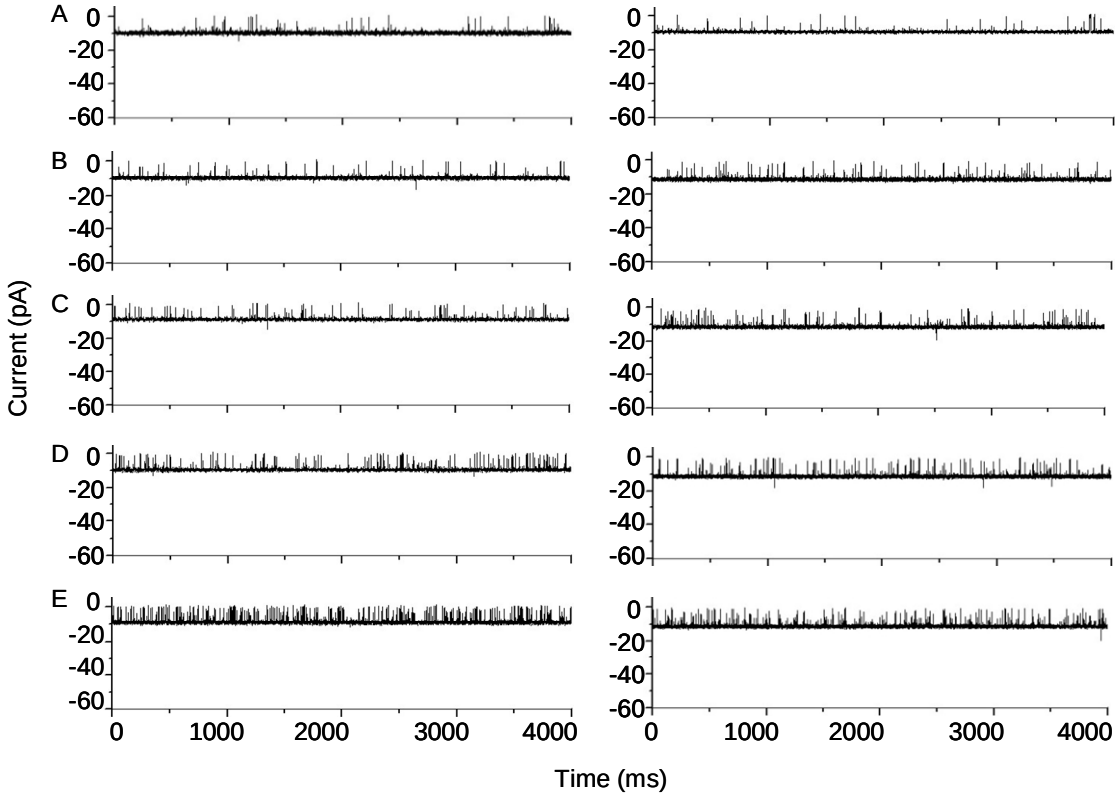

Figure 4.6 Single channel current recording traces, showing the detection of PMPA and CMPA. (*Left*) PMPA. (*Right*) CMPA. (A) - (E) The concentrations of the analytes added were 500 nM, 1 µM, 2 µM, 5 µM, and 10 µM, respectively for PMPA, while 500 nM, 1 µM, 2 µM, 4 µM, and 8 µM, respectively for CMPA. All the experiments were performed at an applied potential of -80mV (*cis* at ground) in a buffer solution containing 1M NaCl and 10 mM Tris·HCl (pH 7.5), and in the presence of 40 µM βCD. Both βCD and PMPA or CMPA were added into the *trans* compartment, while the $(M113K/F147N)_7$ protein pore was added into the *cis* side of the chamber.

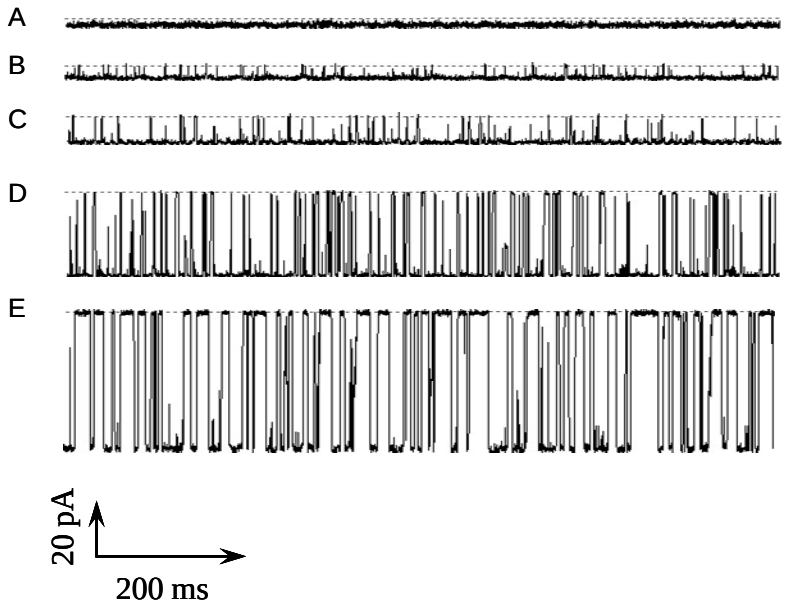

Figure 4.7 Single channel current recording traces, showing the salt effect on PMPA detection. (A) 0.1M NaCl; (B) 0.5M NaCl; (C) 1M NaCl; (D) 3M NaCl; and (E) 5M NaCl; these experiments were performed at -80mV with concentrations of NaCl ranging from 1M to 5M and 10mM Tris·HCl (pH 7.5). Both βCD and PMPA or CMPA were added into the *trans* compartment, while the $(M113K/F147N)_7$ protein pore was added into the *cis* side of the chamber.

4.6 Conclusions

A single-molecule nanopore stochastic sensing approach for the detection of organophosphorus nerve agent hydrolytes PMPA and CMPA was successfully developed. Given its sensitivity, and rapid response, coupled with the recent development of new approaches for building stable and/or portable lipid bilayer platforms[126, 127, 132] and constructing nanopore sensor array,[31] our nanopore sensing method reported in this work is envisioned for further development as a deployable technique for real-time, on-site analysis of nerve agents in environmental monitoring applications.

CHAPTER 5

REAL TIME MONITORING OF PEPTIDE CLEAVAGE USING A NANOPORE PROBE

5.1 Introduction

Interactions among biomolecules (such as proteins, peptides and proteases) are involved in a wide variety of physiological activities within living cells.[133] Evaluating the functional roles of these biologically active molecules and elucidating their interactions will benefit biomedical research.[134] For example, of paramount importance in clinical assessment of neurodegenerative problems including Alzheimer's and Parkinson's diseases is early detection and monitoring of the conformational change of amyloid-β peptide (A-β), as attributed to the proteolytic cleavage of the amyloid-based precursors by β- and γ-secretases.[135,136] Many approaches currently available in the proteomics research rely on peptide cleavage for the identification of proteins and other biomarkers. At present, the majority of studies performed in this area are dependent on expensive and time-consuming techniques that frequently require sample labeling.[137138, 139] Although several label-free approaches have been utilized in the detection of biomarkers and the study of protease-substrate interactions,[133] a definite need remains for a more rapid, lower cost, and easier to use methodology to study protein/peptide cleavage, and for use in enzymatic activity assays.

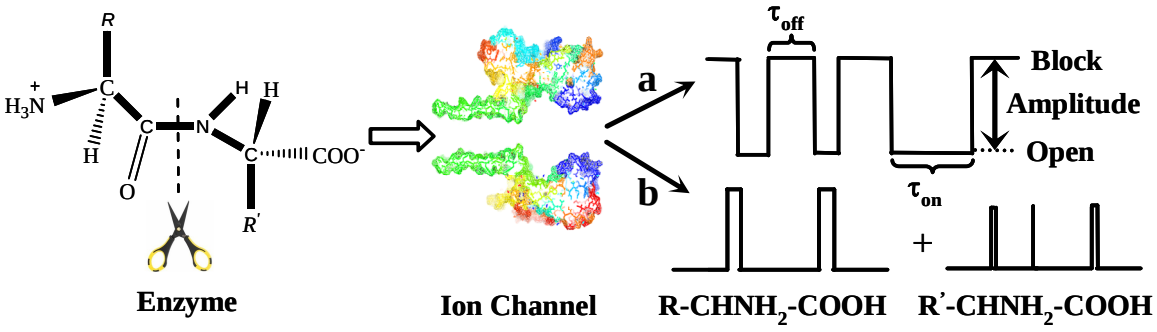

Figure 5.1: Probing peptide-protease interaction in an ion channel. (a) Without the enzyme, the current modulations are caused only by the substrate. (b) With the enzyme, new blockage events having different residence times and/or amplitudes from those of the substrate could be observed due to the breakdown products of the substrate.

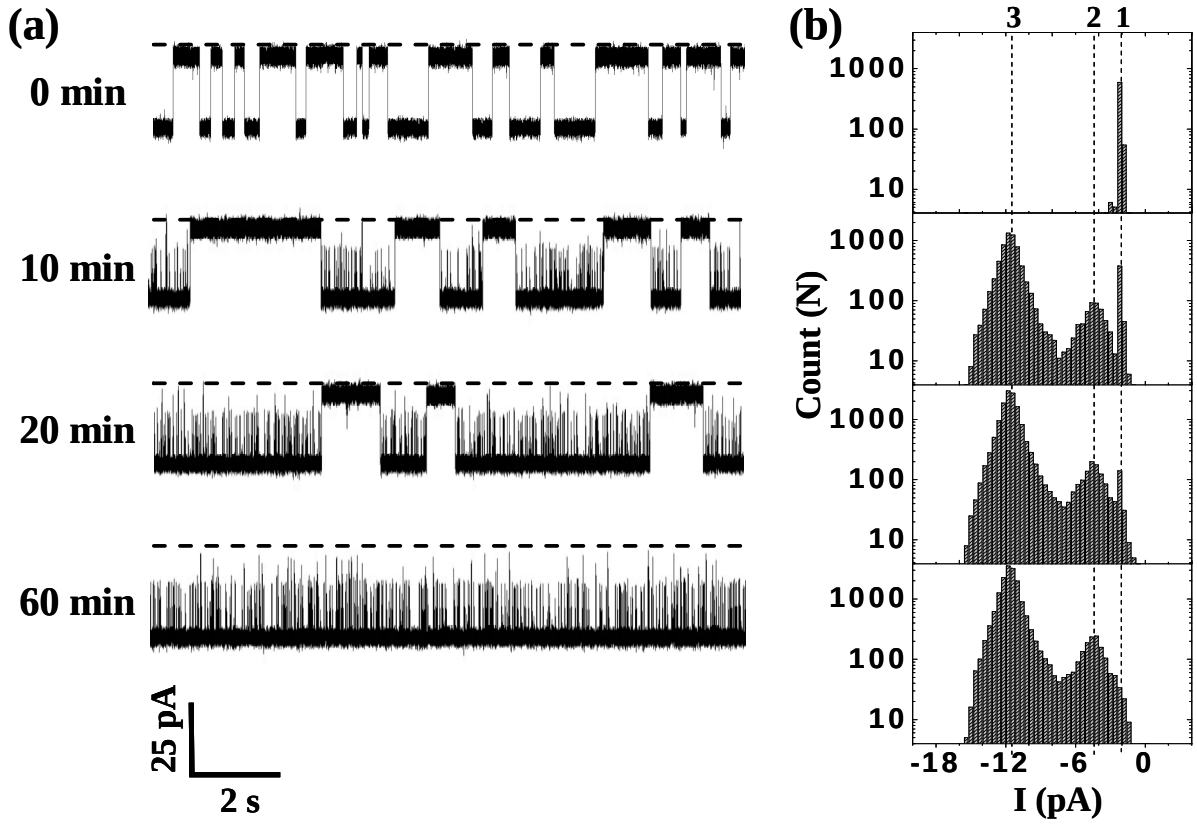

Figure 5.2: Monitoring of A-β (10-20) cleavage by trypsin. (a) Representative segments of a single channel recording trace at various times. Dashed lines represent the levels of zero current; (b) The corresponding time-dependent event amplitude histograms. Dashed lines 1, 2, and 3 represent the mean residual current levels for peptides YEVHHQKLVFF, YEVHHQK, and LVFF, respectively. The experiment was performed at -40 mV with 10 μM A-β (10-20) and 0.025 μM trypsin

Herein we demonstrate that use of a protein channel provides a viable new approach to probe peptide cleavage. It has long been established that ion channels play a pivotal role in the regulation of mass and energy transfer for many biological processes. More recently, it has been clearly established that these nanometer-sized channels offer exciting new possibilities for development of ultrasensitive biosensors, study of biomolecular folding and unfolding, and investigation of covalent and non-covalent bonding interactions.[140,141-145] In the present report, peptide cleavage is monitored by recording peptide translocation through an ion channel in the absence and presence of an enzyme with single-channel recording technique (Figure 5.4). As documented below, our method permits study of protease kinetics based on real-time monitoring of the ionic current modulations arising from the enzyme-peptide interactions. As shown in Figure 5.1, in the absence of the enzyme, the current modulations are caused only by the substrate (Figure 5.1.a). However, after addition of the enzyme to the buffer solution, the substrate will be cleaved into two fragments. Thus, new blockage events having different residence times (τ_{off}) and/or amplitudes from those of the substrate can be observed (Figure 5.1.b).

To demonstrate this concept, an engineered version of alpha-hemolysin (αHL) channel, $(M113F)_7$, was used to study the trypsin cleavage of peptide A-β (10-20). The $(M113F)_7$ protein has been shown to provide a significantly enhanced resolution for biomolecule recognition versus the wild-type αHL pore.[61] Trypsin is commonly used as serine protease to cleave peptide bonds after Arg (R) or Lys (K) amino acid residue.[146] Since the spherical molecular diameter (38Å)[147] of trypsin is larger than that (20 Å) of the αHL transmembrane domain,[19] trypsin can not enter the pore, and hence will not produce current blockage events which might interfere with the

identification of the target peptide(s). Our experimental results (Figure 5.2, t = 0 min) show that, in the absence of trypsin, the buffer solution containing peptide A-β (10-20) produced only a single type of current blockage, one having a large mean residence time of 0.63 ± 0.06 s (Figure 5.2.a and 5.1, Figure 5.5) and a small mean residual current of -1.8 ± 0.3 pA (Figure 5.2.b). In sharp contrast, after addition of trypsin, two new types of current modulation events are clearly observed, both having significantly shorter residence times at 0.85 ± 0.08 ms and 0.75 ± 0.05 ms, and larger mean blockage residual currents at -4.4 ± 0.3 pA, and -12.2 ± 0.6 pA, respectively (Figure 5.2, t =10, 20, and 60 min). These shorter duration blockages are attributed to YEVHHQK (YK-7) and LVFF fragments, the breakdown products of A-β (10-20). Their identities were confirmed by direct measurement of current blockages using both single standards of YK-7 and LVFF peptides as well as 1:1 solution mixtures of these two compounds. As shown in Figure 5.4, and Figure 5.6, blockage events with the two peptides produced similar mean residence times (0.9 ± 0.1 ms and 0.77 ± 0.07 ms, respectively) and residual currents (-4.5 ± 1.0 pA and -14 ± 2 pA, respectively) to those of the A-β (10-20) /trypsin digestion products. Note that the mean residence time (τ_{off}) and/or amplitude of the events can be used as signatures for identifying a peptide, while the event frequency f ($f = 1/\tau_{on}$) could be used to quantify the substrate remaining or the fragments produced (Figure 5.2 , Figure 5.4, and Figure 5.5). The time-dependent event frequency provided further evidence that the enzymatic cleavage process is responsible for the appearance of these new blockage events. With increasing reaction time, the frequency of A-β (10-20) events decrease, while those of fragment events increase, a clear indication that the substrate was being digested by trypsin. In fact, the large duration and small residual current events disappear after approximately one hour digestion, suggesting that all

of the A-β (10-20) substrate is cleaved at that point in time. As an added control, translocation of peptide YYYYYY, which is not a substrate for trypsin, in the $(M113F)_7$ pore was examined. No new types of events and no change in the event τ_{off} or amplitude were observed after addition of trypsin (Figure 5.4, and Figure 5.7), consistent with this analysis.

To determine the enzyme kinetics, quantitative analysis of the above single-channel current recording (Figure 5.2) of the peptide A-β (10-20) digestion by trypsin was performed (see Figure 5.4). From the time curve of the substrate digestion (Figure 5.3.a), we observe that the rate for the A-β (10-20) cleavage decreases rapidly with reaction time. For example, 93.5 ± 3.8 percent of the substrate is cleaved in the first 20 min, whereas only an additional 6.1 ± 0.7 percent of the substrate is digested in the second 20 min. Our observation is reasonable considering that the concentration of the substrate is relatively large in the early stage of the trypsin/A-β (10-20) interaction. A Lineweaver-Burk plot (Figure 5.3.b) using the frequency of the cleavage product LVFF events reveals that the Michaelis constant K_m of the reaction is 59.2 μM, whereas k_{cat} ($k_{cat}=V_{max}/[trypsin]$) is 4.43 s^{-1}. These values agree with those of other studies involving cleavage of A-β peptide, carried out under similar experimental conditions to those involved in the present investigation.[148] Note that the enzymatic activity is influenced by substrate, pH, temperature, and salt concentration.[149]

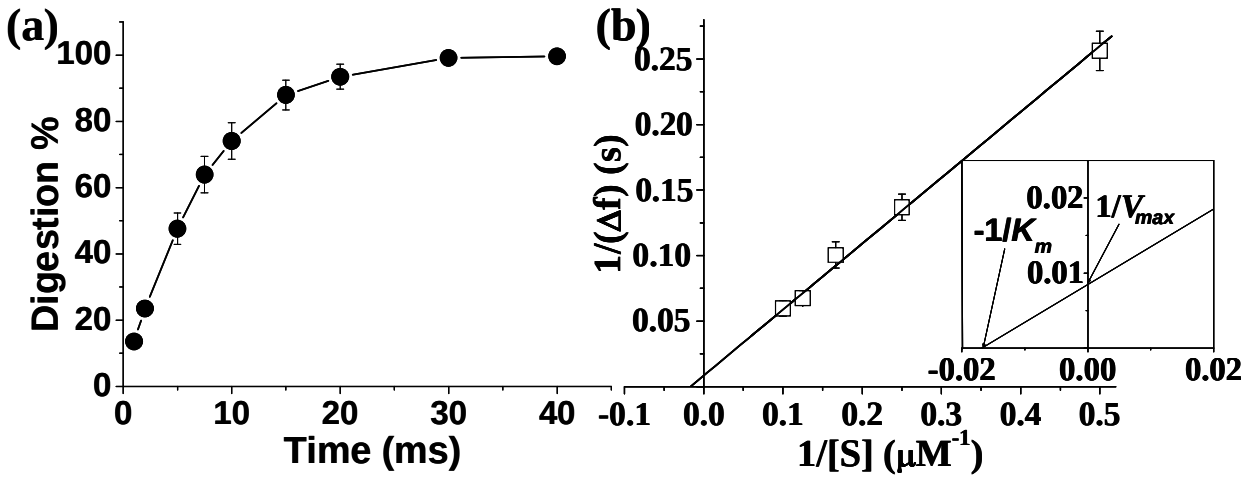

Figure 5.3: Kinetic profiles for the A-β (10-20)/trypsin interaction. (a) Time curve of the digestion with $[substrate]_0$ = 10.0 μM and [trypsin] = 0.025 μM. (b) Lineweaver-Burk plot for the determination of K_m and k_{cat}. The inset of Figure 2b shows an enlarged x- and y-intercept region. The experiments were performed with 0.025 μM trypsin and various concentrations of A-β (10-20).

It should be noted that, at the early stage of the enzymatic reaction, the product concentration is very low (nanomolar range). This requires a relatively long period of time (e.g., 1 min in this work) taken to collect hundreds of individual single molecule events, which are necessary for the statistical analysis of the event frequency. This limitation could be remedied by replacing the event mean frequency with the number of event occurrences in the analysis of enzyme kinetics. Using this approach, the product concentration could be determined in seconds, and a substrate digestion curve similar to Figure 5.3a was obtained (Figure 5.4 and Figure 5.9). Furthermore, in principle, the method developed in this work should be compatible with the analysis of enzymatic reactions involving long peptides / proteins, and complex mixtures. The former could be achieved by using synthetic nanopores with large pore diameters or engineered protein pores which could enhance biomolecular translocation as the sensing element, [91,150] while the latter by only considering the cleavage products and focusing on the frequency increase in their events.

5.2 Experimental section

5.2.1 Materials and reagents

Mutant αHL M113F gene was constructed by site-directed mutagenesis with a WT αHL gene in a T7 vector (pT7–αHL), which has been described elsewhere.[22] The mutant M113F αHL protein monomer was first synthesized by coupled *in vitro* transcription and translation (IVTT) using the *E. coli* T7 S30 Extract System for Circular DNA from Promega (Madison, WI). Subsequently, it was assembled into homoheptamer by adding rabbit red cell membranes and incubating for 1~2 h. The heptamer protein pore was purified by SDS-polyacrylamide gel electrophoresis and stored in aliquots at -80℃. [151]

The substrate amyloid-β peptide (10-20) with a sequence of YEVHHQKLVFF (A-β (10-20)) was purchased from American Peptide Company, Inc. (Sunnyvale, CA). Other peptides, including YEVHHQK (YK-7), LVFF, YYYYYYRYPWF (Y6R-YPWF), YYYYYYR (Y6R), and YPWF were obtained from Biomatik Corporation (Wilmington, DE). All these peptides did not contain any protecting groups at the N- or C-terminus and were supplied in lyophilized form. The purity of these peptides was greater than 95% as verified by high-performance liquid chromatography and mass spectrometry. Lipid 1,2-diphytanoylphosphatidylcholine was purchased from Avanti Polar Lipids (Alabaster, AL). All the other reagents, including trypsin from bovine pancreas, were obtained from Sigma (St. Louis, MO). All the peptides and trypsin were dissolved in HPLC-grade water. All the stock solutions of the peptides were prepared at 0.5 mM each. The concentration of trypsin was 5 μM. All the peptide and trypsin solutions were kept at -80 °C before and after use.

5.2.2 Bilayer experiment and data analysis

A bilayer of 1,2-diphytanoylphosphatidylcholine was formed on an aperture (150 μm) in a Teflon septum (25 μm thick; Goodfellow, Malvern, PA, USA) that divided a planar bilayer chamber into two compartments, *cis* and *trans* (Figure 5.4). The formation of the bilayer was achieved by using the Montal-Mueller method,[23] and monitored by using a function generator (BK precision 4012A; Yorba Linda, CA, USA). In most cases, the lifetime of the bilayer is at least three hours even after insertion of an αHL pore. The experiments were performed under a series of symmetrical buffer conditions with a 2.0 mL solution comprising 1 M NaCl, and 10 mM Tris·HCl (pH 7.5) at 22 ± 1 °C. Unless otherwise noted, the mutant αHL $(M113F)_7$ protein was added to the *cis* compartment, which was connected to "ground", while the peptide and/or trypsin was added to the *trans* compartment. In such a way, after insertion of a single αHL protein channel, the mushroom cap of the αHL channel would be located in the *cis* compartment, while the β-barrel of the αHL protein would insert into the lipid bilayer and connect with the *trans* of the chamber device. The final concentration of the αHL proteins was 0.2–2.0 $ng \cdot mL^{-1}$. Currents were recorded with a patch clamp amplifier (Axopatch 200B, Molecular Devices; Sunnyvale, CA, USA). They were low-pass filtered with a built-in four-pole Bessel filter at 10 kHz and sampled at 50 kHz by a computer equipped with a Digidata 1322 A/D converter (Molecular Devices).

All the peptide digestion experiments in this work were carried out by first recording the peptide translocation in the (M113F)7 pore for at least 10 min in the absence of trypsin, and then recording for at least another 80 min in the presence of trypsin. The control experiments with single peptide standards and 1:1 solution mixtures of two

peptides were recorded for at least 10 min without trypsin. Each experiment was repeated at least 3 times. The mean conductance, inter-event interval (□on), and residence time (τoff) were obtained by using clampfit software. Specifically, conductance values were obtained from the amplitude histograms after the peaks were fit to Gaussian functions. Values of □on and □off for the peptide events were obtained from the open state (1) and close state (0) dwell time histograms, respectively by fitting the distributions to single exponential functions by the Levenberg-Marquardt procedure.[10]

In terms of all the peptide digestion experiments, the time of t = 0 min represents the period in which the substrate digestion by trypsin has not yet begun. Note that, a ~ 30-s period of addition of trypsin to the solution and stirring was also included in the time of t = 0 min, but this period was not included in the analysis of the peptide events (see Figure 5.4). All the amplitude histograms were created based on the events collected in a 10-min period of recording. For example, as shown in Figure 5.2b, the amplitude histogram at t = 0 min was generated from a 10-min recording of the peptide A-β (10-20) translocation in the $(M113F)_7$ pore without trypsin, while that of t = 10 min was obtained from a 10-min recording of digestion of A-β (10-20) by trypsin in the period from t = 0 min to t =10 min (note that, here, t = 0 min starts after addition of trypsin and stirring). Similarly, the amplitude histogram at t = 20 min was created based on the events collected in the period of t = 10 min to t = 20 min from the single-channel trace, while that of t = 60 min was obtained from the events recorded in the period of from t = 50 min to t = 60 min.

5.3 Time curve of the substrate digestion

It should be noted that, in a certain amount of trypsin (e.g., 0.025 μM in this work), the concentration of the substrate peptide A-β (10-20) consumed in a given period of time t should be equal to that of the peptide fragment LVFF (or YK-7) produced. From the supporting information Figure 5.5.a, it is clear that the frequency f ($f = 1/\tau_{on}$) of the events of a certain peptide is directly proportional to its concentration. Therefore, the digestion percentage of the substrate at a specific time t could be calculated by using the following equation:

$$\text{Cleavage (\%)} = f_t / f_0 \times 100\%$$

where the value of f_0 is the event frequency of peptide LVFF (or YK-7) produced after all of the substrate peptide A-β (10-20) has been digested by trypsin in the protein pore, whereas the value of f_t represents the event frequency of the product LVFF (or YK-7) after the substrate-trypsin enzymatic reaction occurred for a period of time t.

To obtain the plot of substrate digestion percentage with reaction time, all the events collected in a 1-min segment (from 60 min to 61 min) of the single channel current recording trace was used to calculate f_0, while the values of f_t at various digestion times were obtained based on all the events recorded from a period of 1 min around that time t. For example, $f_{t=2\ min}$ were calculated from all the events collected from t = 1 min to t = 2 min; and $f_{t=10\ min}$ were obtained based on all the events collected from t = 9 min to t = 10 min. A typical illustration at digestion time t = 5 min is shown in Figure 5.2. Note that our experimental results (Figure 5.1) show that all of the substrate peptide A-β (10-20) has been cleaved by trypsin into two peptide fragments

(i.e., LVFF and YK-7) in one hour. Therefore, the concentration of the product LVFF after one hour enzymatic reaction would be equal to the initial concentration of the substrate.

To facilitate the analysis of LVFF events, the overall inter-event interval τ_{on} and frequency f_{total} ($f_{total} = 1/\tau_{on}$) of all of the three different types of events (including A-β (10-20), LVFF, and YK-7) were first obtained. Then, the frequency of LVFF events was calculated based on the equation: $f = pf_{total}$, where p is the percentage of the LVFF events in all of the three types of events. [152]

5.3.1 Determination of enzyme kinetics

To determine the Michaelis-Menten kinetic constants K_m and V_{max}, a series of single-channel current recording experiments with translocation of the substrate peptide A-β (10-20) in the $(M113F)_7$ pore with trypsin was carried out, where we kept the concentration of the trypsin constant at 0.025 μM, but varied the substrate concentration, ranging from 2.0 μM to 10.0 μM. The frequency of the cleavage product LVFF events at a digestion time of 5 min (i.e., $f_{t=5min}$) was calculated by using the same approach as described in the previous section “Time curve of the substrate digestion”. Since the solution contained only the substrate at t = 0 min, the concentration of the peptide fragment LVFF produced in the 5 min digestion period, i.e., the rate ν of the reaction, would be proportional to the change in the frequency, Δf ($\Delta f = f_{t=5min}$), of the LVFF events. Plotting of the reciprocals of the substrate concentrations vs. the values of $1/\Delta f$ yields the "double-reciprocal" or Lineweaver-

Burk curve, as shown in Figure 5.3b. The K_m was calculated from the x-intercept, while V_{max} was obtained from the y-intercept of the linear fit. The value of k_{cat} could be calculated by using the equation $k_{cat} = V_{max}$ / [enzyme], where [enzyme] is the concentration of the enzyme. It should be mentioned that the value of V_{max} obtained from this Lineweaver-Burk curve is the frequency of the LVFF events. The value of V_{max} in $\mu M \cdot s^{-1}$ could be calculated from the relationship between the frequency of LVFF events and its concentration. The substrate digestion experimental results (Figure 5.3.a and Table 5.1) show that the relationship between the frequency of LVFF events and its concentration conforms to the equation: Y = 3.548X, where Y is the event frequency *f* (in s^{-1}), while X is the LVFF concentration (in μM). Note that for the accurate determination of K_m and V_{max}, the use of the initial rate of the enzymatic reaction at various substrate concentrations is desired. Figure 5.3.a shows that the substrate digestion percentage increases linearly approximately from t = 0 min to t = 5 min, thus suggesting that the reaction velocities at digestion times from 0 to 5 min are close to initial rate of the enzymatic reaction. Furthermore, given a certain period of time frame (e.g., 1 min), since more events could be collected at t = 5 min than those recorded at a digestion time less than 5 min, thus facilitating data analysis, the frequency of the LVFF events at t = 5 min was employed in this work to construct the Lineweaver-Burk plot.

5.3.2 Trypsin cleavage of peptide YYYYYYRYPWF

To further document the utility of nanopore technology as an effective label-free approach to monitoring peptide cleavage and to determining enzyme kinetics, trypsin cleavage of the peptide YYYYYYRYPWF was also examined, again using the mutant $(M113F)_7$ pore. As in the case of the A-β (10-20) substrate, trypsin cleaves peptide bonds after Arg or Lys amino acid residue. Therefore, addition of trypsin to the buffer solution containing YYYYYYRYPWF would be expected to produce two fragments, i.e., YYYYYYR and YPWF. As shown in Figure 5.2a, at an applied potential of -40 mV and t = 0 min (i.e., in the absence of trypsin), we observe a single type of events having a large mean dwell time (1.6 ± 0.2 s) and residual current of -1.6 ± 0.1 pA. These events were produced by the substrate YYYYYYRYPWF. In contrast, with addition of trypsin to the solution, two new types of blockage events are clearly observed. One type of events exhibited a slightly larger mean residual current (-3.8 ± 0.5 pA) but a significantly smaller event mean dwell time (62 ± 5 ms) to those of the substrate. As revealed by calibration runs with single standards (Figure 5.2a), these events are attributed to the presence of YYYYYYR product molecules. The second new blockage events, having mean residual currents at -14.5 pA and at -9.8 pA, are attributed to YPWF, the second cleavage product (Figure 5.2a). Furthermore, with increasing digestion time, the frequency of the YYYYYYRYPWF substrate events decrease and no events attributable to this compound are observed after 3 hours of reaction. In contrast, event frequencies of the two product peptide fragments increase with the reaction time. Similar phenomenon was also observed at +40 mV, where two new types of blockage events in the current trace are identified, again demonstrating that the YYYYYYRYPWF substrate is cleaved into two new peptide

fragments (Figures 6.0 and 6.2). Taken together, the combined results suggest that the translocation of peptide YYYYYYRYPWF in the mutant $(M113F)_7$ pore is mainly attributed to diffusion but not electrophoretic driving.

5.4 Conclusions

In summary, we report a rapid new label-free method to monitor peptide cleavage and to obtain quantitative chemical kinetic information on enzymatic processes. Given the need for such information, such as in disease diagnostics and drug discovery, further development of this technique into miniature nanopore sensing systems, including systems having more automated controls, is currently underway. In addition, given the fact that properly engineered protein pores can differentiate the sequences of short peptides,[61] we believe this peptide/protein cleavage approach offers the potential for further development as a novel rapid label free protein sequencing technique.

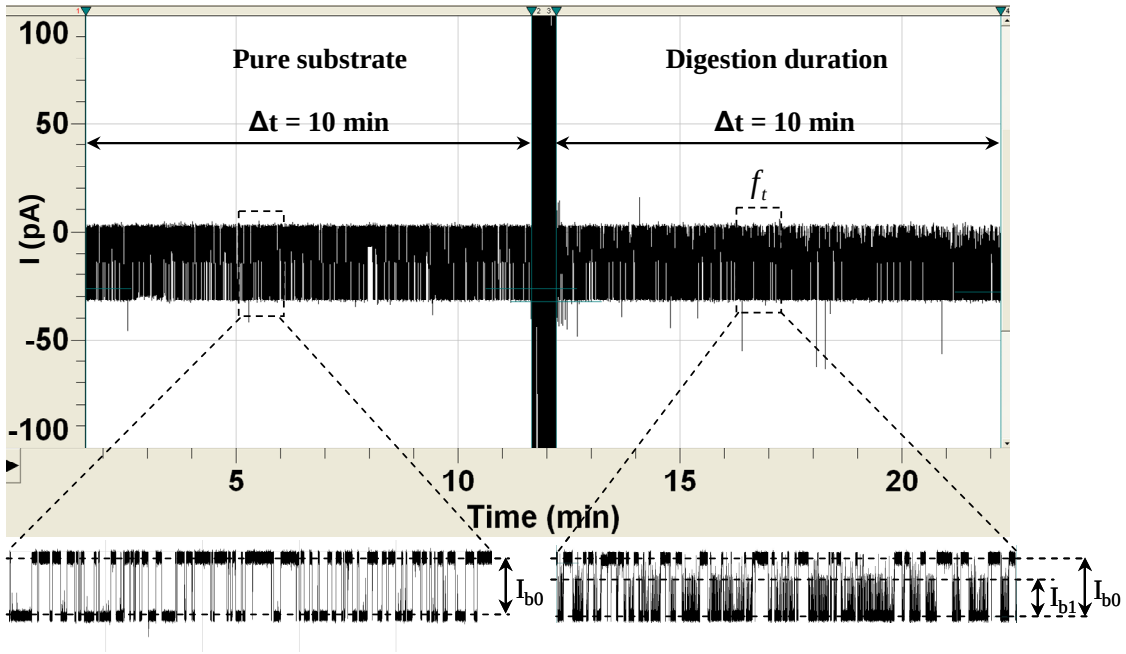

Figure 5.4: Calculation of f_t from a ~ 20 min single channel recording trace, where the translocation of peptide A-β (10-20) in the αHL $(M113F)_7$ pore in the absence and presence of trypsin was recorded for 10 min, respectively. Note that, after addition of trypsin, the buffer solution was stirred for ~ 30 seconds (from ~ 11min40s to ~ 12 min10s in this example current recording trace). Typical magnified 1-min segment of the trace without trypsin was shown in the left lower panel, while that with trypsin and used for the calculation of $f_{t=5min}$ (i.e., the event frequency after the substrate-trypsin enzymatic reaction occurred for 5 min) was presented in the right lower panel. The experiment was performed at -40 mV (*cis* at ground) with a 2.0 mL solution comprising 1 M NaCl and 10 mM Tris·HCl (pH 7.5). The initial concentration of the substrate was 10 µM and that of trypsin was 0.025 µM.

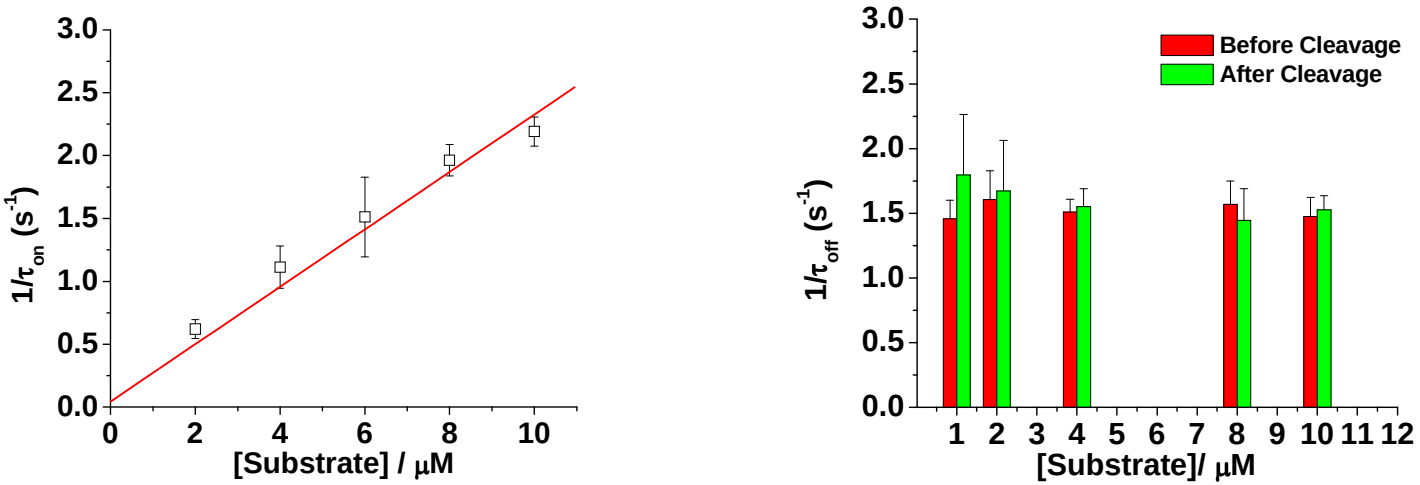

Figure 5.5: The effect of the substrate concentration on current blockage events. (a) Plot of event frequency ($1/\tau_{on}$) as a function of peptide A-β (10-20) concentration, showing that the event frequency is proportional to the peptide concentration, and hence can be used to quantify the substrate remaining or the peptide fragments produced; and (b) Plot of $1/\tau_{off}$ as a function of A-β (10-20) concentration, demonstrating that the mean residence time of events for a given molecule does not change with concentration or in the presence of other matrix components, and hence can be used to identify a compound. The experiment was performed at -40 mV (*cis* at ground) under a series of symmetrical buffer conditions with a 2.0 mL solution comprising 1 M NaCl and 10 mM Tris·HCl (pH 7.5). The concentration of trypsin was 0.025 μM. Note that the mean residence time (τ_{off}) before cleavage in Figure S2b was calculated based on the peptide A-β (10-20) events collected in a period of 10 min in the absence of trypsin, while the residence time after cleavage in Figure S2b was obtained based on the A-β (10-20) events recorded for 10 min after addition of trypsin to the buffer solution.

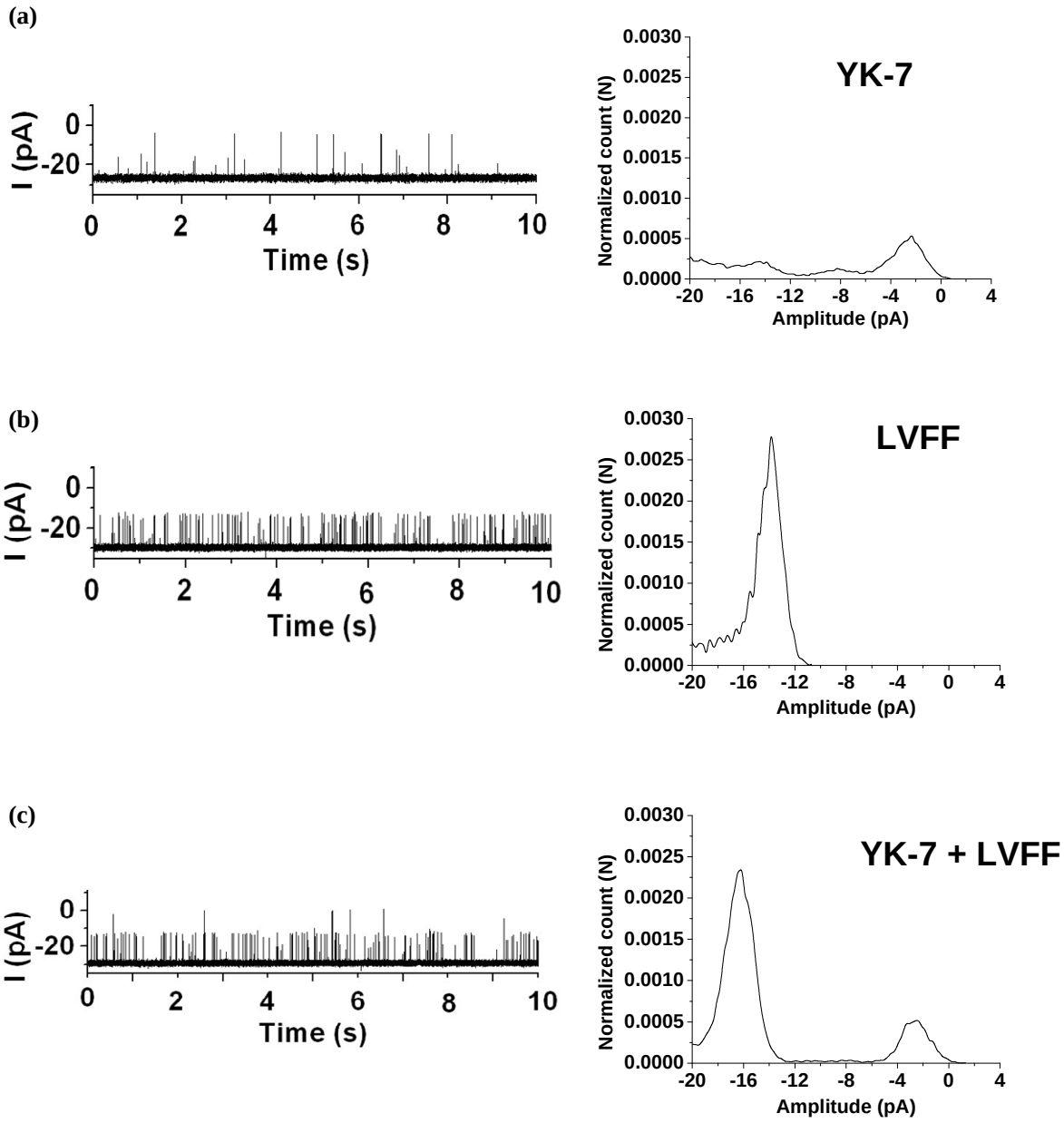

Figure 5.6: Control experiments with peptides YK-7 and LVFF, confirming the identities of the cleavage products of A-β (10-20) in the presence of trypsin. Typical single-channel recording traces and their corresponding all-points histograms for (a) YK-7; (b) LVFF; and (c) a mixture of YK-7 and LVFF (1:1 ratio). The experiment was performed at -40 mV under a series of symmetrical buffer conditions with a 2.0 mL solution comprising 1 M NaCl and 10 mM Tris·HCl (pH 7.5).

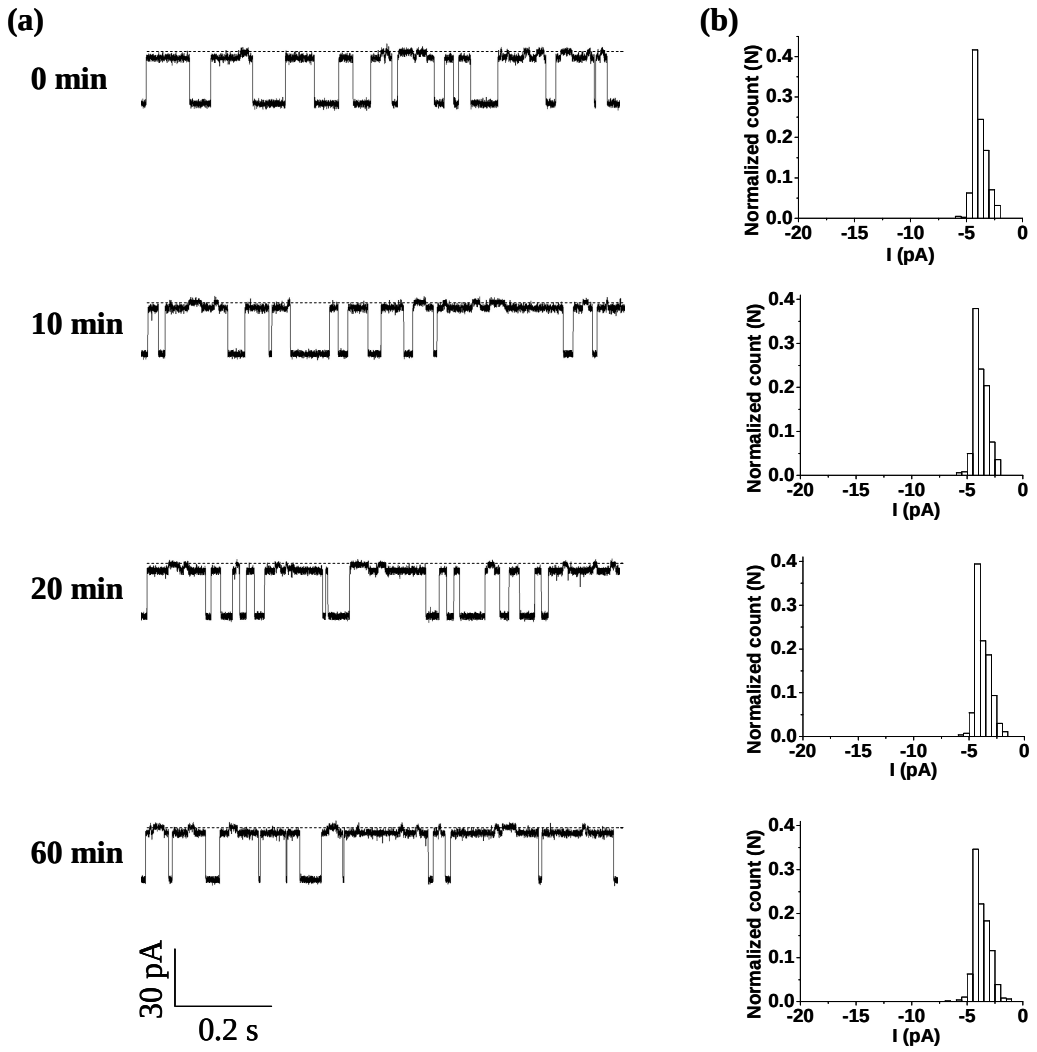

Figure 5.7: Translocation of peptide YYYYYY in the mutant αHL $(M113F)_7$ pore in the absence and presence of trypsin. (a) Representative segments of a single channel recording trace, and (b) the corresponding event amplitude histograms at various times. The experiment was performed at -40 mV with 5 μM YYYYYY and 0.025 μM trypsin. Dashed lines represent the levels of zero current. Note that the segment at t= 0 min was taken from the single channel trace before addition of trypsin, while other segments were taken after addition of trypsin to the solution and stirring. The event amplitude histograms in Figure 5.8b were obtained based on the events collected from a period of 1 min around the time shown in Figure 5.8a.

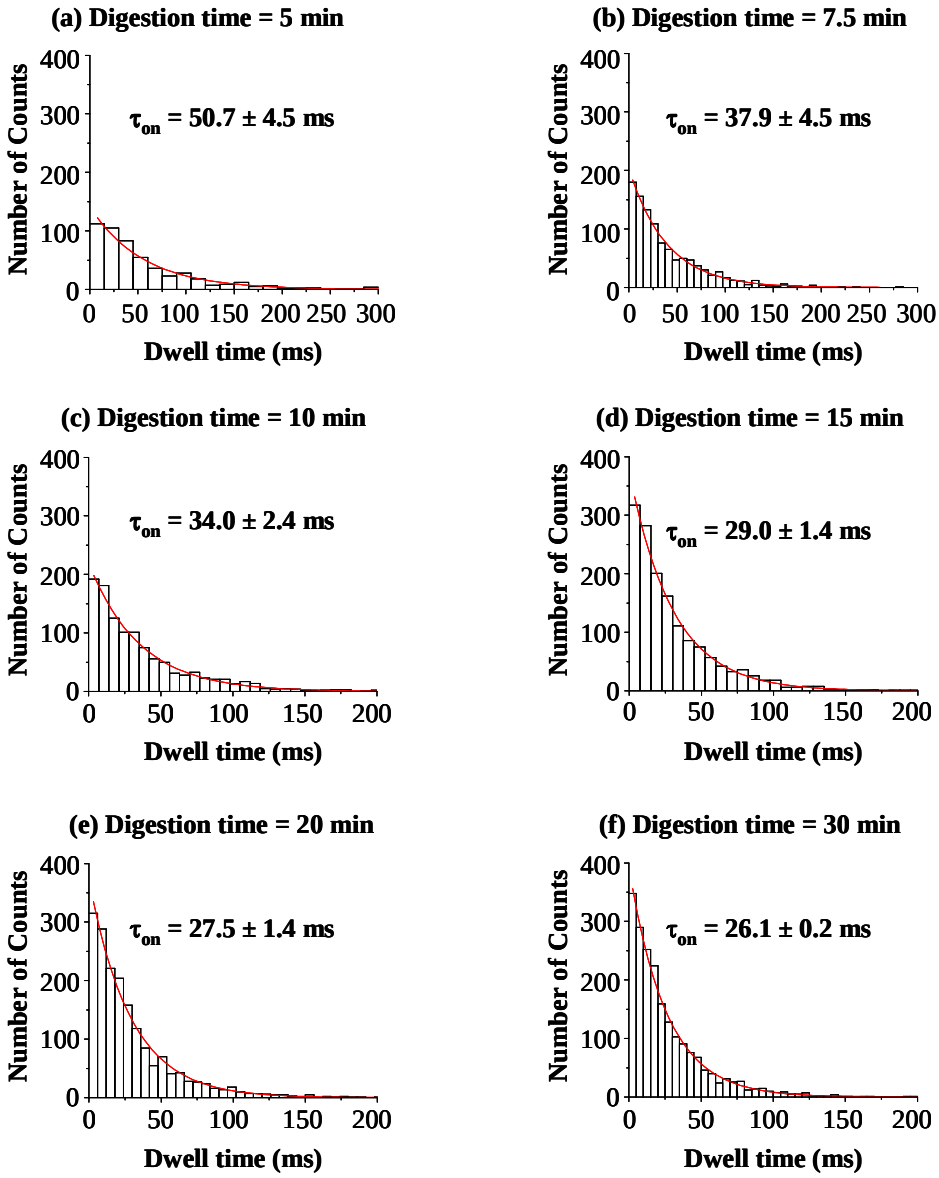

Figure 5.8: Representative inter-event interval (τ_{on}) histograms at various digestion times. The experiment was performed at -40 mV with the translocation of 10 µM peptide A-β (10-20) through the mutant αHL $(M113F)_7$ pore in the presence of 0.025 µM trypsin. The red solid lines in the inter-event interval histograms are fits of the event distributions. Note that all of the three different types of events (including A-β (10-20), LVFF, and YK-7) were included in the analysis.

Table 5.1 Effect of digestion time on the event frequency of the cleavage product LVFF[a]

Digestion Time (min)	τ_{on}[b] (ms)	$1/\tau_{on}$ (s^{-1})	Percentage of LVFF events (%)	LVFF Event frequency f_t (s^{-1})
1	132 ± 16	7.7 ± 1.0	62.8 ± 3.5	4.8 ± 0.6
2	94.6 ± 10.0	10.7 ± 1.1	76.9 ± 1.3	8.3 ± 0.8
5	50.7 ± 4.5	19.9 ± 1.8	85.0 ± 2.4	16.9 ± 1.7
7.5	37.9 ± 4.5	26.7 ± 3.2	89.4 ± 1.5	22.9 ± 2.4
10	34.0 ± 2.4	29.6 ± 2.1	88.9 ± 1.2	26.3 ± 2.0
15	29.0 ± 1.4	34.6 ± 1.8	90.3 ± 0.8	31.2 ± 1.6
20	27.5 ± 1.4	36.5 ± 1.8	91.0 ± 0.9	33.2 ± 1.3
30	26.1 ± 0.2	38.4 ± 0.3	90.5 ± 0.4	35.2 ± 0.7
40	25.7 ± 0.6	38.9 ± 1.0	91.1 ± 1.8	35.3 ± 0.3
61	25.7 ± 0.4	38.9 ± 0.5	91.1 ± 1.4	35.5 ± 0.2

[a] The experiment was performed at -40 mV with the translocation of 10 μM peptide A-β (10-20) through the mutant αHL $(M113F)_7$ pore in the presence of 0.025 μM trypsin.

[b] τ_{on} was calculated based on all of the three different types of events (including A-β (10-20), LVFF, and YK-7) collected in a period of 1 min around a specific digestion time t.

Table 5.2 Effect of the substrate A-β (10-20) concentration on the event frequency $f_{t=5min}$ [a] of the cleavage product LVFF [b]

Substrate concentration (μM)	τ_{on} [c] (ms)	$1/\tau_{on}$ (s^{-1})	Percentage of LVFF events (%)	LVFF event frequency $f_{t=5min}$ (s^{-1})
2	226 ± 16	4.6 ± 0.4	88.1 ± 0.7	4.0 ± 0.3
4	117 ± 10	8.7 ± 0.7	85.1 ± 0.6	7.4 ± 0.6
6	89.8 ± 9.8	11.4 ± 1.2	89.4 ± 0.8	10.2 ± 1.1
8	58.3 ± 6.5	17.3 ± 1.9	86.2 ± 2.4	14.9 ± 1.2
10	50.7 ± 4.5	19.9 ± 1.8	85.0 ± 2.4	16.9 ± 1.7

[a] $f_{t=5\ min}$ is the event frequency of the cleavage product LVFF at a digestion time of 5 min.

[b] The experiments were performed at -40 mV with the translocation of peptide A-β (10-20) at various concentrations through the mutant αHL $(M113F)_7$ pore in the presence of 0.025 μM trypsin.

[c] τ_{on} was calculated based on all of the three different types of events (including A-β (10-20), LVFF, and YK-7) collected in a period of 1 min from t = 4 min to t = 5 min.

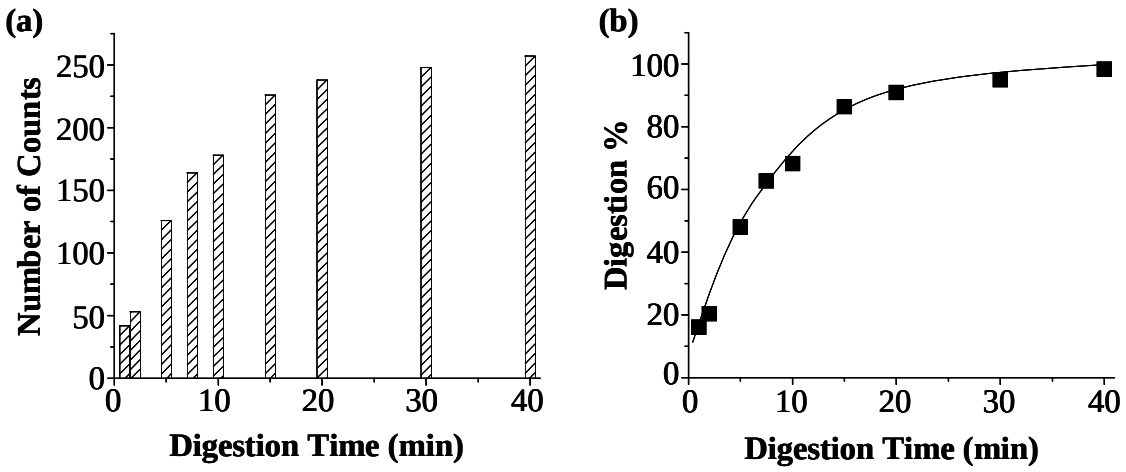

Figure 5.9: Time curve of the substrate digestion. Plots of (a) number of occurrences of the cleavage product LVFF events and (b) substrate digestion percentage vs. digestion time. The experiment was performed at -40 mV with the translocation of 10 μM peptide A-β (10-20) through the mutant αHL $(M113F)_7$ pore in the presence of 0.025 μM trypsin. The number of counts was obtained based on all the LVFF events collected from a period of 6 seconds around a specific digestion time t. For example, the number of counts at t = 2 min was calculated from all the LVFF events recorded from t = 1.9 min to t = 2.0 min; and that at t = 10 min was obtained based on all the LVFF events collected from t = 9.9 min to t = 10 min. Note that the number of event occurrences reported in Figure 5.9a were corrected values, which were obtained by dividing the actual number of counts by the percentage of the open channel state. This correction eliminates the variation in the long duration blockage events of the substrate peptide A-β (10-20) between different digestion times.

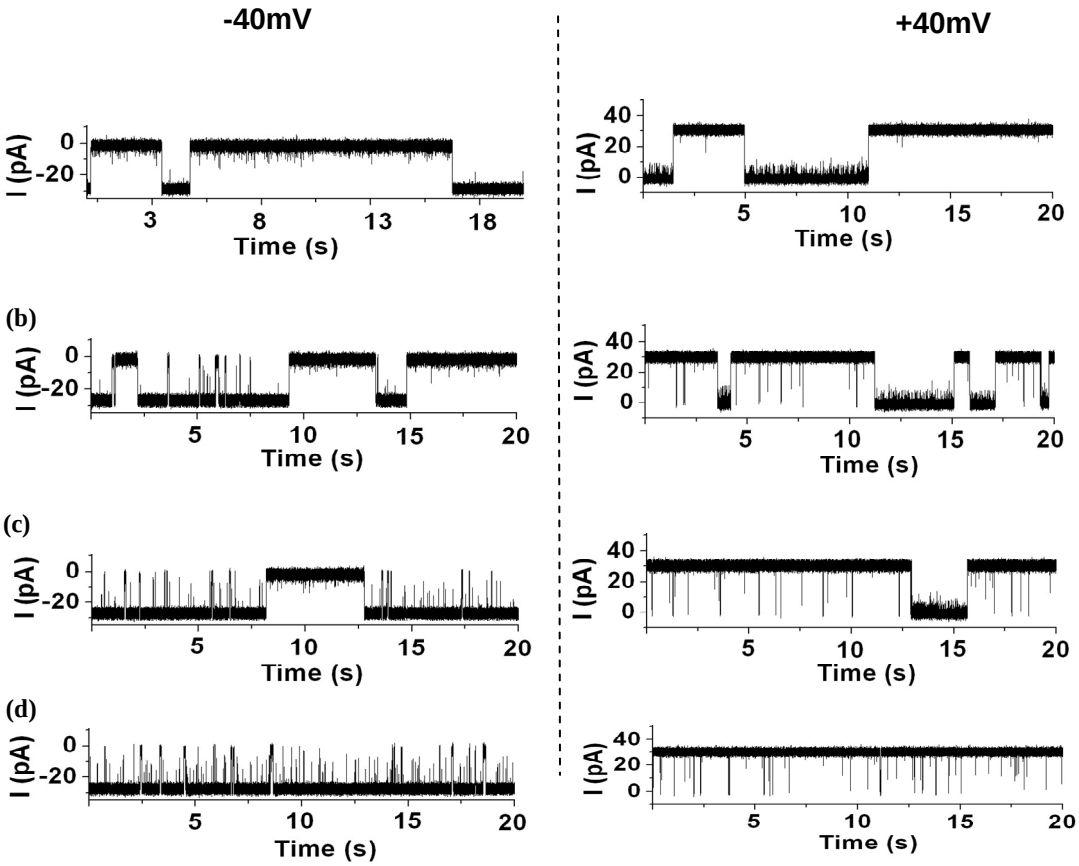

Figure 5.10: Cleavage of peptide YYYYYYRYPWF by trypsin. Representative segments of the single-channel current recording of the substrate-trypsin reaction at various times of (a) t = 0 min, (b) t = 10 min, (c) t = 60 min, and (d) t =180 min. The experiments were performed at both -40 mV(*left*) and +40 mV (*right*) with a 2.0 mL solution comprising 1 M NaCl and 10 mM Tris·HCl (pH 7.5). The concentration of substrate was 1.0 µM and that of trypsin was 0.15 µM.

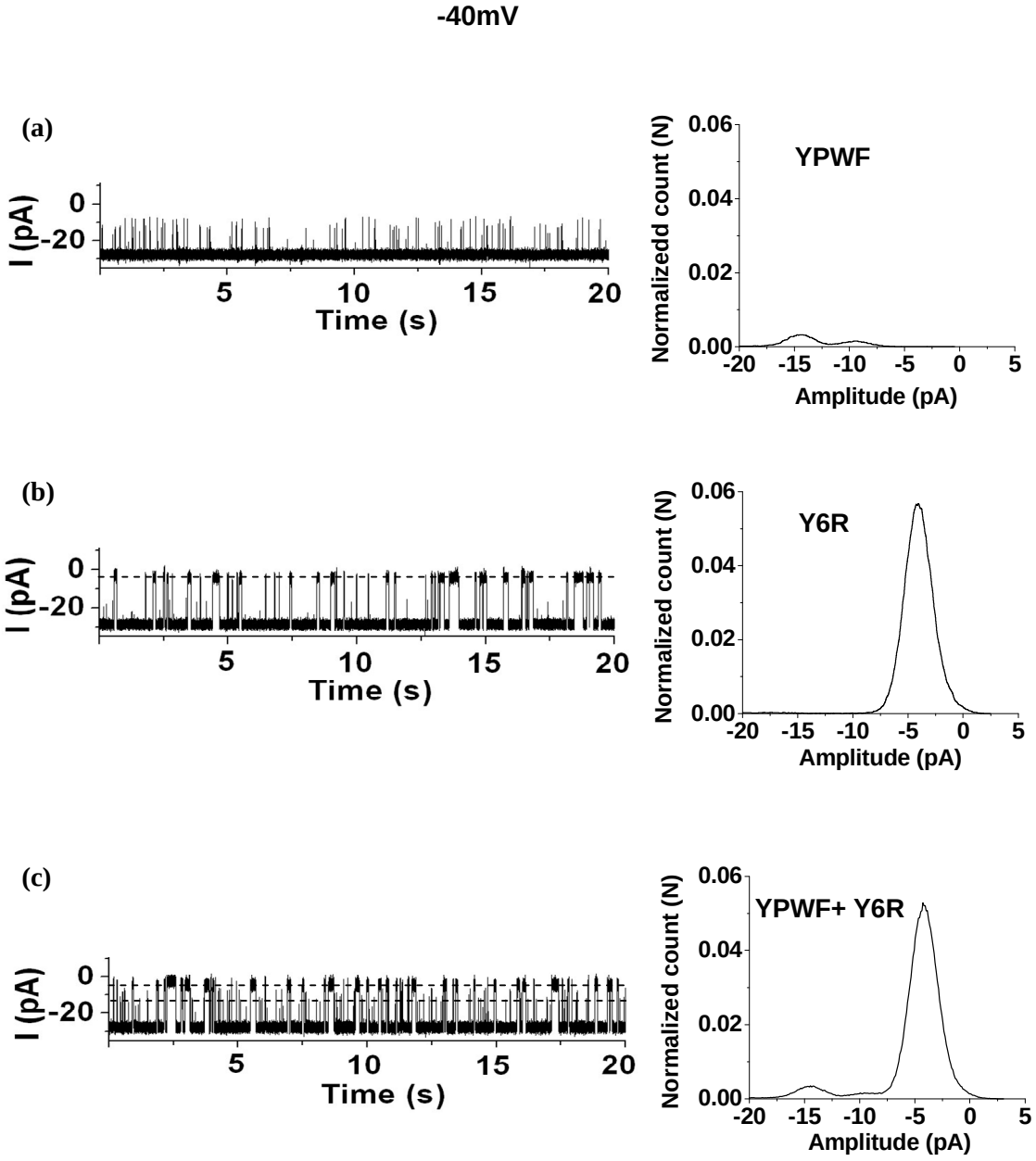

Figure 5.11: Control experiments with peptides Y6R and YPWF, confirming the identities of the cleavage products of YYYYYYRYPWF in the presence of trypsin. Typical single-channel recording traces and the corresponding all-points histograms for (a) YPWF, (b) Y6R, and (c) a mixture of YPWF and Y6R (1:1 ratio). The experiment was performed at -40 mV (*cis* at ground) under a series of symmetrical buffer conditions with a 2.0 mL solution comprising 1 M NaCl and 10 mM Tris·HCl (pH 7.5). Note that two different amplitude level events were observed for YPWF. These events may be attributed to the two different directions in which YPWF entered the $(M113F)_7$ pore. This phenomenon was also found in some DNA and RNA molecules

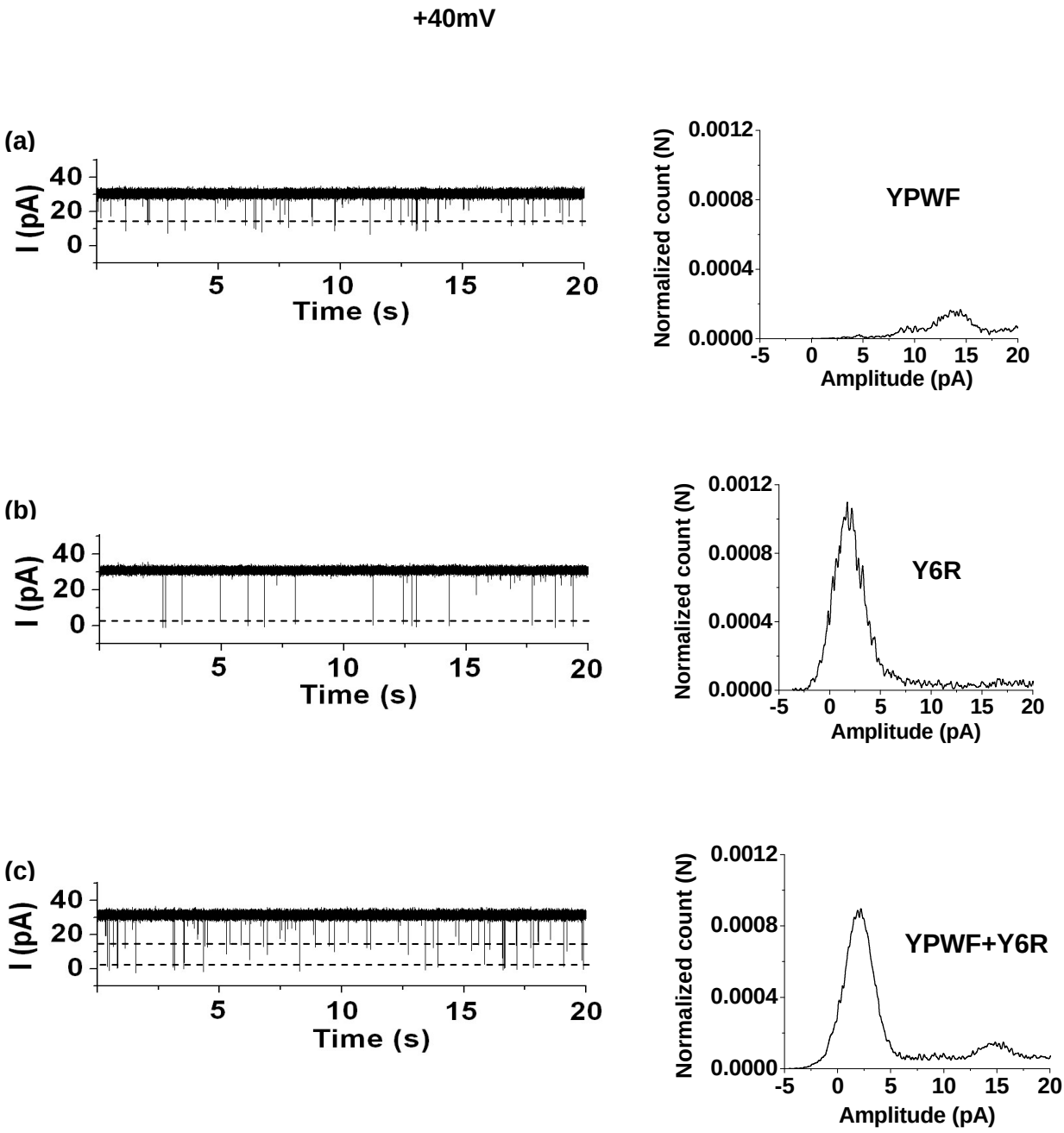

Figure 5.12: Control experiments with peptides Y6R and YPWF, confirming the identities of the cleavage products of YYYYYYRYPWF in the presence of trypsin. Typical single-channel recording traces and the corresponding all-points histograms for (a) YPWF, (b) Y6R, and (c) a mixture of YPWF and Y6R (1:1 ratio). The experiment was performed at +40 mV (*cis* at ground) under a series of symmetrical buffer conditions with a 2.0 mL solution comprising 1 M NaCl and 10 mM Tris·HCl (pH 7.5).

CHAPTER 6

SUMMARY

Nanopore DNA sequencing has emerged as the one of the most promising DNA sequencing schemes among other DNA sequencing methods. The α-Hemolysin protein nanopore has advantages over other nanopores and is widely used for nanopore sensing applications. The basis behind nanopore sensing is that single analyte molecules traversing through the nanopore cause characteristic event signatures that are unique to each analyte. Stochastic analysis of these event signatures allow the identification of the analyte. A limiting factor with nanopore DNA sequencing is the high translocation rates of DNA polynucleotide molecules through the nanopore, thus reducing the resolution of event signatures. The work described in this dissertation is mainly focused on slowing the DNA translocation through the α-Hemolysin nanpore.

In Chapter 2, we have shown that electrolyte solutions containing organic cations can significantly decrease the translocation rate. Compared to commonly used NaCl/KCl solutions, ionic liquid solutions resulted in a reduction of approximately 2 orders of magnitude. We interpret this decrease in DNA translocation rate as being due to the complex formation of Butyl-methyl-imidazolium cation with the negatively charged DNA strand. Five different DNA samples were discriminated with enhanced resolution.

Chapter 3 describes another approach to reducing the translocation rate by using acidic electrolyte solutions. Acidic electrolyte solutions resulted in rapid translocation events (~ 4 to 10 μs per base) as well as reduced translocation rates (~ 60 to 287 μs per base). Moreover, an increase of open channel conductance in the presence of acidic electrolyte solutions was also observed, helping to enhance the resolution of event signatures.

According to our knowledge, this is the first instance of using ionic liquid solutions for decreasing the DNA translocation rate. Slowing the passage of DNA through the nanopore by changing the electrolyte solution provides for a more convenient and effective strategy compared with other strategies that have been employed so far. We believe our strategies would provide new avenues for nanopore DNA sequencing, especially with synthetic nanopores. However, further theoretical, computational and experimental studies will be needed to better interpret these results.

Chapter 4 describes detection of organophosphorus nerve agent hydrolytes PMPA and CMPA with stochastic nanopore sensors. The mutant $(M113F/K147N)_7$ protein pore with βCD as a molecular adapter have been employed to screen the nerve agent hydrolytes. This is the first reported instance of detecting organophosphorus nerve agent hydrolytes with stochastic nanopore sensors.

A novel label free method to study the peptide cleavage and the corresponding enzymatic kinetics is described in chapter five. Peptide cleavage is studied with the mutant $(M113F)_7$ nanopore. Cleavage of the substrate A-β (10-20) by the enzyme

trypsin was carried out in the presence of $(M113F)_7$ protein nanopore. Translocation of the resulting peptides were recorded. $(M113F)_7$ has shown an enhanced resolution in the identification and discrimination of peptides compared to $(WT)_7$. Therefore, it has been shown that engineered protein nanopores can be employed in studying peptide cleavage and the corresponding enzyme kinetics.

APPENDIX A

STRUCTURE OF BUTYL-METHYL-IMIDAZOLIUM CHLORIDE

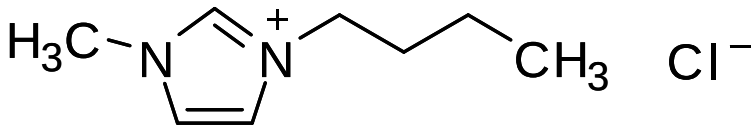

APPENDIX B

RIGHTS AND PERMISSIONS

Chapter 2: Reproduced with permission from Journal of Physical Chemistry B (2009), 113(40), 13332-13336; “Slowing DNA translocation through nanopores using a solution containing organic salts” by Ranulu Samanthi de Zoysa, Dilani A. Jayawardhana, Qitao Zhao, Deqiang Wang, Daniel W. Armstrong, Xiyun Guan. Copyright © 2009 American Chemical Society .

Chapter 4: Reproduced with permission from from Journal of Sensors and Actuators, B: Chemical (2009), B139(2), 440-446; ” Detection of nerve agent hydrolytes in an engineered nanopore” by Deqiang Wang, Qitao Zhao, Ranulu Samanthi de Zoysa, Xiyun Guan. Copyright © 2009 Elsevier.

Chapter 5: Reproduced with permission from from Journal of American Chemical Society, B: (2009), 131(18), 6324-6325; ” Real-Time Monitoring of Peptide cleavage Using a Nanopore Probe” by, Qitao Zhao, Ranulu Samanthi de Zoysa, Deqiang Wang, Dilani A. Jayawardhana, Xiyun Guan. Copyright © 2009 American Chemical Society.

REFERENCES

(1) Bayley, H.; Cremer, P. S. Stochastic sensors inspired by biology. *Nature (London, U. K.)* **2001***, 413*, 226-230.

(2) Schmidt, J. Stochastic sensors. *J. Mater. Chem.* **2005***, 15*, 831-840.

(3) Hladky, S. B.; Haydon, D. A. Discreteness of conductance change in bimolecular lipid membranes in the presence of certain antibiotics. *Nature (London)* **1970***, 225*, 451-453.

(4) Krasil'nikov, O. V.; Ternovskii, V. I.; Tashmukhamedov, B. A. Properties of conductivity channels induced in phospholipid bilayer membranes by alpha-staphylotoxin. *Biofizika* **1981***, 26*, 271-276.

(5) Kasianowicz, J. J.; Brandin, E.; Branton, D.; Deamer, D. W. Characterization of individual polynucleotide molecules using a membrane channel. *Proc Natl Acad Sci U S A* **1996***, 93*, 13770-13773.

(6) Kasianowicz, J. J.; Bezrukov, S. M. Protonation dynamics of the alpha-toxin ion channel from spectral analysis of pH-dependent current fluctuations. *Biophys J* **1995***, 69*, 94-105.

(7) Cheley, S.; Gu, L.; Bayley, H. Stochastic sensing of nanomolar inositol 1,4,5-trisphosphate with an engineered pore. *Chem. Biol.* **2002***, 9*, 829-838.

(8) Braha, O.; Gu, L. Q.; Zhou, L.; Lu, X.; Cheley, S.; Bayley, H. Simultaneous stochastic sensing of divalent metal ions. *Nat Biotechnol* **2000***, 18*, 1005-1007.

(9) Shin, S.; Luchian, T.; Cheley, S.; Braha, O.; Bayley, H. Kinetics of a reversible covalent-bond-forming reaction observed at the single-molecule level. *Angew. Chem. , Int. Ed.* **2002***, 41*, 3707-3709.

(10) Jayawardhana, D. A.; Crank, J. A.; Zhao, Q.; Armstrong, D. W.; Guan, X. Nanopore Stochastic Detection of a Liquid Explosive Component and Sensitizers Using Boromycin and an Ionic Liquid Supporting Electrolyte. *Anal. Chem. (Washington, DC, U. S.)* **2009***, 81*, 460-464.

(11) Kang, X.; Cheley, S.; Guan, X.; Bayley, H. Stochastic Detection of Enantiomers. *J. Am. Chem. Soc.* **2006***, 128*, 10684-10685.

(12) Movileanu, L.; Howorka, S.; Braha, O.; Bayley, H. Detecting protein analytes that modulate transmembrane movement of a polymer chain within a single protein pore. *Nat. Biotechnol.* **2000***, 18*, 1091-1095.

(13) Howorka, S.; Nam, J.; Bayley, H.; Kahne, D. Stochastic detection of monovalent and bivalent protein-ligand interactions. *Angew. Chem. , Int. Ed.* **2004***, 43*, 842-846.

(14) Meller, A.; Nivon, L.; Brandin, E.; Golovchenko, J.; Branton, D. Rapid nanopore discrimination between single polynucleotide molecules. *Proc. Natl. Acad. Sci. U. S. A.* **2000***, 97*, 1079-1084.

(15) Howorka, S.; Cheley, S.; Bayley, H. Sequence-specific detection of individual DNA strands using engineered nanopores. *Nat Biotechnol* **2001***, 19*, 636-639.

(16) de Zoysa, R. S. S.; Jayawardhana, D. A.; Zhao, Q.; Wang, D.; Armstrong, D. W.; Guan, X. Slowing DNA Translocation through Nanopores Using a Solution Containing Organic Salts. *J. Phys. Chem. B* **2009***, 113*, 13332-13336.

(17) Gu, L.; Braha, O.; Conlan, S.; Cheley, S.; Bayley, H. Stochastic sensing of organic analytes by a pore-forming protein containing a molecular adapter. *Nature (London)* **1999***, 398*, 686-690.

(18) Bhakdi, S.; Tranum-Jensen, J. Alpha-toxin of Staphylococcus aureus. *Microbiol. Rev.* **1991***, 55*, 733-751.

(19) Song, L.; Hobaugh, M. R.; Shustak, C.; Cheley, S.; Bayley, H.; Gouaux, J. E. Structure of staphylococcal Î±-hemolysin, a heptameric transmembrane pore. *Science (Washington, D. C.)* **1996***, 274*, 1859-1866.

(20) Menestrina, G. Ionic channels formed by Staphylococcus aureus alpha-toxin: voltage-dependent inhibition by divalent and trivalent cations. *J Membr Biol* **1986***, 90*, 177-190.

(21) Fussle, R.; Bhakdi, S.; Sziegoleit, A.; Tranum-Jensen, J.; Kranz, T.; Wellensiek, H. J. On the mechanism of membrane damage by Staphylococcus aureus alpha-toxin. *J Cell Biol* **1981***, 91*, 83-94.

(22) Zhao, Q.; Jayawardhana, D. A.; Guan, X. Stochastic study of the effect of ionic strength on noncovalent interactions in protein pores. *Biophys. J.* **2008***, 94*, 1267-1275.

(23) Montal, M.; Mueller, P. Formation of bimolecular membranes from lipid monolayers and a study of their electrical properties. *Proc. Nat. Acad. Sci. U. S. A.* **1972***, 69*, 3561-3566.

(24) Movileanu, L.; Schmittschmitt, J. P.; Scholtz, J. M.; Bayley, H. Interactions of peptides with a protein pore. *Biophys. J.* **2005***, 89*, 1030-1045.

(25) Li, J.; Stein, D.; McMullan, C.; Branton, D.; Aziz, M. J.; Golovchenko, J. A. Ion-beam sculpting at nanometer length scales. *Nature (London, U. K.)* **2001***, 412*, 166-169.

(26) Li, J.; Gershow, M.; Stein, D.; Brandin, E.; Golovchenko, J. A. DNA molecules and configurations in a solid-state nanopore microscope. *Nat. Mater.* **2003***, 2*, 611-615.

(27) Storm, A. J.; Chen, J. H.; Zandbergen, H. W.; Dekker, C. Translocation of double-strand DNA through a silicon oxide nanopore. *Phys Rev E Stat Nonlin Soft Matter Phys* **2005***, 71*, 051903.

(28) Yeh, I.; Hummer, G. Nucleic acid transport through carbon nanotube membranes. *Proc. Natl. Acad. Sci. U. S. A.* **2004***, 101*, 12177-12182.

(29) Nardin, C.; Hirt, T.; Leukel, J.; Meier, W. Polymerized ABA Triblock Copolymer Vesicles. *Langmuir* **2000***, 16*, 1035-1041.

(30) Nardin, C.; Winterhalter, M.; Meier, W. Giant Free-Standing ABA Triblock Copolymer Membranes. *Langmuir* **2000***, 16*, 7708-7712.

(31) Zhao, Q.; Wang, D.; Jayawardhana, D. A.; Guan, X. Stochastic sensing of biomolecules in a nanopore sensor array. *Nanotechnology* **2008***, 19*, 505504/1-505504/8.

(32) Akeson, M.; Branton, D.; Kasianowicz, J. J.; Brandin, E.; Deamer, D. W. Microsecond time-scale discrimination among polycytidylic acid, polyadenylic acid, and polyuridylic acid as homopolymers or as segments within single RNA molecules. *Biophys. J.* **1999***, 77*, 3227-3233.

(33) Branton, D.; Deamer, D. W.; Marziali, A.; Bayley, H.; Benner, S. A.; Butler, T.; Di Ventra, M.; Garaj, S.; Hibbs, A.; Huang, X.; Jovanovich, S. B.; Krstic, P. S.; Lindsay, S.; Ling, X. S.; Mastrangelo, C. H.; Meller, A.; Oliver, J. S.; Pershin, Y. V.; Ramsey, J. M.; Riehn, R.; Soni, G. V.; Tabard-Cossa, V.; Wanunu, M.; Wiggin, M.; Schloss, J. A. The potential and challenges of nanopore sequencing. *Nat. Biotechnol.* **2008***, 26*, 1146-1153.

(34) Bayley, H. Sequencing single molecules of DNA. *Curr. Opin. Chem. Biol.* **2006***, 10*, 628-637.

(35) Jett, J. H.; Keller, R. A.; Martin, J. C.; Marrone, B. L.; Moyzis, R. K.; Ratliff, R. L.; Seitzinger, N. K.; Shera, E. B.; Stewart, C. C. High-speed DNA sequencing: an approach based upon fluorescence detection of single molecules. *J. Biomol. Struct. Dyn.* **1989***, 7*, 301-309.

(36) Astier, Y.; Braha, O.; Bayley, H. Toward Single Molecule DNA Sequencing: Direct Identification of Ribonucleoside and Deoxyribonucleoside 5'-Monophosphates by Using an Engineered Protein Nanopore Equipped with a Molecular Adapter. *J. Am. Chem. Soc.* **2006***, 128*, 1705-1710.

(37) Wu, H.; Astier, Y.; Maglia, G.; Mikhailova, E.; Bayley, H. Protein Nanopores with Covalently Attached Molecular Adapters. *J. Am. Chem. Soc.* **2007***, 129*, 16142-16148.

(38) Sauer-Budge, A. F.; Nyamwanda, J. A.; Lubensky, D. K.; Branton, D. Unzipping Kinetics of Double-Stranded DNA in a Nanopore. *Phys. Rev. Lett.* **2003***, 90*, 238101/1-238101/4.

(39) Zwolak, M.; Di Ventra, M. Electronic Signature of DNA Nucleotides via Transverse Transport. *Nano Lett.* **2005***, 5*, 421-424.

(40) Zikic, R.; Krstic, P. S.; Zhang, X. -.; Fuentes-Cabrera, M.; Wells, J.; Zhao, X. Reply to "Comment on 'Characterization of the tunneling conductance across DNA bases' ". *Phys. Rev. E: Stat. , Nonlinear, Soft Matter Phys.* **2007***, 76*, 013902/1-013902/2.

(41) Heng, J. B.; Aksimentiev, A.; Ho, C.; Marks, P.; Grinkova, Y. V.; Sligar, S.; Schulten, K.; Timp, G. Stretching DNA Using the Electric Field in a Synthetic Nanopore. *Nano Lett.* **2005***, 5*, 1883-1888.

(42) Gracheva, M. E.; Xiong, A.; Aksimentiev, A.; Schulten, K.; Timp, G.; Leburton, J. Simulation of the electric response of DNA translocation through a semiconductor nanopore-capacitor. *Nanotechnology* **2006***, 17*, 622-633.

(43) Sigalov, G.; Comer, J.; Timp, G.; Aksimentiev, A. Detection of DNA Sequences Using an Alternating Electric Field in a Nanopore Capacitor. *Nano Lett.* **2008***, 8*, 56-63.

(44) Drmanac, R.; Drmanac, S.; Chui, G.; Diaz, R.; Hou, A.; Jin, H.; Jin, P.; Kwon, S.; Lacy, S.; Moeur, B.; Shafto, J.; Swanson, D.; Ukrainczyk, T.; Xu, C.; Little, D. Sequencing by hybridization (SBH): advantages, achievements, and opportunities. *Adv. Biochem. Eng. /Biotechnol.* **2002***, 77*, 75-101.

(45) Zwolak, M.; Di Ventra, M. Physical approaches to DNA sequencing and detection. *Los Alamos Natl. Lab. , Prepr. Arch. , Phys.* **2007**, 1-26, arXiv:0708.2724v1 [physics.bio-ph].

(46) Aksimentiev, A.; Heng, J. B.; Timp, G.; Schulten, K. Microscopic kinetics of DNA translocation through synthetic nanopores. *Biophys. J.* **2004***, 87*, 2086-2097.

(47) Aksimentiev, A.; Schulten, K. Imaging Î±-hemolysin with molecular dynamics: Ionic conductance, osmotic permeability, and the electrostatic potential map. *Biophys. J.* **2005***, 88*, 3745-3761.

(48) Muthukumar, M.; Kong, C. Y. Simulation of polymer translocation through protein channels. *Proc Natl Acad Sci U S A* **2006***, 103*, 5273-5278.

(49) Liu, H.; Qian, S.; Bau, H. H. The effect of translocating cylindrical particles on the ionic current through a nanopore. *Biophys. J.* **2007***, 92*, 1164-1177.

(50) Meller, A.; Nivon, L.; Branton, D. Voltage-Driven DNA Translocations through a Nanopore. *Phys. Rev. Lett.* **2001***, 86*, 3435-3438.

(51) Franca, L. T. C.; Carrilho, E.; Kist, T. B. L. A review of DNA sequencing techniques. *Q. Rev. Biophys.* **2002***, 35*, 169-200.

(52) AnonymousRFA-HG-04-003: REVOLUTIONARY GENOME SEQUENCING TECHNOLOGIES -- THE $1000 GENOME *http://grants1.nih.gov/grants/guide/rfa-files/RFA-HG-04-003.html* (accessed 3/3/2011, 2011).

(53) Meller, A.; Branton, D. Single molecule measurements of DNA transport through a nanopore. *Electrophoresis* **2002***, 23*, 2583-2591.

(54) Sanchez-Quesada, J.; Saghatelian, A.; Cheley, S.; Bayley, H.; Ghadiri, M. R. Single DNA rotaxanes of a transmembrane pore protein. *Angew. Chem. , Int. Ed.* **2004***, 43*, 3063-3067.

(55) Purnell, R. F.; Mehta, K. K.; Schmidt, J. J. Nucleotide Identification and Orientation Discrimination of DNA Homopolymers Immobilized in a Protein Nanopore. *Nano Lett.* **2008***, 8*, 3029-3034.

(56) Welton, T. Room-Temperature Ionic Liquids. Solvents for Synthesis and Catalysis. *Chem. Rev. (Washington, D. C.)* **1999***, 99*, 2071-2083.

(57) Nakashima, K.; Kubota, F.; Maruyama, T.; Goto, M. Feasibility of ionic liquids as alternative separation media for industrial solvent extraction processes. *Ind. Eng. Chem. Res.* **2005***, 44*, 4368-4372.

(58) Anderson, J. L.; Armstrong, D. W.; Wei, G. -. Ionic Liquids in Analytical Chemistry (Anal. Chem. 2006, 78, 2893-2902). *Anal. Chem. (Washington, DC, U. S.)* **2007***, 79*, 4247.

(59) Welton, T. Ionic liquids in catalysis. *Coord. Chem. Rev.* **2004***, 248*, 2459-2477.

(60) Galinski, M.; Lewandowski, A.; Stepniak, I. Ionic liquids as electrolytes. *Electrochim. Acta* **2006***, 51*, 5567-5580.

(61) Zhao, Q.; Jayawardhana, D. A.; Wang, D.; Guan, X. Study of Peptide Transport through Engineered Protein Channels. *J. Phys. Chem. B* **2009***, 113*, 3572-3578.

(62) Butler, T. Z.; Gundlach, J. H.; Troll, M. Ionic current blockades from DNA and RNA molecules in the Î±-hemolysin nanopore. *Biophys. J.* **2007***, 93*, 3229-3240.

(63) Miller, C. Coupling of water and ion fluxes in a potassium(1+)-selective channel of sarcoplasmic reticulum. *Biophys. J.* **1982***, 38*, 227-230.

(64) Colquhoun, D.; Hawkes, A. G.; Sakmann, B., Neher, E., In *The principles of stochastic interpretation of ion-channel mechanisms. In Single-Channel Recording;* 1983; pp 135-175.

(65) Zamyatnin, A. A. Amino acid, peptide, and protein volume in solution. *Annu. Rev. Biophys. Bioeng.* **1984***, 13*, 145-165.

(66) Kawano, R.; Schibel, A. E. P.; Cauley, C.; White, H. S. Controlling the Translocation of Single-Stranded DNA through Î±-Hemolysin Ion Channels Using Viscosity. *Langmuir* **2009***, 25*, 1233-1237.

(67) Maglia, G.; Restrepo, M. R.; Mikhailova, E.; Bayley, H. Enhanced translocation of single DNA molecules through Î±-hemolysin nanopores by manipulation of internal charge. *Proc. Natl. Acad. Sci. U. S. A.* **2008***, 105*, 19720-19725.

(68) Gu, L.; Cheley, S.; Bayley, H. Prolonged residence time of a noncovalent molecular adapter, Î²-cyclodextrin, within the lumen of mutant Î±-hemolysin pores. *J. Gen. Physiol.* **2001***, 118*, 481-493.

(69) Marziali, A.; Akeson, M. New DNA sequencing methods. *Annu. Rev. Biomed. Eng.* **2001***, 3*, 195-223.

(70) Zhang, J.; Shklovskii, B. I. Effective charge and free energy of DNA inside an ion channel. *Phys. Rev. E: Stat. , Nonlinear, Soft Matter Phys.* **2007***, 75*, 021906/1-021906/10.

(71) Shen, X.; Xu, G.; Shao, C. The effect of K+, Na+ doping on infrared emissivity of lanthanum manganites. *Solid State Commun.* **2009***, 149*, 852-854.

(72) Berthod, A.; Kozak, J. J.; Anderson, J. L.; Ding, J.; Armstrong, D. W. Ionic liquid-alkane association in dilute solutions. *Theor. Chem. Acc.* **2007***, 117*, 127-135.

(73) Wang, J.; Cheng, D.; Chen, X.; Du, Z.; Fang, Z. Direct Extraction of Double-Stranded DNA Into Ionic Liquid 1-Butyl-3-methylimidazolium Hexafluorophosphate and Its Quantification. *Anal. Chem.* **2007***, 79*, 620-625.

(74) Xie, Y. N.; Wang, S. F.; Zhang, Z. L.; Pang, D. W. *J. Phys. Chem. B* **2008***, 12*, 9864-9864-9868.

(75) Fologea, D.; Uplinger, J.; Thomas, B.; McNabb, D. S.; Li, J. Slowing DNA Translocation in a Solid-State Nanopore. *Nano Lett.* **2005***, 5*, 1734-1737.

(76) Keyser, U. F.; Koeleman, B. N.; Van Dorp, S.; Krapf, D.; Smeets, R. M. M.; Lemay, S. G.; Dekker, N. H.; Dekker, C. Direct force measurements on DNA in a solid-state nanopore. *Nat. Phys.* **2006***, 2*, 473-477.

(77) Benner, S.; Chen, R. J. A.; Wilson, N. A.; Abu-Shumays, R.; Hurt, N.; Lieberman, K. R.; Deamer, D. W.; Dunbar, W. B.; Akeson, M. Sequence-specific detection of individual DNA polymerase complexes in real time using a nanopore. *Nat. Nanotechnol.* **2007***, 2*, 718-724.

(78) Gershow, M.; Golovchenko, J. A. Recapturing and trapping single molecules with a solid-state nanopore. *Nat. Nanotechnol.* **2007***, 2*, 775-779.

(79) Guan, X.; Gu, L.; Cheley, S.; Braha, O.; Bayley, H. Stochastic sensing of TNT with a genetically engineered pore. *ChemBioChem* **2005***, 6*, 1875-1881.

(80) Wang, D.; Zhao, Q.; de Zoysa, R. S. S.; Guan, X. Detection of nerve agent hydrolytes in an engineered nanopore. *Sens. Actuators, B* **2009***, B139*, 440-446.

(81) Braha, O.; Walker, B.; Cheley, S.; Kasianowicz, J. J.; Song, L.; Gouaux, J. E.; Bayley, H. Designed protein pores as components for biosensors. *Chem. Biol.* **1997***, 4*, 497-505.

(82) Gao, C.; Ding, S.; Tan, Q.; Gu, L. Method of creating a nanopore-terminated probe for single-molecule enantiomer discrimination. *Anal. Chem. (Washington, DC, U. S.)* **2009***, 81*, 80-86.

(83) Lee, S. B.; Mitchell, D. T.; Trofin, L.; Nevanen, T. K.; Soederlund, H.; Martin, C. R. Antibody-based bio-nanotube membranes for enantiomeric drug separations. *Science (Washington, DC, U. S.)* **2002***, 296*, 2198-2200.

(84) Luchian, T.; Shin, S.; Bayley, H. Single-molecule covalent chemistry with spatially separated reactants. *Angew. Chem. , Int. Ed.* **2003***, 42*, 3766-3771.

(85) Shim, J. W.; Tan, Q.; Gu, L. Single-molecule detection of folding and unfolding of the G-quadruplex aptamer in a nanopore nanocavity. *Nucleic Acids Res.* **2009***, 37*, 972-982.

(86) Talaga, D. S.; Li, J. Single-Molecule Protein Unfolding in Solid State Nanopores. *J. Am. Chem. Soc.* **2009***, 131*, 9287-9297.

(87) Zhao, Q.; de Zoysa, R. S. S.; Wang, D.; Jayawardhana, D. A.; Guan, X. Real-Time Monitoring of Peptide Cleavage Using a Nanopore Probe. *J. Am. Chem. Soc.* **2009***, 131*, 6324-6325.

(88) Storm, A. J.; Storm, C.; Chen, J.; Zandbergen, H.; Joanny, J.; Dekker, C. Fast DNA Translocation through a Solid-State Nanopore. *Nano Lett.* **2005***, 5*, 1193-1197.

(89) Stoddart, D.; Heron, A. J.; Mikhailova, E.; Maglia, G.; Bayley, H. Single-nucleotide discrimination in immobilized DNA oligonucleotides with a biological nanopore. *Proc. Natl. Acad. Sci. U. S. A.* **2009***, 106*, 7702-7707, S7702/1-S7702/11.

(90) Clarke, J.; Wu, H.; Jayasinghe, L.; Patel, A.; Reid, S.; Bayley, H. Continuous base identification for single-molecule nanopore DNA sequencing. *Nat. Nanotechnol.* **2009***, 4*, 265-270.

(91) Jovanovic-Talisman, T.; Tetenbaum-Novatt, J.; McKenney, A. S.; Zilman, A.; Peters, R.; Rout, M. P.; Chait, B. T. Artificial nanopores that mimic the transport selectivity of the nuclear pore complex. *Nature (London, U. K.)* **2009***, 457*, 1023-1027.

(92) Mitchell, N.; Howorka, S. Chemical tags facilitate the sensing of individual DNA strands with nanopores. *Angew. Chem. , Int. Ed.* **2008***, 47*, 5565-5568.

(93) Cockroft, S. L.; Chu, J.; Amorin, M.; Ghadiri, M. R. A Single-Molecule Nanopore Device Detects DNA Polymerase Activity with Single-Nucleotide Resolution. *J. Am. Chem. Soc.* **2008***, 130*, 818-820.

(94) Maglia, G.; Henricus, M.; Wyss, R.; Li, Q.; Cheley, S.; Bayley, H. DNA strands from denatured duplexes are translocated through engineered protein nanopores at alkaline pH. *Nano Lett* **2009***, 9*, 3831-3836.

(95) Luan, B.; Aksimentiev, A. Electro-osmotic screening of the DNA charge in a nanopore. *Phys. Rev. E: Stat. , Nonlinear, Soft Matter Phys.* **2008***, 78*, 021912/1-021912/4.

(96) Bates, M.; Burns, M.; Meller, A. Dynamics of DNA molecules in a membrane channel probed by active control techniques. *Biophys. J.* **2003***, 84*, 2366-2372.

(97) Hooijschuur, E. W. J.; Kientz, C. E.; Brinkman, U. A. T. Analytical separation techniques for the determination of chemical warfare agents. *J. Chromatogr. , A* **2002***, 982*, 177-200.

(98) Yang, Y. Chemical Detoxification of Nerve Agent VX. *Acc. Chem. Res.* **1999***, 32*, 109-115.

(99) Witkiewicz, Z.; Mazurek, M.; Szulc, J. Chromatographic analysis of chemical warfare agents. *J. Chromatogr.* **1990***, 503*, 293-357.

(100) Hooijschuur, E. W.; Kientz, C. E.; Brinkman, U. A. Determination of alkylphosphonic acids by microcolumn liquid chromatography with gradient elution coupled on-line with flame photometric detection. *J Chromatogr A* **2001***, 907*, 165-172.

(101) Kingery, A. F.; Allen, H. E. Ion chromatographic separation of closely related nerve agent degradation products using an organic modifier to provide selectivity. *Anal. Chem.* **1994***, 66*, 155-159.

(102) Melanson, J. E.; Wong, B. L. -.; Boulet, C. A.; Lucy, C. A. High-sensitivity determination of the degradation products of chemical warfare agents by

capillary electrophoresis-indirect UV absorbance detection. *J. Chromatogr. , A* **2001***, 920*, 359-365.

(103) Pardasani, D.; Mazumder, A.; Gupta, A. K.; Kanaujia, P. K.; Tak, V.; Dubey, D. K. Determination of hydrolytic degradation products of nerve agents by injection port fluorination in gas chromatography/mass spectrometry for the verification of the Chemical Weapons Convention. *Rapid Commun. Mass Spectrom.* **2007***, 21*, 3109-3114.

(104) Richardson, D. D.; Caruso, J. A. Derivatization of organophosphorus nerve agent degradation products for gas chromatography with ICPMS and TOF-MS detection. *Anal. Bioanal. Chem.* **2007***, 388*, 809-823.

(105) Smith, J. R.; Shih, M. L. Analysis of the degradation compounds of chemical warfare agents using liquid chromatography/mass spectrometry. *J. Appl. Toxicol.* **2001***, 21*, S27-S34.

(106) Guilbault, G. G.; Kristoff, J.; Owens, D. Detection of organophosphorus compounds with a coated piezoelectric crystal. *Anal. Chem.* **1985***, 57*, 1754-1756.

(107) Grate, J. W.; McGill, R. A. Dewetting Effects on Polymer-Coated Surface Acoustic Wave Vapor Sensors. *Anal. Chem.* **1995***, 67*, 4015-4019.

(108) Nieuwenhuizen, M. S.; Harteveld, J. L. N. Studies on a surface acoustic wave (SAW) dosimeter sensor for organophosphorus nerve agents. *Sens. Actuators, B* **1997***, B40*, 167-173.

(109) Zhou, Y.; Yu, B.; Shiu, E.; Levon, K. Potentiometric Sensing of Chemical Warfare Agents: Surface Imprinted Polymer Integrated with an Indium Tin Oxide Electrode. *Anal. Chem.* **2004***, 76*, 2689-2693.

(110) Tomchenko, A. A.; Harmer, G. P.; Marquis, B. T. Detection of chemical warfare agents using nanostructured metal oxide sensors. *Sens. Actuators, B* **2005***, B108*, 41-55.

(111) Cadwell, K. D.; Lockwood, N. A.; Nellis, B. A.; Alf, M. E.; Willis, C. R.; Abbott, N. L. Detection of organophosphorus nerve agents using liquid crystals supported on chemically functionalized surfaces. *Sens. Actuators, B* **2007***, B128*, 91-98.

(112) Zuo, G.; Li, X.; Li, P.; Yang, T.; Wang, Y.; Cheng, Z.; Feng, S. Detection of trace organophosphorus vapor with a self-assembled bilayer functionalized SiO2 microcantilever piezoresistive sensor. *Anal. Chim. Acta* **2006***, 580*, 123-127.

(113) Sohn, H.; Letant, S.; Sailor, M. J.; Trogler, W. C. Detection of Fluorophosphonate Chemical Warfare Agents by Catalytic Hydrolysis with a Porous Silicon Interferometer. *J. Am. Chem. Soc.* **2000***, 122*, 5399-5400.

(114) Zourob, M.; Simonian, A.; Wild, J.; Mohr, S.; Fan, X.; Abdulhalim, I.; Goddard, N. J. Optical leaky waveguide biosensors for the detection of organophosphorus pesticides. *Analyst (Cambridge, U. K.)* **2007***, 132*, 114-120.

(115) Simonian, A. L.; Good, T. A.; Wang, S. -.; Wild, J. R. Nanoparticle-based optical biosensors for the direct detection of organophosphate chemical warfare agents and pesticides. *Anal. Chim. Acta* **2005***, 534*, 69-77.

(116) Joshi, K. A.; Prouza, M.; Kum, M.; Wang, J.; Tang, J.; Haddon, R.; Chen, W.; Mulchandani, A. V-Type Nerve Agent Detection Using a Carbon Nanotube-Based Amperometric Enzyme Electrode. *Anal. Chem.* **2006***, 78*, 331-336.

(117) Jenkins, A. L.; Bae, S. Y. Molecularly imprinted polymers for chemical agent detection in multiple water matrices. *Anal. Chim. Acta* **2005***, 542*, 32-37.

(118) Wallace, K. J.; Morey, J.; Lynch, V. M.; Anslyn, E. V. Colorimetric detection of chemical warfare simulants. *New J. Chem.* **2005***, 29*, 1469-1474.

(119) Zhang, S.; Swager, T. M. Fluorescent Detection of Chemical Warfare Agents: Functional Group Specific Ratiometric Chemosensors. *J. Am. Chem. Soc.* **2003***, 125*, 3420-3421.

(120) Levitsky, I.; Krivoshlykov, S. G.; Grate, J. W. Rational design of a Nile Red/polymer composite film for fluorescence sensing of organophosphonate vapors using hydrogen bond acidic polymers. *Anal. Chem.* **2001***, 73*, 3441-3448.

(121) Shulga, O. V.; Palmer, C. Detection of V-type nerve agent degradation products at electrodes modified by PPy/PQQ using CaCl2 as supporting electrolyte. *Anal. Bioanal. Chem.* **2006***, 385*, 1116-1123.

(122) Choi, N.; Kwak, J.; Lim, Y.; Bahn, T.; Yun, K.; Kim, J.; Huh, J.; Lee, D. Classification of chemical warfare agents using thick film gas sensor array. *Sens. Actuators, B* **2005***, B108*, 298-304.

(123) Meier, D. C.; Taylor, C. J.; Cavicchi, R. E.; Edward, W. V.; Ellzy, M. W.; Sumpter, K. B.; Semancik, S. Chemical warfare agent detection using MEMS-compatible microsensor arrays. *IEEE Sens. J.* **2005***, 5*, 712-725.

(124) Tan, H. Y.; Loke, W. K.; Tan, Y. T.; Nguyen, N. A lab-on-a-chip for detection of nerve agent sarin in blood. *Lab Chip* **2008***, 8*, 885-891.

(125) Hill, H. H., Jr.; Martin, S. J. Conventional analytical methods for chemical warfare agents. *Pure Appl. Chem.* **2002***, 74*, 2281-2291.

(126) Kang, X.; Cheley, S.; Rice-Ficht, A. C.; Bayley, H. A Storable Encapsulated Bilayer Chip Containing a Single Protein Nanopore. *J. Am. Chem. Soc.* **2007***, 129*, 4701-4705.

(127) White, R. J.; Ervin, E. N.; Yang, T.; Chen, X.; Daniel, S.; Cremer, P. S.; White, H. S. Single Ion-Channel Recordings Using Glass Nanopore Membranes. *J. Am. Chem. Soc.* **2007***, 129*, 11766-11775.

(128) Loftsson, T.; Duchene, D. Cyclodextrins and their pharmaceutical applications. *Int. J. Pharm.* **2007***, 329*, 1-11.

(129) Rekharsky, M. V.; Inoue, Y. Complexation Thermodynamics of Cyclodextrins. *Chem. Rev. (Washington, D. C.)* **1998***, 98*, 1875-1917.

(130) Matsuno, Y.; Osono, C.; Hirano, A.; Sugawara, M. Single-channel recordings of gramicidin at agarose-supported bilayer lipid membranes formed by the tip-dip and painting methods. *Anal. Sci.* **2004***, 20*, 1217-1221.

(131) Piao, H.; Marx, R. B.; Schneider, S.; Irvine, D. A.; Staton, J. Analysis of VX nerve agent hydrolysis products in wastewater effluents by ion chromatography with amperometric and conductivity detection. *J. Chromatogr. , A* **2005***, 1089*, 65-71.

(132) Shim, J. W.; Gu, L. Q. Stochastic Sensing on a Modular Chip Containing a Single-Ion Channel. *Anal. Chem.* **2007***, 79*, 2207-2213.

(133) Roepe, P. D. A peptide needle in a signaling haystack. *Nat. Genet.* **2001***, 27*, 6-8.

(134) Schatz, P. J. Use of peptide libraries to map the substrate specificity of a peptide-modifying enzyme: a 13 residue consensus peptide specifies biotinylation in Escherichia coli. *Biotechnology (N Y)* **1993***, 11*, 1138-1143.

(135) Barnham, K. J.; Kenche, V. B.; Ciccotosto, G. D.; Smith, D. P.; Tew, D. J.; Liu, X.; Perez, K.; Cranston, G. A.; Johanssen, T. J.; Volitakis, I.; Bush, A. I.; Masters, C. L.; White, A. R.; Smith, J. P.; Cherny, R. A.; Cappai, R. Platinum-based inhibitors of amyloid-Î² as therapeutic agents for Alzheimer's disease. *Proc. Natl. Acad. Sci. U. S. A.* **2008***, 105*, 6813-6818.

(136) Aidley, D. j.; Stanfield, P. R. *Ion Channels: Molecules in Action* **1996**, 59-112.

(137) Lee, H.; Sun, E.; Ham, D.; Weissleder, R. Chip-NMR biosensor for detection and molecular analysis of cells. *Nat. Med. (N. Y. , NY, U. S.)* **2008***, 14*, 869-874.

(138) Clements, A.; Johnston, M. V.; Larsen, B. S.; McEwen, C. N. Fluorescence-Based Peptide Labeling and Fractionation Strategies for Analysis of Cysteine-Containing Peptides. *Anal. Chem.* **2005***, 77*, 4495-4502.

(139) Urbaniak, M. D.; Yashunsky, D. V.; Crossman, A.; Nikolaev, A. V.; Ferguson, M. A. J. Probing Enzymes Late in the Trypanosomal Glycosylphosphatidylinositol Biosynthetic Pathway with Synthetic Glycosylphosphatidylinositol Analogues. *ACS Chem. Biol.* **2008***, 3*, 625-634.

(140) Mozsolits, H.; Aguilar, M. Surface plasmon resonance spectroscopy: an emerging tool for the study of peptide-membrane interactions. *Biopolymers* **2002***, 66*, 3-18.

(141) Strop, P.; Brunger, A. T. Refractive index-based determination of detergent concentration and its application to the study of membrane proteins. *Protein Sci.* **2005***, 14*, 2207-2211.

(142) Raorane, D. A.; Lim, M. D.; Chen, F. F.; Craik, C. S.; Majumdar, A. Quantitative and Label-Free Technique for Measuring Protease Activity and Inhibition using a Microfluidic Cantilever Array. *Nano Lett.* **2008***, 8*, 2968-2974.

(143) Salisbury, C. M.; Maly, D. J.; Ellman, J. A. Peptide Microarrays for the Determination of Protease Substrate Specificity. *J. Am. Chem. Soc.* **2002***, 124*, 14868-14870.

(144) Vestergaard, M.; Kerman, K.; Saito, M.; Nagatani, N.; Takamura, Y.; Tamiya, E. A rapid label-free electrochemical detection and kinetic study of Alzheimer's amyloid beta aggregation. *J. Am. Chem. Soc.* **2005***, 127*, 11892-11893.

(145) Knudsen, S. M.; Lee, J.; Ellington, A. D.; Savran, C. A. Ribozyme-Mediated Signal Augmentation on a Mass-Sensitive Biosensor. *J. Am. Chem. Soc.* **2006***, 128*, 15936-15937.

(146) Evnin, L. B.; Vasquez, J. R.; Craik, C. S. Substrate specificity of trypsin investigated by using a genetic selection. *Proc. Natl. Acad. Sci. U. S. A.* **1990***, 87*, 6659-6663.

(147) Diaz, J. F.; Balkus, K. J.,Jr Enzyme immobilization in MCM-41 molecular sieve. *J. Mol. Catal. B: Enzym.* **1996***, 2*, 115-126.

(148) Sahasrabudhe, S. R.; Brown, A. M.; Hulmes, J. D.; Jacobsen, J. S.; Vitek, M. P.; Blume, A. J.; Sonnenberg, J. L. Enzymic generation of the amino terminus of the Î²-amyloid peptide. *J. Biol. Chem.* **1993***, 268*, 16699-16705.

(149) Murthy, S. N. S.; Kostman, J.; Dinoso, V. P.,Jr Effect of pH, substrate, and temperature on tryptic activity of duodenal samples. *Dig. Dis. Sci.* **1980***, 25*, 289-294.

(150) Wolfe, A. J.; Mohammad, M. M.; Cheley, S.; Bayley, H.; Movileanu, L. Catalyzing the Translocation of Polypeptides through Attractive Interactions. *J. Am. Chem. Soc.* **2007***, 129*, 14034-14041.

(151) Cheley, S.; Braha, O.; Lu, X.; Conlan, S.; Bayley, H. A functional protein pore with a "retro" transmembrane domain. *Protein Sci* **1999***, 8*, 1257-1267.

(152) Movileanu, L.; Cheley, S.; Bayley, H. Partitioning of individual flexible polymers into a nanoscopic protein pore. *Biophys. J.* **2003***, 85*, 897-910.

BIOGRAPHICAL INFORMATION

Samanthi de Zoysa was born in Galle, Sri Lanka. She did her undergraduate studies at Rajarata University of Sri Lanka and obtained her BS degree in 2003. She also completed a special degree in chemistry from Institute of Chemistry, Ceylon in 2002. After working as an assistant lecturer at the Open University of Sri Lanka, she moved to the United States in 2005 to pursue her doctoral studies in chemistry at the University of Texas at Arlington. She began working with Prof. Richard X. Guan in 2008. Her research interests include chemical and biochemical analysis with nanopore sensors. She obtained her PhD in 2011.